

AD-A255 618



AFOSR-TR- 92 0033

2

**HIGH RESOLUTION GEOLOGICAL SITE
CHARACTERIZATION UTILIZING GROUND
MOTION DATA**

S DTIC ELECTE D
A SEP 14 1992

Approved for public distribution unlimited

**ANNUAL REPORT
GRANT AFOSR-89-0176
1 NOVEMBER 90 - 31 OCTOBER 91**

This document has been approved for public release and sale; its distribution is unlimited.

**PI: BRIAN W STUMP
DEPARTMENT OF GEOLOGICAL SCIENCES
SOUTHERN METHODIST UNIVERSITY
DALLAS, TEXAS 75275-0395**

26 JUNE 92

92 09 11 030

92-25076



91698

AIR FORCE ON BEHALF OF AFOSR
1992-12

18 AUG 1992

406857

26 June 92

Annual: 1 Nov 90 - 31 Oct 91

HIGH RESOLUTION GEOLOGICAL SITE CHARACTERIZATION
UTILIZING GROUND MOTION DATA, AFOSR-89-0176

G-AFOSR-89-0176

61102F

AUTHORS

B. Stump, C. Hayward, C. Pearson, M. Bogaards,
M. Craven and R. Reinke

2309

A2

REPORTING ORGANIZATION NAME(S) AND ADDRESS(ES)

Southern Methodist University
Department of Geological Sciences
Dallas, Texas 75275-0395

REPORT NUMBER

SMU G-10

SPONSORING/MONITORING AGENCY NAME(S) AND ADDRESS(ES)

AFOSR/NL
Building 410
Bolling AFB, DC 20332-6448
Dr. Dickinson

SPONSORING/MONITORING AGENCY REPORT NUMBER

Approved for public release;
distribution unlimited.

Work in the past reporting period has been focused in four areas all related to our task of shallow geological site characterization using seismic waves. The first area of emphasis is documented in, Comparison of Sources for Shallow Seismic Imaging: Radiation, Energy and Bandwidth by Hayward and Pearson. This paper contrasts a variety of shallow seismic sources for P and S waves. The second paper, Characterization of the Shallow Weathered Zone with Complete Seismograms is by Bogaards and Stump. This work documents the separation of stochastic and deterministic wave propagation effects in the shallow weathered zone. The status of a parallel investigation designed to use the surface wave arrivals in constraining near-surface Q's and velocities is discussed in the third contribution by Mike Craven. Finally, the comparison of site characterization information is made to waveform variability observed from high explosive testing in Experimental Studies of Stochastic Geologic Influences on Near-Source Ground Motions by Reinke and Stump.

SUBJECT TERMS

Seismology, P and S sources, stochastic and deterministic wave propagation, surface wave inversions

NUMBER OF PAGES

11 PAGES CODE

17 SECURITY CLASSIFICATION OF REPORT

unclassified

18 SECURITY CLASSIFICATION OF THIS PAGE

unclassified

19 SECURITY CLASSIFICATION OF ABSTRACT

unclassified

20 LIMITATION OF ABSTRACT

(UL)

Comparison of Sources for Shallow Seismic Imaging: Radiation, Energy and Bandwidth

Chris Hayward
Craig Pearson

Southern Methodist University
Geophysics Department
Dallas, Texas 75275

Accession For	
NTIS	✓
ERIC	
USGPO	
Justification	
By	
Date	
Accession No.	
Doc	Spec
A-1	

July 24, 1992

DTEC QUALITY INSPECTED 3

1 **Abstract**

2 An experiment to characterize the radiation pattern, energy flux and bandwidth
3 of three P and six S seismic sources was conducted in conjunction with source reflection
4 comparison experiments southwest of Houston, Texas in low velocity, unsaturated,
5 unconsolidated sands. Each source was positioned in the center of a 10 meter circle of
6 28 two-component (transverse and radial horizontal) 10 Hz wide band geophones and
7 recorded at 1000 samples/second onto 16-bit dataloggers. Source azimuthal radiation
8 patterns in general agree with theoretical calculations, however, significant geologic and
9 topographic path effects are evident. A thin low velocity surficial layer produces in high
10 amplitude surfaces waves and refracted arrivals further complicating the results. The low
11 Q materials limited the recorded bandwidth making it difficult to separate the body and
12 surface waves at the short 10 meter offset. Some of the shear sources exhibit complex
13 time signatures and poor repeatability due to either source precursors and reverberations
14 or significant alteration of source region during each shot. Further comparisons of the
15 sources reveal differences in total and component partitioned energy flux, spectrums, and
16 reflected energy. Further field experiments are warranted to separate the source
17 characteristics from the complexities imposed by the media.

18 **Introduction**

19 Choosing an appropriate source for shallow, high resolution seismic reflection
20 surveys has always been difficult, but is critical to the eventual success of a shallow P, S
21 or a combined P and S survey. Commonly users have considered cost, spectral
22 characteristics, convenience and efficiency, energy, repeatability and safety in their
23 analysis (Knapp and Steeples, 1986). A number of studies describe the performance,
24 spectral character, energy, application, and cost of common sources suitable for shallow
25 high resolution P wave reflection profiling (Miller et al. 1992, 1989, 1986). These
26 sources have been successfully applied to shallow engineering, groundwater, mining and
27 environmental problems (Steeple and Miller, 1990; Jongerious and Helbig, 1988; Pullan
28 and MacAulay, 1987; Birkelo et al., 1987; Hunter et al., 1984; Ruskey, 1981; Schepers,
29 1975).

30 Since 1986, the SEG Engineering and Groundwater Committee has conducted
31 source tests in various geologic settings (Miller et al., 1986; 1989) demonstrating P wave
32 sources that may have application to the shallow seismic domain. These tests are
33 designed to evaluate sources in a realistic geologic setting by comparing reflector
34 imaging properties (SNR and bandwidth) among the sources for a single shot record of a
35 traditional CDP 2 d layout. Typically, the geophones are arranged in a typical pattern for
36 acquiring shallow CDP data in an area, and then every source is fired several times into
37 the array, usually several times with various prefilters and gains. Because every real
38 survey works under specific constraints often different from the tests, the test results,
39 shot records, spectra, SNR plots and energy histograms, are normally presented without
40 recommendations as to which source is 'best'. This principle, to let the data speak for
41 itself, is also part of the ground rules established by the Committee prior to the tests.

1 From comparing the source tests made with the same sources and recording
2 parameters in various areas, it is apparent that the choice of a source depends strongly on
3 the nature of the surface layer. Sources such as surface guns which show strong promise
4 in areas with consolidated surface materials or a shallow water table, are not much better
5 than simple hammer sources in areas with loose sand on the surface. The spectral
6 content and relative energy received also depends strongly on the surface geology. Thus,
7 for P wave profiling, it is not expected that a single source will be the best choice in all
8 areas. The choice of an appropriate source will depend on the nature of the problem.

9 Since 1984 there has been a heightened interest in combined P and S wave
10 reflection profiling for shallow engineering and groundwater problems (Stumpel, H, et.
11 al. 1984; Hasbrouck, W. P., 1986,1988; Goforth and Hayward, 1992). Typical
12 applications for these surveys include profiling in areas where P surveys don't work, such
13 as areas with high Q_p , areas with strong water saturation contrasts; description of
14 sediment parameters such as gas or water saturation; detection of fissures and faults; and
15 mapping shallow aquicludes. However, the routine use of shear surveys in engineering
16 applications is more limited than that of P waves. Most of the published shear surveys
17 are pilot demonstrations of the method, rather than full scale investigations.

18 A number of different shear wave sources suitable for shallow investigations
19 have been proposed and used (Edelmann, 1985), but comparison among sources have not
20 been routinely done. Generally, each study chooses and uses a single source, generally
21 the most convenient, but occasionally the one invented for the particular project. There
22 has been no comprehensive tests of shear sources as there have for P sources. However,
23 since the results of the P source tests revealed that the surface conditions play a large roll
24 in the selection of an appropriate source, the same conclusion is expected for the S
25 sources. Unfortunately, to this point there have been no comprehensive tests of shallow
26 S sources in a wide variety of surface materials.

27 For most conventional P wave point sources, such as vertical forces like
28 hammers, weight drops, small vibrators and surface guns, and explosive forces such as
29 the buffalo gun, small caps, and dynamite, the radiation pattern for the energy is
30 considered cylindrically symmetric although extreme changes in the near source material
31 properties can modify this. This symmetry considerably simplifies the tests, since it's not
32 necessary to measure but one azimuth from the source. Since energy radiates equally in
33 all azimuths from all sources, it's not necessary to consider directivity when choosing a
34 source. Any source beam forming or pattern directivity must be made with multiple
35 source shooting, something that is usually prohibitively expensive in shallow acquisition.

36 For shear wave interpretation though, the problem of source directivity is
37 important. For example, the uninitiated would not expect to generate a great deal of
38 shear energy that could be detected with horizontal phones by using a vertical source.
39 However, for some ray paths, the horizontal shear energy is substantial (Kahler and
40 Meissner, 1983). For horizontal point force sources at the free surface, the radiation is
41 no longer cylindrically symmetric, although torsional point sources do show cylindrical
42 symmetry. Just as in the simpler P wave case, near source material property differences

1 can modify the directivity. Furthermore, many existing sources are not simple point
2 sources but have finite dimensions and may include more complex motions. An
3 understanding of the radiation pattern of seismic sources is necessary to their proper use
4 in shallow exploration. For example, shallow 3D and VSP shear surveys make use of
5 energy from more than one azimuth or inclination from the source.

6 The investigation of source radiation patterns from land seismic sources has
7 been pursued intermittently for some time (Hirona, 1948) but have usually considered
8 vertical (Miller and Pursey, 1954), torsional (Dorn, 1984) or horizontal (Cherry, 1962)
9 vibrators or explosive sources (Heelan, 1952) common in traditional reflection profiling
10 used for oil exploration. Field studies of various sources are also comparatively rare and
11 generally concentrate on those sources used in conventional exploration (Arnold, 1977;
12 Robertson and Corrigan, 1983).

13 Recently, in association with the 1991 annual SEG convention in Houston,
14 Texas, the Committee sponsored an extended set of tests similar to previous source tests,
15 but for the first time including both P and S sources and three component recordings.
16 Most of the previously tested P sources were included in the test plus a number of
17 different shear sources. Like the previous tests, this test involved repeated shots from
18 various sources into a typical CDP receiver spread which was recorded through various
19 prefilters on a typical 24 channel wireline recording system. P sources were recorded
20 into high frequency vertical phones, while S sources were recorded into horizontal
21 phones or in some cases three component phones.

22 Since 1989, we at SMU have been studying azimuthal radiation patterns from
23 a small surface shear source used for site characterization and shallow refraction or
24 reflection experiments. We fielded the source south of Houston as one of the invited
25 shear sources. In conjunction with the SEG test, we fielded an associated experiment at
26 the test site, but with a much different design to supplement the more conventional
27 source tests in characterizing selected small to intermediate energy level sources.

28 In contrast to the Committee experiment which tested over 20 different source
29 configurations, we selected only nine sources concentrating on shear sources and shot
30 each source with an single configuration (the Committee tests extended to testing sources
31 in many configurations, such as powder load, hammer weights, or charge weight). These
32 nine sources are an inclined fence post driver shear source referred to as the BEAR
33 (Goforth and Hayward, 1992), a torsional vane source called the arrow (Brown, 1966), a
34 plank shear source (Kobayashi, 1959), a strike plate shear source (Hasbrouck, 1983), a
35 rotational trip hammer striking a vertical blow; Miller and Pursey, 1956), a modified
36 Buffalo gun shear source (Pullan and MacAulay, 1987; Murphy, 1977), a horizontal
37 pneumatic hammer called the SWIG (Shear Wave Impluse Generator) (Liu, 1985), a fifty
38 caliber surface gun in a dry 1 m hole (Miller, et. al. 1992), and a small 1/12 pound
39 dynamite in a dry 1 m hole (Heelan, 1953). Each of these sources was hypothesized to
40 produce some shear energy although three sources (the dynamite, surface gun, and
41 vertical hammer) are traditionally used during P wave surveys.

1 **Geologic Setting**

2 The tests were conducted on the Caldwell Executive Golf Course, south of
3 Rosenberg, Texas (the largest and most modern golf course between Beasley and
4 Needville and approximately 45 miles southwest of Houston Texas, in Quaternary
5 Beaumont Formation of the Gulf Coastal Plain (Figure 1). The experiment was
6 performed in a rough near a service road, in low velocity, unsaturated, unconsolidated
7 sands. Other than native grass, there was no significant vegetation. Surface relief was a
8 maximum of 1/2 m. over the test bed. From conversations with Mr. Caldwell the land
9 owner, we established the depth to the water table was approximately 10 m, and that the
10 surficial materials were unconsolidated sand down to that point.

11 The conventional SEG source test was conducted along the shore of a small
12 clay lined pond to improve high frequency coupling. Our survey was conducted
13 approximately 150 m ESE of the SEG test.

14 **Reconnaissance Survey**

15 We performed a reconnaissance survey to estimate the optimum offset for the
16 radiation pattern test. In particular, we wished to avoid choosing an offset near or
17 beyond the first refraction critical distance where emergent arrivals would complicate the
18 analysis. Because the surficial material was highly attenuative, we preferred the near
19 offsets where there was the best chance of recording a broad band signal.

20 The initial survey was done with a 12 channel, 10 bit, fixed gain, engineering
21 seismograph and hammer. A transposed survey in one direction was done for both P and
22 SH sources. The P survey used a single 10 Hz Mark Product L410 for each group, with
23 3 m group spacing. Three blows of a 12 lb. hammer on a steel plate were stacked to
24 produce each record and the hammer moved by 0.5 m. The SH records were collected
25 using a single 40 Hz Mark Product L410 for each group and a 12 pound hammer on the
26 side of an L shaped plate as the source. Again three blows were stacked to produce each
27 record.

28 A clear break on the P section (Figure 2) at 16.5 m and 75 ms indicates the
29 arriving head wave from the water table. The section also shows a shallow reflector at
30 70 ms, although its close proximity to the Rayleigh wave noise cone makes it difficult to
31 identify on field records. No other reflector was visible. As is common in
32 unconsolidated materials, material velocity is less than air velocity, making air-wave
33 interference a problem when picking first break arrivals. We tried a number of low cut
34 filters to eliminate the strong ground roll, but were not able to materially improve the
35 section. The apparent event at 220 ms is probably an aliased noise wave or side swiped
36 ground wave since its dominant frequency is so low. Since the area was flat, a simple
37 refraction interpretation was assumed to derive a model for P wave velocity (Figure 3a).
38 A thin layer of very low velocity material (probably the loose dry soil zone) overlies an
39 8.8 m low velocity material which in turn overlies the water table. This agrees with the
40 approximate depth to the water table given by the owner. Since P velocities are below

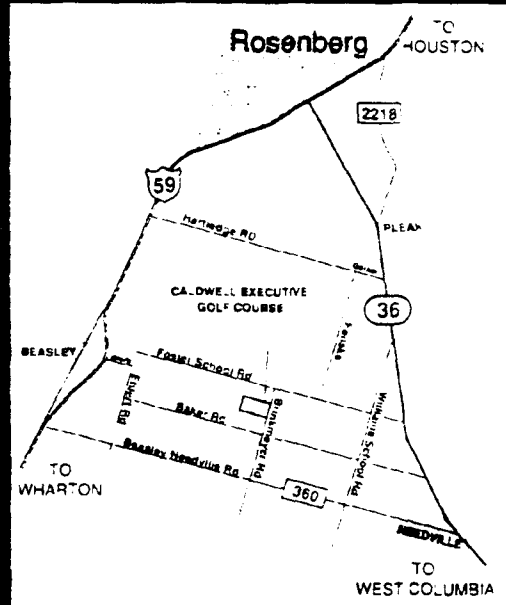


Figure 1. Location map of the test site south of Rosenberg, Texas on the Caldwell Executive Golf Course (the most modern golf course between Needville and Beasley.)

1 the free air velocity, first arrivals are complicated by the air wave. It was disappointing
2 to note that we could resolve no reflectors on the P section in this area. The SEG
3 committee experiment was able to resolve them by moving receivers adjacent to the pond
4 where near receiver coupling was improved.

5 The shear section (Figure 2b) has no obvious refraction cross over. Since the
6 source produced some P energy and a strong air wave, initial arrivals at the far offsets
7 may be obscured. The strong high frequency ring at the farther offsets is probably
8 parasitic P or air wave on the horizontal geophones. A minor break was interpreted at 35
9 m offset, but this gives a velocity of 200 m/s, nearly that of the P layer (Figure 3b). If
10 this truly is a SH refraction break, then the velocity model must clearly be wrong. An
11 obvious reflection at 195 ms has no equivalent on the P section. Furthermore, while the
12 only P reflection is contaminated by ground roll at moderate offsets, the shear section is
13 not obscured by the noise cone even at significant offsets. We believe this is another
14 case where S profiling may work better than P (Goforth and Hayward, 1992).

15 Acquisition

16 The source characterization array was composed of 28 stations evenly
17 distributed on the circumference of a circle of 10 m. radius (Figure 4) to give an
18 interstation spacing of 2.25 m (12.6 degrees interval angle). Each station consisted of
19 two horizontal (one radial and one transverse) Mark Products L-410, 10 Hz geophones
20 damped to 0.6 of critical on 15 cm spikes. A single vertical Mark Products L-410, 10
21 Hz. geophone damped to 0.6 critical on a 7 cm spike was added at station 8 to provide a
22 measure of the vertical energy. The 10 m. offset was within the direct P wave first
23 arrival window, and avoided including shrubbery, small trees, and significant topography
24 within the array. While a 10 m range is not adequate for good separation of body and
25 surface waves, it provides a better measure of the horizontally propogating source energy
26 while minimizing noise and surface statics effects.

27 Each source was carefully positioned at the center of the array with all shear
28 sources activated in the direction of station 8. Sources which created significant surface
29 damage, i.e. dynamite and surface guns, were offset slightly from the center so that the
30 near source area for each firing would be in undisturbed ground. Destructive sources
31 were done last to avoid source region damage during tests of less destructive sources.
32 All sources were positioned within 1/2 m of the array center.

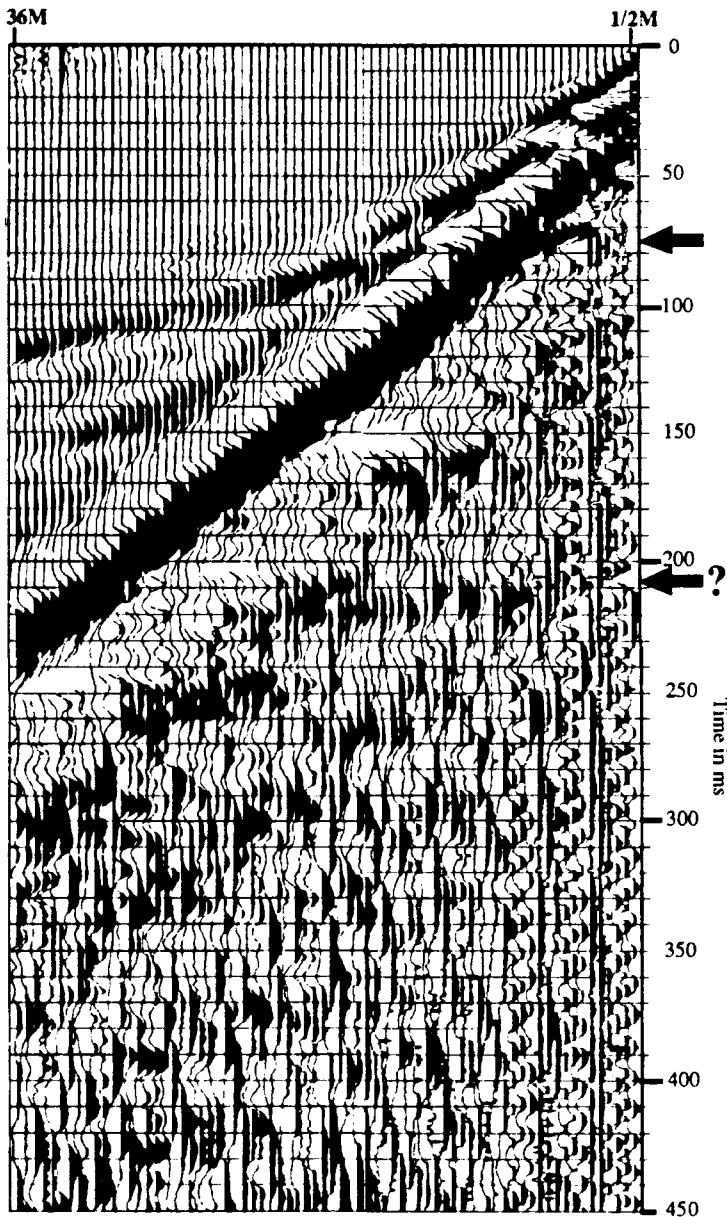
33 All non destructive sources were fired several times to firmly seat and couple
34 the source to the ground. Several activations of each non destructive source were
35 recorded so that coherence calculations could be made for source repeatability. Each
36 shear source was fired in both polarities, again for repeatability studies. Two of the light
37 weight shear sources were activated in several orientations to allow separation of source
38 radiation pattern differences from local receiver and path effects. Time constraints in the
39 field prevented us from conducting the same set of comprehensive tests on every source.

40 Ten, 6-channel, 16-bit fixed gain recorders (Reftek 72 A DAS units)
41 telemetered 1 second, 1 ms. sample interval, records to a RefTek 44D array controller via

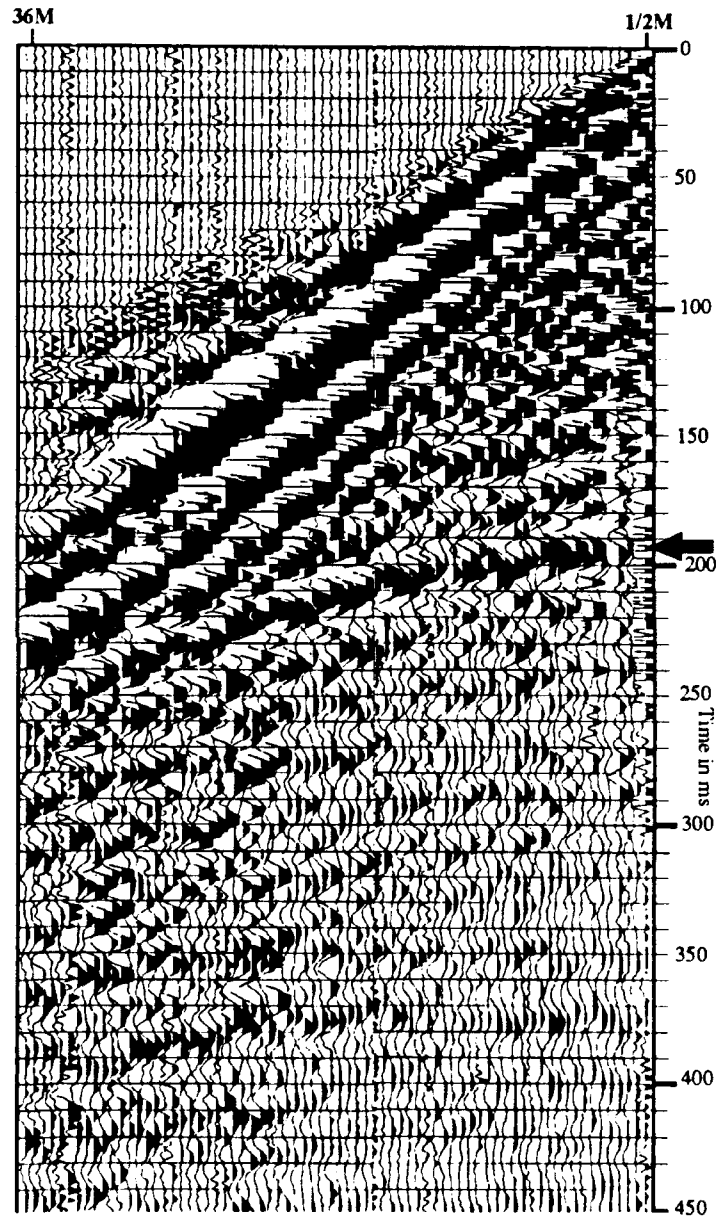
Caldwell Executive Golf Course Refraction/Reflection Survey

Compressional Section (Hammer Source)

Shear Section (Hammer Source)



(a)



(b)

Figure 2. Reconnaissance Survey. The near offset and group interval are both 0.5 m. The far offset is 36 m. The compressional section (2a) shows an obvious reflection at 75 ms, but noise wave interference makes it difficult to detect in the field at trace spacings beyond about 1.5 m. The shear section (2b) shows a clear reflection at approximately 180 ms, but the refraction breaks are obscured by the P direct arrival and air wave.

GEOLOGIC MODEL

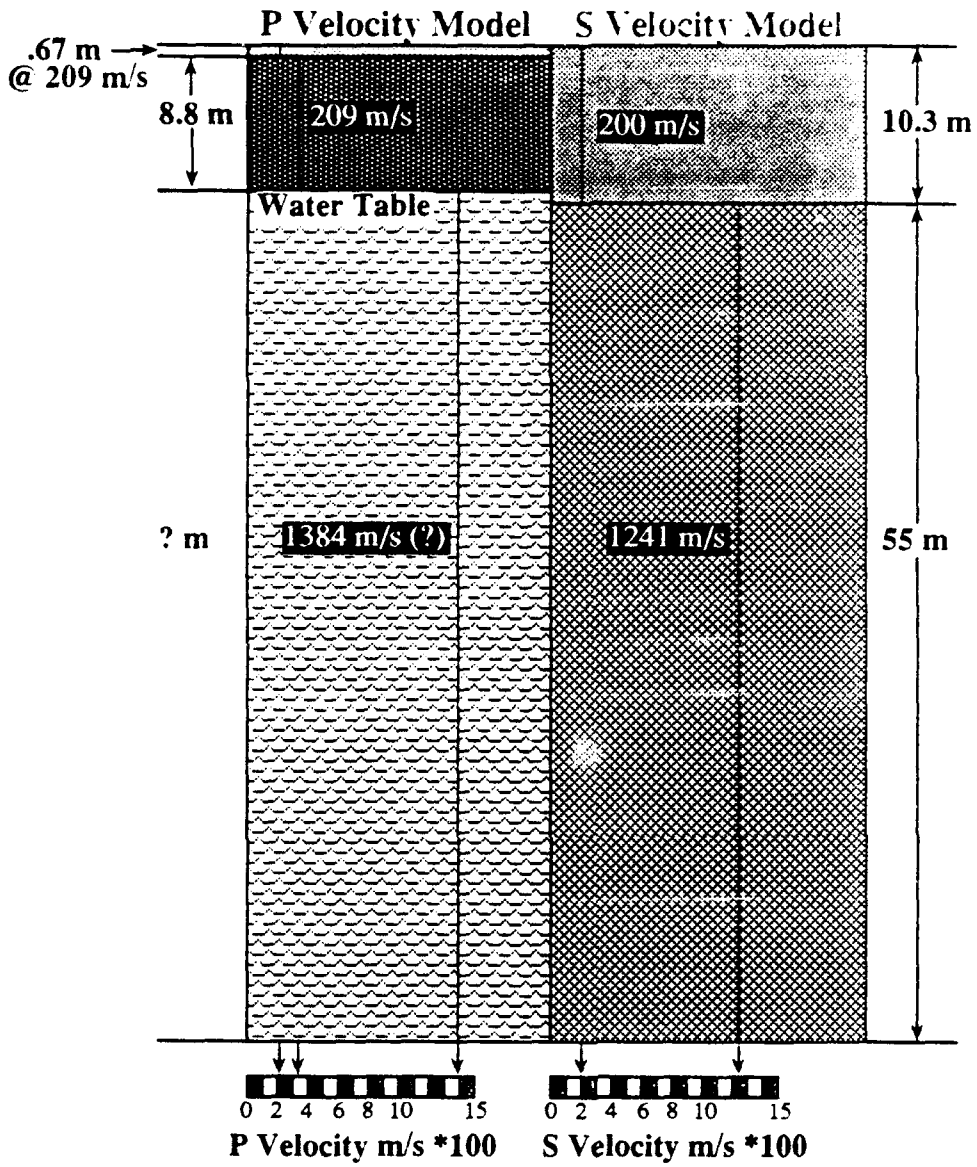


Figure 3.

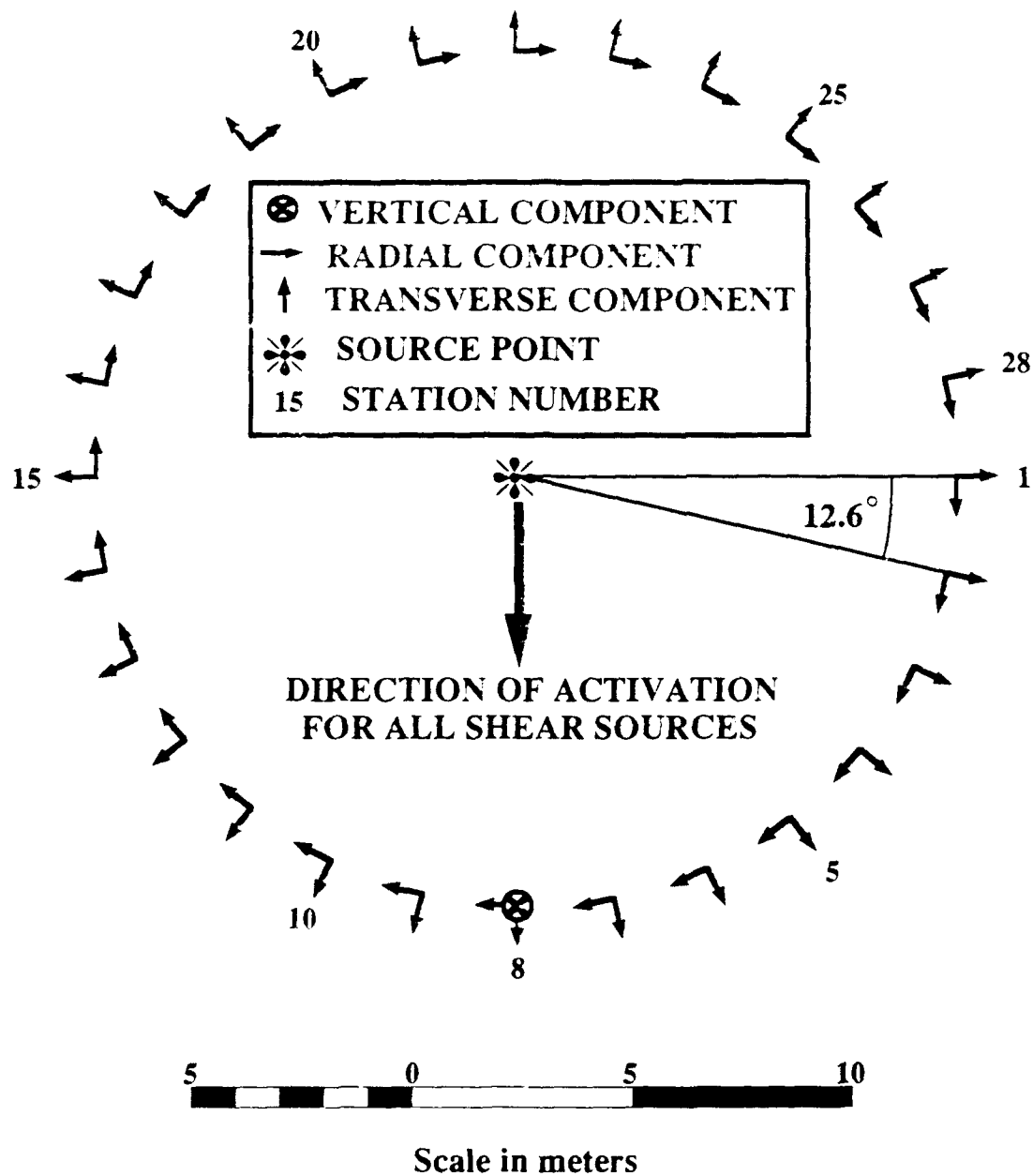


Figure 4. Plan view of Array Layout. The 28 two horizontal component stations are laid out in a ten mile radius. The station numbers are shown on the perimeter of the array. All sources were located within 1/2 m of the center of the array. Receiver orientations were checked at the start and finish of the experiment to confirm they were within a few degrees of

1 wireline. The data were previewed in the field, stored on hard disk, and later archived on
2 8 mm tape. The amplifier front end have a self noise of XXX nV rms and the equipment
3 has an instantaneous dynamic range of 96 dB. Selectable preamplifier gains were
4 carefully adjusted for each source to avoid clipping throughout the record while retaining
5 maximum dynamic range.

6 The time break was derived from a 10 Hz vertical or horizontal geophone
7 planted within 10 cm of the source and processed through an Input/Output XXXX XXXX
8 time break generator. To measure any source precursors, the data acquisition system was
9 programmed to record 100 ms prior to the time break and 900 ms after the time break.
10 With the exception of analog anti alias filters, no prefiltering was applied during
11 acquisition.

12 **Results**

13 We deployed 9 different sources within the source characterization array,
14 including both P and S type sources. Because we wished to confine all sources to a 1/2
15 m. area at the center of the array and wished to minimize ground damage in the area, we
16 were limited in the number of destructive tests that could be accommodated at the array
17 center. For this reason, we used only one configuration (generally the nominal or easiest
18 to field) and energy level for each major source type, .

19 For each source, the total horizontal power of the source is determined by
20 calculating the RMS power of all recorded horizontal channels. All calculations for each
21 source were then normalized to this power. Surprisingly, even though the individual
22 source power varied by more than on hundred (Figure 5), and P and S source types are
23 included, the power is distributed so that each source is about twice the power of the
24 previous one. This result was entirely unplanned, but suggests that besides the various
25 mechanisms tested, each source type also has a natural design energy niche.

26 For all the sources, the proportion of radial to total horizontal power is nearly
27 constant. Sources which are designed to produce P energy produce relatively small
28 amounts of transverse energy. While it's difficult to make strong generalizations with
29 only 4 points, the proportion of radial to transverse power of the P sources seem to
30 increase slightly with increasing power. P sources radiate only one tenth of their energy
31 as transverse energy. All shear sources produce equal amounts of both radial and
32 transverse energy, which agrees with theoretical arguments. We elected to concentrate
33 on S sources since these should have the most interesting radiation pattern and this is of
34 particular importance to reflection profiling. Therefore we ignored the various low
35 energy P sources common in other experiments.

36 Sources included common manual hammer sources, a pneumatic, a hydraulic,
37 and two explosive sources (Figure 6a,8a and 10a). Each source presented unique
38 deployment requirements. Generally, the high energy sources required more effort than
39 the low. Deployment times in this test ranged from a few minutes to over one half hour.
40 However because these times included a lot of initial setup time, it is likely that they are

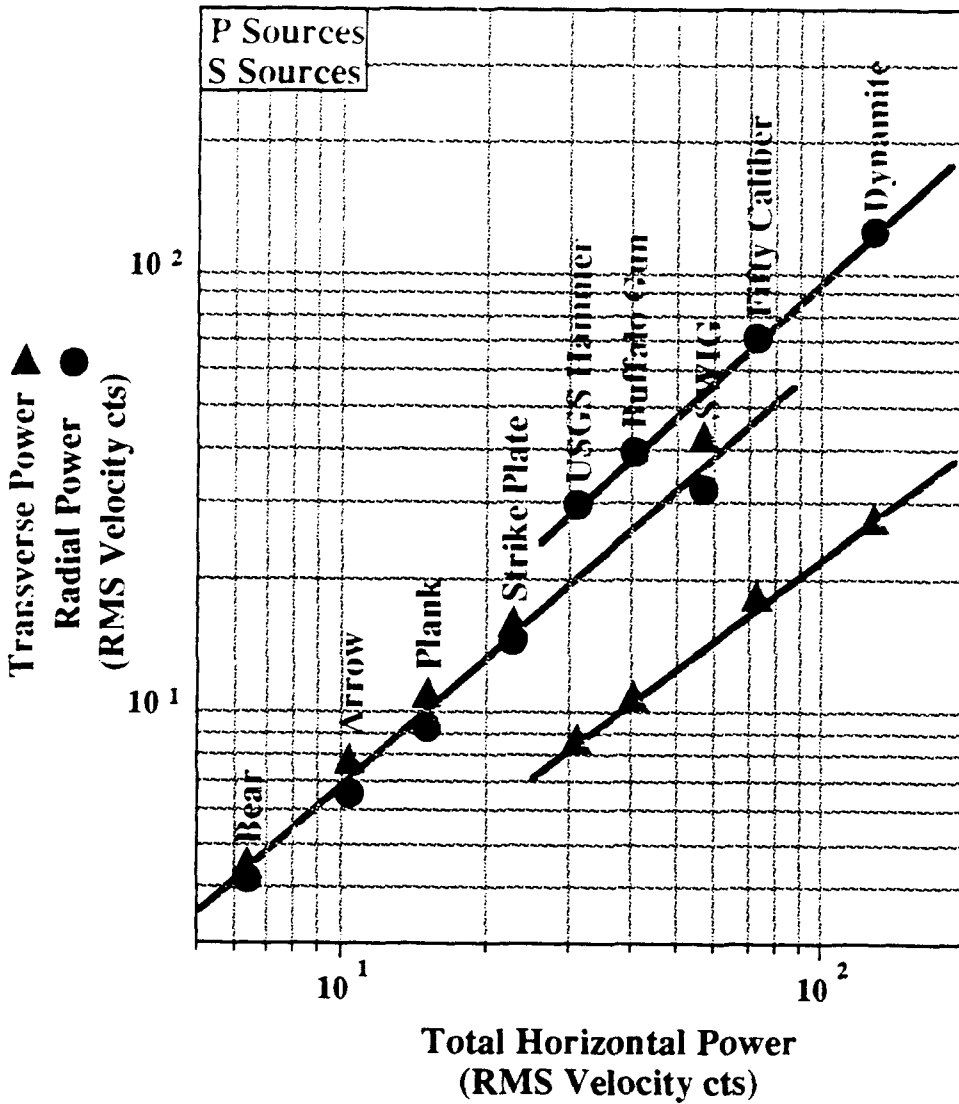


Figure 5. Total Relative Horizontal Received Power. The observed received power spans two orders of magnitude at amazingly equal increments. For all the sources of one type (P or S) the proportion of radial to transverse power is nearly constant. Shear sources have slightly more power in the transverse than in the radial, while for P sources, the transverse power is only 1/10 of the radial.

1 not representative of production work. Costs for each of the complete field sources range
2 from under \$50 to over \$50,000.

3 **Source Characterization**

4 Eight separate characteristics of each of the sources are presented for
5 comparison in Tables 1 through 6 and Figures 6 through 11. The sources for each table
6 and accompanying figure are arranged in columns 1-3, from least to most energetic
7 irrespective of source type. Each of Figures 6-11 is accompanied by an adjacent table
8 (Tables 1-6). Figure 6, 8, and 10 present a picture of the source, the accompanying time
9 domain records, azimuthal radiation pattern and the reflection section. Row 1 shows a
10 photograph of the source in a typical field operation or deployment mode. Row 2, the
11 time series, shows the radial velocity traces in cyan and the transverse velocity in red. A
12 single scale factor is used for each source. The small numbers around the outside are the
13 station numbers as shown in Figure 4. The dotted timing line marks 100 ms, while a
14 dashed line marks 75 ms. Instrument response has been deconvolved from all data. Row
15 3, the radiation pattern, shows the relative RMS power in each trace (radial in cyan,
16 transverse in red, overlap in magenta, and total power in blue) displayed as the radius in
17 polar coordinates. Each source is normalized to the maximum power observed for the
18 source. Dotted grid lines indicate 6 dB increments. The final row on Figures 6,8, and 10
19 are the time series AGC scaled to show late reflection energy. For tractional shear
20 sources, the traces are symmetrically rotated to show Sh (cyan) and Sv (red) components
21 as labeled above the section. Otherwise, they show radial (color) and transverse (color)
22 components.

23 Figures 7,9, and 11 present the particle motion and spectral information for
24 each source. Row 1 is a particle motion plot. The outermost ring shows particle motion
25 from the time series plots (first 200 ms) with a small + plotted at 75 ms. Colors change
26 every 50 ms. Inner rings show successive 100 ms windows on the AGC reflection
27 section. Row 2, the mean spectra display's the average spectra for all traces. Power
28 spectra for each azimuth and mean spectra \pm one standard deviation are displayed. The
29 mean radial spectrum is plotted in red and the mean transverse spectrum is plotted in
30 cyan. Rows 3 and 4 are the contoured transverse and radial spectra respectively. For
31 each trace, power spectra are calculated using a 1024 point Hamming window applied to
32 the original 1000 point detrended and padded time series. These are then contoured as a
33 function of azimuth and frequency (labeled in cyan on the lower vertical radius) from DC
34 at the outside to 150 Hz at the center. The power scale is shown to the right.

35 Each source presented unique deployment requirements. Generally, the high
36 energy sources required more operational effort than the low. Deployment times in this
37 test ranged from a few minutes to over 1/2 hour. However, since these times include
38 some mobilization time, they only generally reflect the actual shot time during normal
39 production. Costs range from under \$50 to over \$10,000.

40 **General Results**

41 In all the time series displays (Figures 6,8,10, row 2) traces around stations 1
42 and 10 are anomalous. Geophone coupling and near receiver geology, or propagation

1 path affected traces near stations 1 and 10. Of particular interest are the high amplitude
2 transverse signals on some of the P wave sources. The dominance of either of the cyan
3 or red (transverse and radial) on these displays makes it obvious which sources are P and
4 which are S. The P sources are dominated by radial energy and therefore have an overall
5 blue cast to them while the tractional S sources have both cyan and blue alternating in
6 opposite quadrants. The exception is the torsional arrow source with equal radial and
7 transverse energy in all quadrants.

8 Radiation patterns (Figures 6,8,10, row 3) also clearly indicate P, shear and
9 torsional sources. Distortions of as much as 6 dB may be due to receiver coupling and
10 near receiver geology or path effects. Like the time series in row 2, the radiation patterns
11 strikingly demonstrate the differences in P and S sources. Again, except for the arrow,
12 the shear sources show classic Sh and Sv cosine dipolar radiation patterns, while the P
13 sources show a classic isotropic radially dominated radiation pattern.

14 No compressional reflection could be recognized in either the reconnaissance
15 survey (Figure XX) or on any of the P source tests (Figures 6,8,10, row 4). But the shear
16 reflection at 300 ms (clearest on the SWIG, Figure 10, row 4) does give an indication of
17 suitability of a source for shear reflection work. Note that the reflector becomes
18 progressively more difficult to follow when examining the SWIG, strike plate, plank,
19 arrow and bear. This is an indication of the total energy available from the source. In
20 field operation, stacking the shots would likely improve the low energy source sections
21 considerably.

22 Overall particle motion (Figures 7,9,11, row 1) is as expected for each source
23 type; however, details and later arrivals are complex. Also some receivers show distinct
24 receiver related anomalies.

25 The mean spectra (Figures 7,9,11, row 2) indicate that there is little spectral
26 difference among individual stations. Low energy sources show well defined high
27 frequency energy, whereas the higher energy sources are dominated by lower
28 frequencies. While the high energy sources are less efficient at high frequencies, they
29 still produce more high frequency energy in an absolute sense. However, making use of
30 the available high frequency energy will likely require substantial field prefiltering.
31 Compressional sources have radial energy levels ten times greater than transverse, while
32 shear sources are generally evenly balanced. Overall peak power varies by a thousand
33 times. Bandwidth and bandshape for the sources differ significantly possible reflecting
34 the dominant surface wave component out to 30 Hz.

35 Transverse spectra (Figures 7,9,11, row 3) show little overall variation in
36 shape vs. azimuth although average power does vary. Shear sources show clear nodes up
37 to 60 Hz. Above 60 Hz the pattern becomes chaotic as a result of noise or scattering
38 from local geologic inhomogeneties.

39 Radial spectra (Figures 7,9,11, row 4) show that P sources change little in
40 spectra as a function of azimuth. Small nodes are visible at low frequencies for shear
41 sources.

1 Shear sources separate well in azimuthal as well as power variations within
2 these transverse plots and P sources show significant scattered components relating
3 closely to the anomalous complex areas of propagation shown in the time series and
4 particle motion diagrams. The radial spectra for tractional Sh sources show radiation of
5 P-Sv energy parallel to the source activation direction, while the P sources show a
6 circularly symmetric energy radiation.

7 **Specific Results**

8 As is evident from Figure 5, and the organization of Figures 6 through 11,
9 there are two overall first order differences among the sources. First except for the
10 arrow, there are only two different source radiation patterns, one for the P sources, and
11 one for the S sources. Second, the major difference between the various sources of one
12 type is the total source energy. Figure 12 shows the relative power at station 8, the only
13 three component station, as measured on each of the components. Since station 8 is at
14 the Sh radiation node, the transverse power should be a minimum for dipolar shear
15 sources. For each of the sources except the arrow, the vertical power falls somewhere
16 between radial and transverse power. For the arrow, vertical power is the least energetic
17 component of the source itself. The vertical power falls between the radial and
18 transverse except for the SWIG and the arrow.

19 Because most of the previous analysis examines the dominant energy in the
20 direct and surface waves, we windowed a small section around the shear reflector at 350-
21 400 ms (Figure 13). Low energy shear and high energy P sources generate
22 approximately equal Sh and Sv reflected power. The strike plate and SWIG source
23 generate nearly twice the Sh power as Sv power, while the buffalo gun has
24 approximately twice the Sv as Sh. While the USGS hammer appears to produce equal
25 Sh and Sv, this is not considered reflection energy, but part of a complex source function.

26 **Conclusions**

- 27 1. A wide range of low to intermediate energy P and S sources are suitable for shallow
28 seismic work.
- 29 2. High energy sources generally take longer to deploy.
- 30 3. All P sources and the arrow torsional source appear isotropic. Tractional S sources
31 are bipolar, producing Sh radiation patterns perpendicular to and P/Sv radiation
32 patterns parallel to the source activation direction.
- 33 4. Source signatures vary significantly from source to source.
- 34 5. Radiation patterns are consistent in amplitude and phase with theory.
- 35 6. Spectral shape appears constant with azimuth, but varies from source to source.
36 Generally, the higher power sources have peak power at lower frequencies.
- 37 7. Although the acquisition layout was adequate for first order characterization,
38 significant receiver variability complicates additional analysis.
- 39 8. The received power is dominated by the surface wave. A 10 m offset does not
40 produce sufficient first arrival to surface wave separation for more detailed analysis.

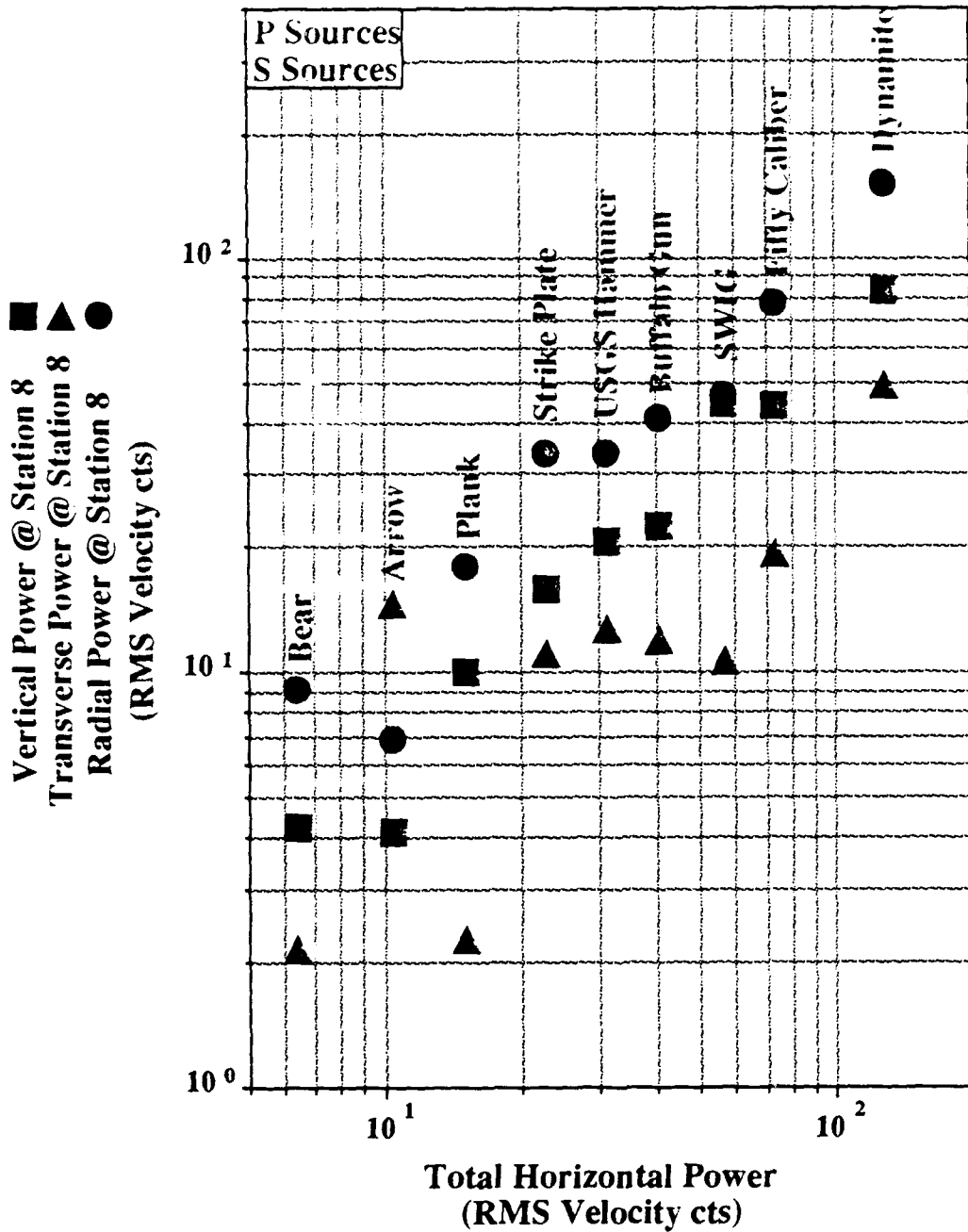


Figure 12. The received power for each component at station 8 is plotted vs. the total power for each source. Shear sources are labeled in red and P sources in blue. Total relative received power spans 2 orders of magnitude at almost equal increments throughout the total power scale.

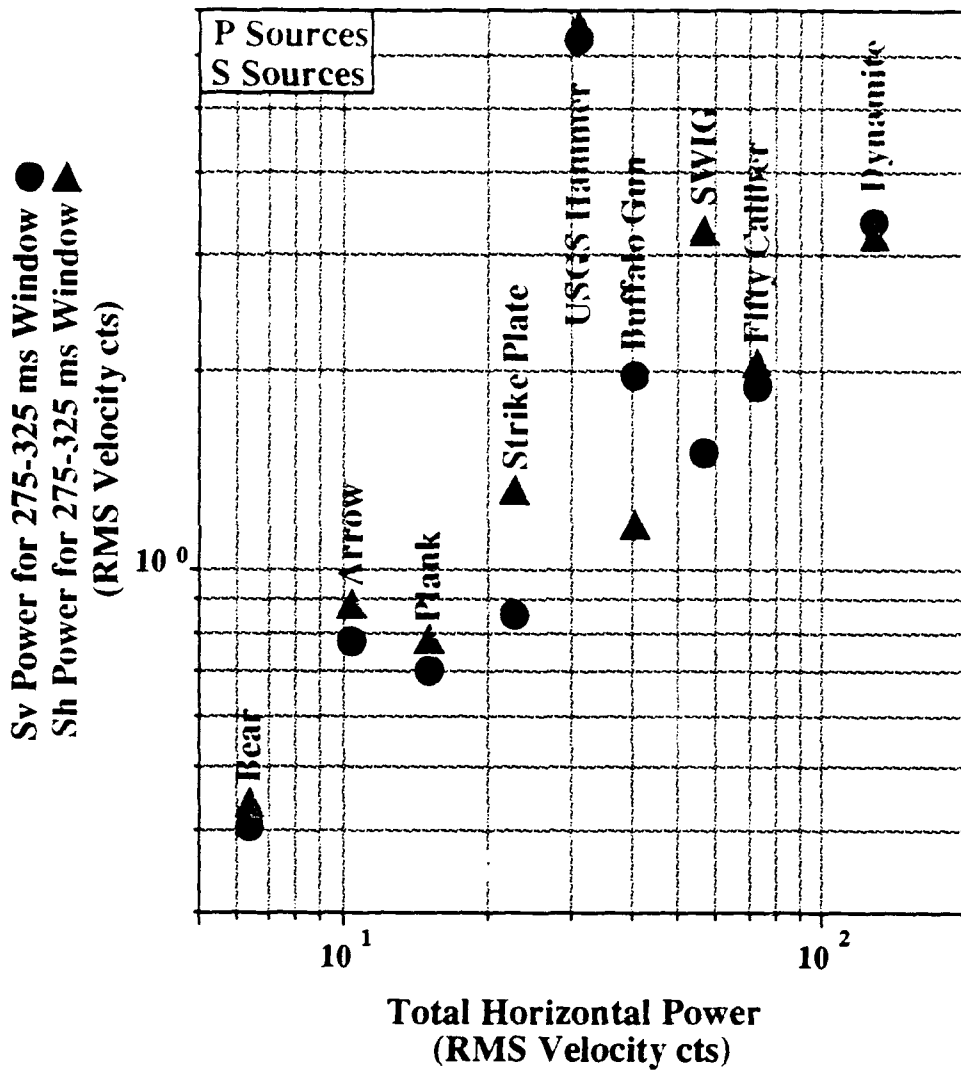


Figure 13. Reflected power for each of the sources. Shear sources are labeled in red and P sources in blue. In general, the larger difference in Sv and Sh power correlates with a more visible shear reflection. The large offset for the USGS Hammer is an indication that the energy is part of a complex source function rather than reflected energy.

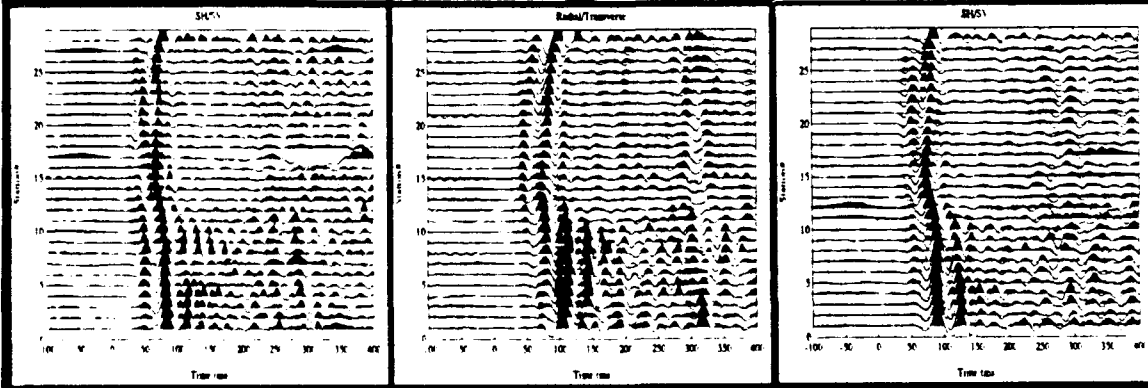
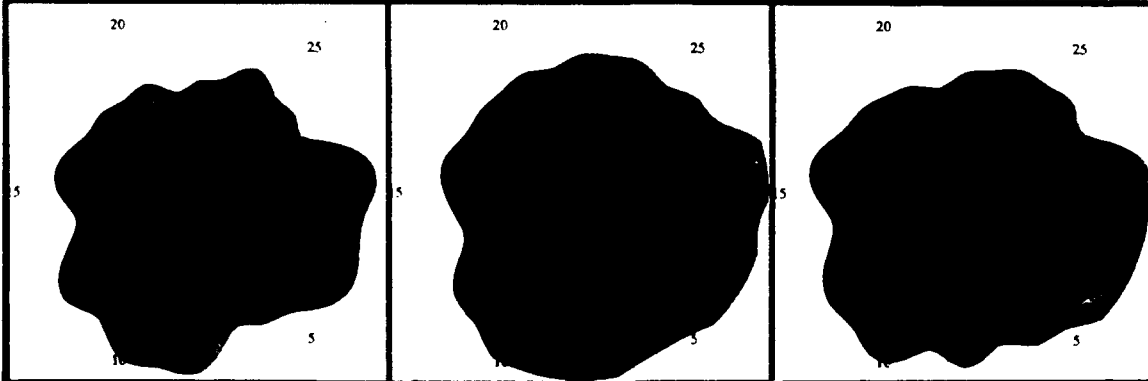
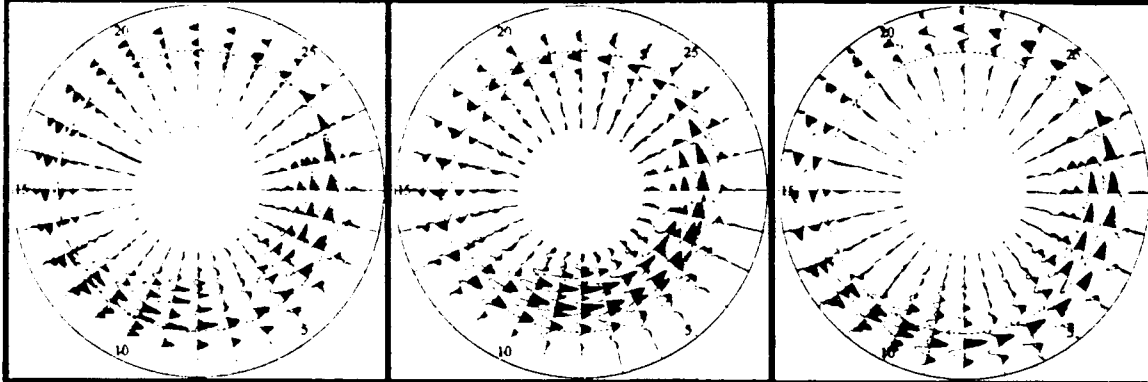
- 1 9. The high frequency portion of the spectra is attenuated by the low Q materials. At
2 other test beds, some sources may efficiently radiate useful high frequency
3 components.

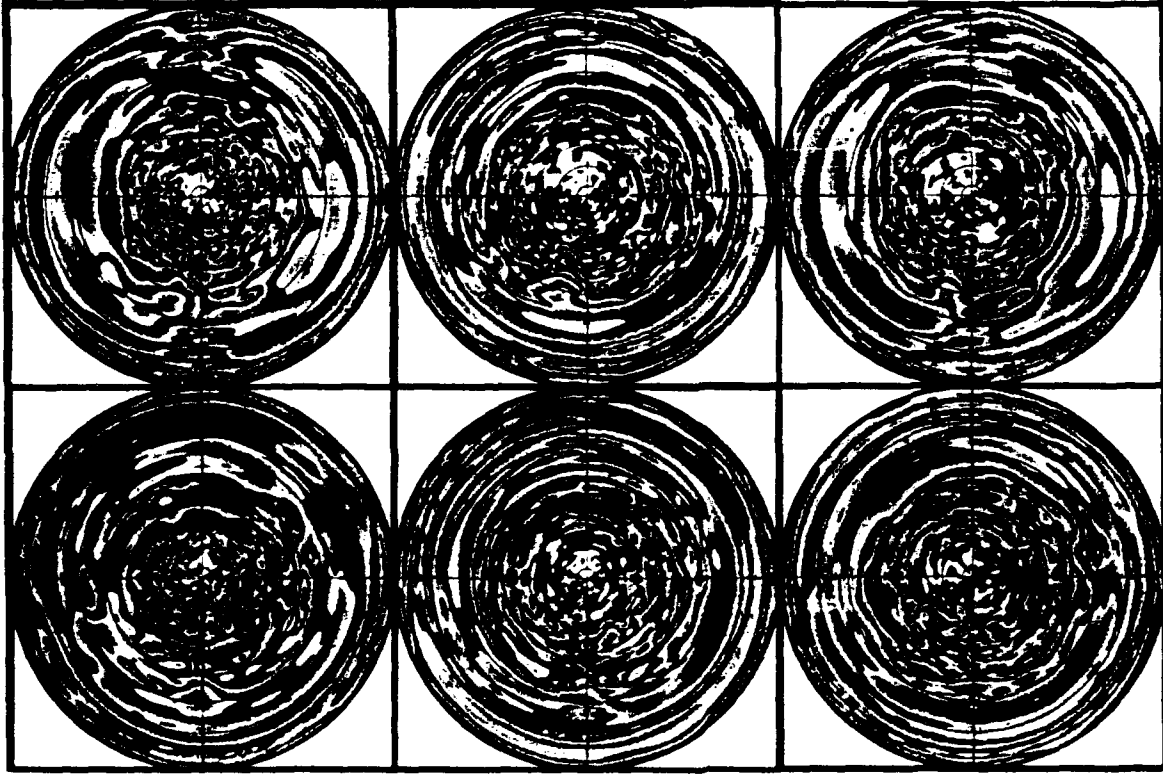
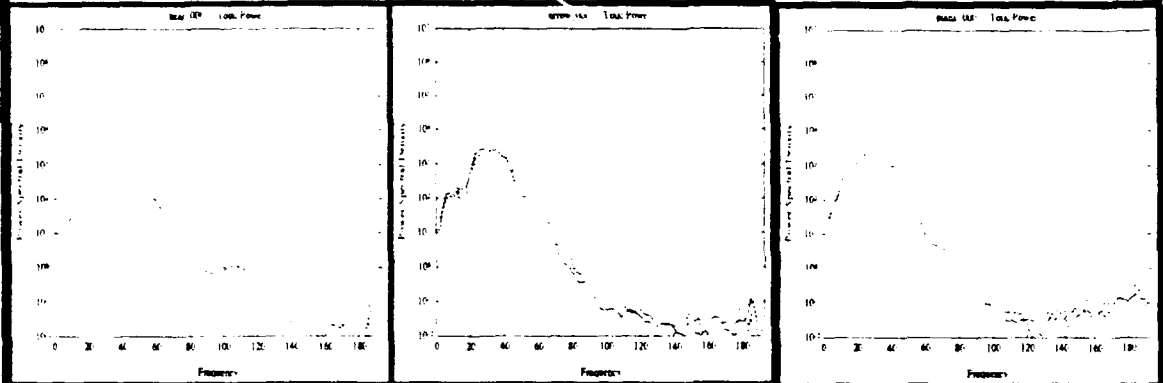
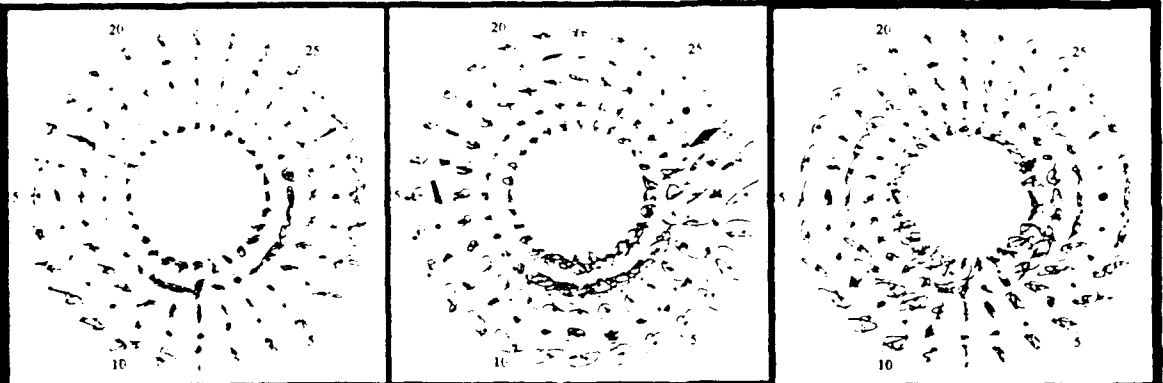
4 **Further Work**

- 5 1. Increase 3D spatial sampling density and range with 3 component receiver stations to
6 more fully characterize the entire source wave field.
- 7 2. Choose a high Q test bed to record an increased source bandwidth. A test bed
8 approximating a thick layer over a half space for both shear and compressional
9 velocity will allow better measurements of reflected power and horizontally
10 propagating power. Sites with a deep water table, thin beds, or strong variations in
11 material properties should be avoided.
- 12 3. Acquire multiple shots of each source for source repeatability, time break
13 repeatability, and stacking limit tests.
- 14 4. Rotate sources expected to show dipolar radiation patterns through a reasonable
15 number of azimuths to measure azimuthal independence of source excitation
16 direction.
- 17 5. Perform detailed reconnaissance surveys prior to source tests to characterize the test
18 bed and provide guidelines for receiver array design.
- 19 6. Include compressional (P, Sv), tractional (P, Sh, Sv), and torsional (Sh) sources to
20 provide a wide range of source types and power levels.
- 21 7. Compute synthetic seismograms using equivalent source models and a velocity model
22 determined from reconnaissance surveys. Compare the synthetics to observed wave
23 forms to verify the adequacy of the calculated source model.
- 24 8. Document each source's deployment and operational characteristics including
25 triggering requirements, functional source controls available, and costs relating to
26 fabrication, maintenance, and operation.
- 27 9. Conduct high g measurements on the source and in the near source nonlinear regime
28 to determine the total source power, source coupling characteristics in surficial
29 materials, efficiency of wavefield generation, and the areal extent of nonlinear
30 material response as driven by the source.
- 31 10. Conduct measurements in various surficial materials with various Poisson's ratios.
32 Also the tests should include both vertical and horizontal phones.

Table 1 Descriptions of Figure 6.

	Bear	Arrow	Caged Plank
Sources	A steel breaker bar is driven into the ground with a common fence post driver. When used as a shear source, the bar is driven in at an angle to impart a tractional force into the ground.	A torsional source consisting of an arrow shaped vane driven into the ground. A sledge hammer impacts an attached lever arm at the surface to induce a net torque on the arrow vane.	A traditional hammer and plank tractional source modified to include steel reinforced end plates. The plank is coupled to the ground by vehicle weight and small teeth on each end plate.
Time Series	While the bear exhibited the least power of any source tested, adequate signal to noise ratio from a single activation is achieved. Anomalous high amplitude time series are evident centered about stations 2 and 10. Radial motion is enhanced in the source activation direction.	The arrow produces unique time series which are not dominated by radial or transverse motion. Anomalous amplitudes are evident between stations 27 and 12 clockwise.	The caged plank produces time series exhibiting the bipolar character of tractional sources. Transverse amplitudes dominate in directions perpendicular to the source activation while radial amplitudes dominate parallel to the source direction. Anomalous amplitudes are evident in the right and lower quadrant.
Radiation	The bear produces transverse radiation with degradation in the nodal areas and significant variance from theoretical in azimuth. The radial radiation is enhanced in the activation direction and does not display well developed nodal structure.	The arrow produces transverse radiation approaching isotropic as expected for a point torque source. Degradation is evident in the development of small nodes perpendicular to the activation direction (parallel to the vane). Radial radiation is approximately elliptical with major axis corresponding to the nodal development in transverse radiation.	The caged plank produces bipolar transverse radiation with a well developed node in the direction of activation and degradation of the node on the side of the source being struck. Radial radiation is enhanced in the direction of activation and anomalous radiation sub parallel to the radial nodal plane is evident.
Reflections	As a result of low power output, the bear does not generate a coherent shear reflector (cyan) at ~ 300 ms from a single shot. Signal stacking would be necessary to improve the signal to noise ratio for reflected power. Components are rotated into SV/SH components	A coherent shear reflection signal (cyan) is not evident from the single shot of the arrow source. Signal stacking would be necessary to improve the signal to noise ratio for reflected power. Components are displayed as radial and transverse due to the isotropic nature of the source.	The output power of the caged plank is not adequate to produce a coherent shear (cyan) reflector from one shot. Signal stacking would be necessary to improve the signal to noise ratio. Components are rotated into Sh and Sv components.





10-22
 10-25
 10-30
 10-35
 10-40
 10-45
 10-50
 10-55
 10-60

Table 2 Descriptions of Figure 7.

	Bear	Arrow	Caged Plank
P a r t i c l e M o t i o n	The bear particle motion exhibits well polarized radial component but weakly polarized transverse components. Later time intervals exhibits anomalous amplitudes in right and lower quadrants.	The arrow shows significant azimuthal variation in particle motion ranging from high amplitude elliptical motion in the SE half of the array to lower amplitude polarized motion in the NW half of the array.	The caged plank exhibits highly polarized components at the radiation field maxima with linearly polarized radial at station 8 (P) and linearly polarized transverse at station 15 (Sh). Complex at intermediate angles.
M e a n S p e c t r a	The mean spectra of the bear source are dominately radial from 10 to 60 Hz. Transverse power is greatest below 10 Hz and above 60 Hz to the system noise level at 130 Hz	The arrow source exhibits ~ equal transverse and radial power at all frequencies out to 100 Hz. The radial component has greater variance throughout the frequency band.	The caged plank spectra are dominantly radial from 20 to 70 Hz and dominantly transverse elsewhere out to 100 Hz. Variance of both radial and transverse is low.
T r a n s v e r s e S p e c t r a	The bear produces azimuthal transverse spectra with obvious nodal development through frequencies from 10 to 80 Hz. Anomalous patches of power between 25 and 60 Hz in the east and south quadrants are observed as for all shear sources.	The arrow exhibits complex power distribution in the radial spectra with dominant power in the east and south. Most power is limited to frequencies from 20 to 50 Hz.	The caged plank exhibits good development of the north-south nodal plane. Power is concentrated to the east and south at frequencies from 10 to 80 Hz.
R a d i a l S p e c t r a	The bear radial spectra show weak development of the expected radial radiation patten in frequencies with no apparent nodal plane. Maximum power is contained between 30 and 50 Hz in the direction of source activation.	Transverse spectra of the arrow are isotropic from 15 to 55 Hz at lower power levels with anomalous power in the east through south quadrants between 25 and 50 Hz.	The caged plank exhibits little development of radial nodal structure throughout the frequency band 15 to 50 Hz.

**S
u
m
m
a
r
y**

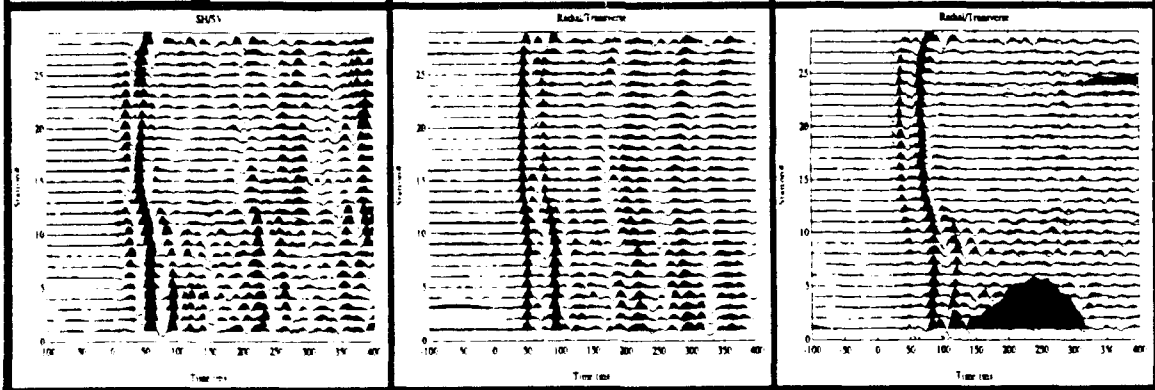
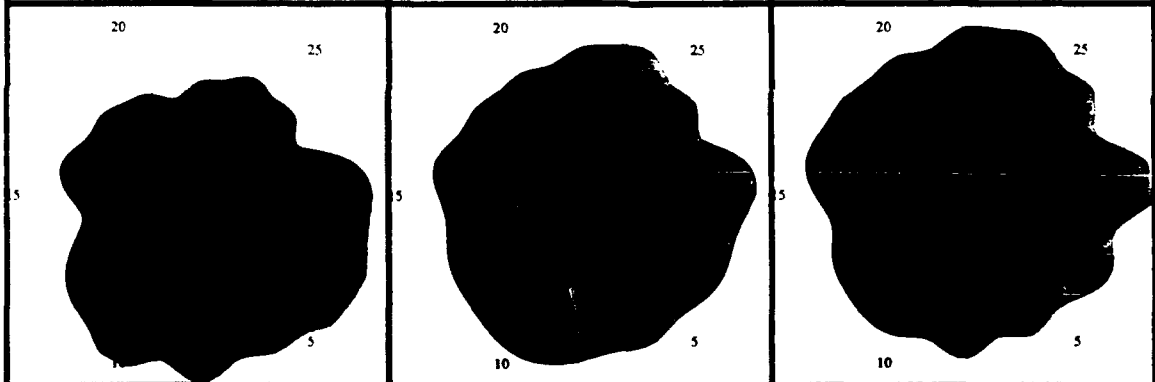
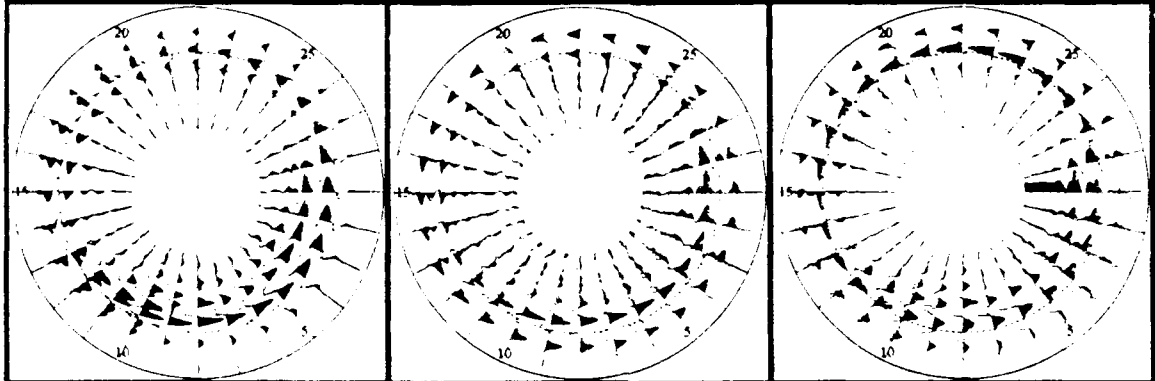
The bear is a cheap, low energy shear source with a surprisingly wide bandwidth. Some blows may ring, but stacking and careful selection can produce a usable section. The single blow does not image the reflector well.

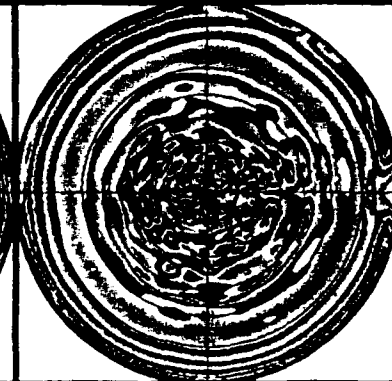
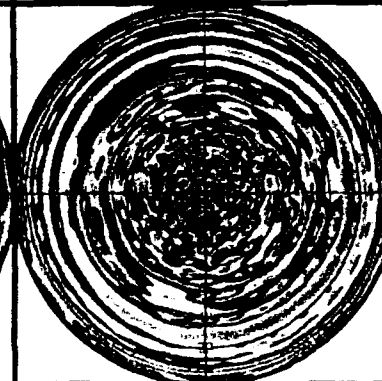
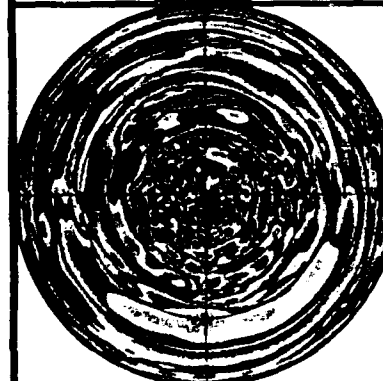
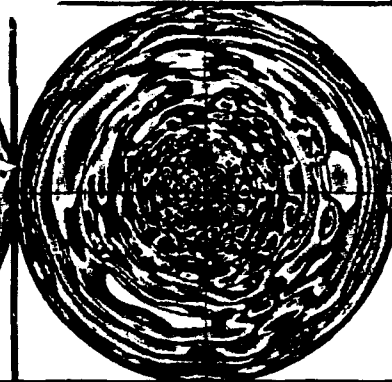
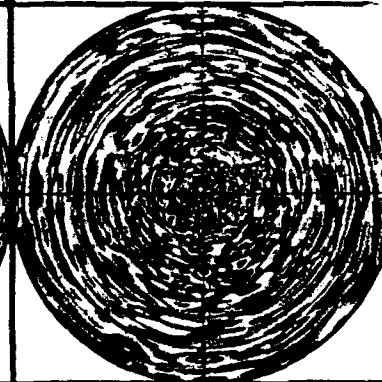
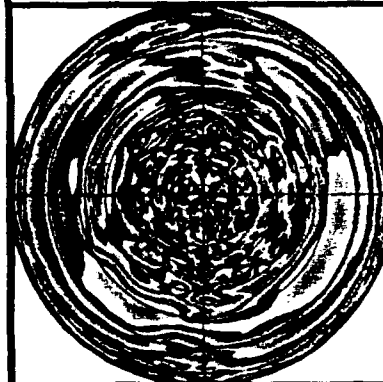
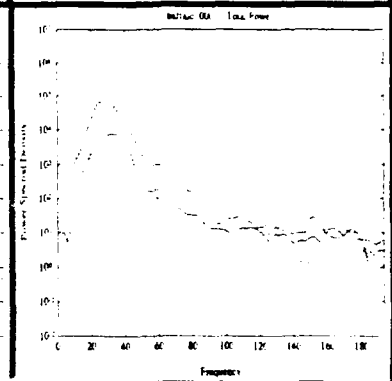
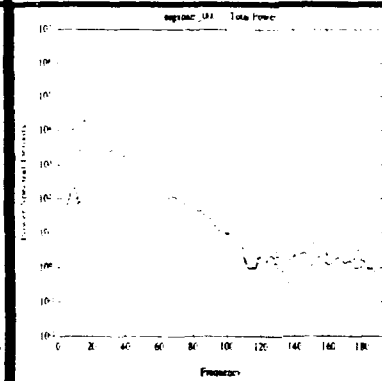
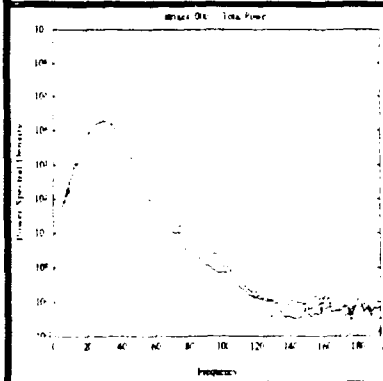
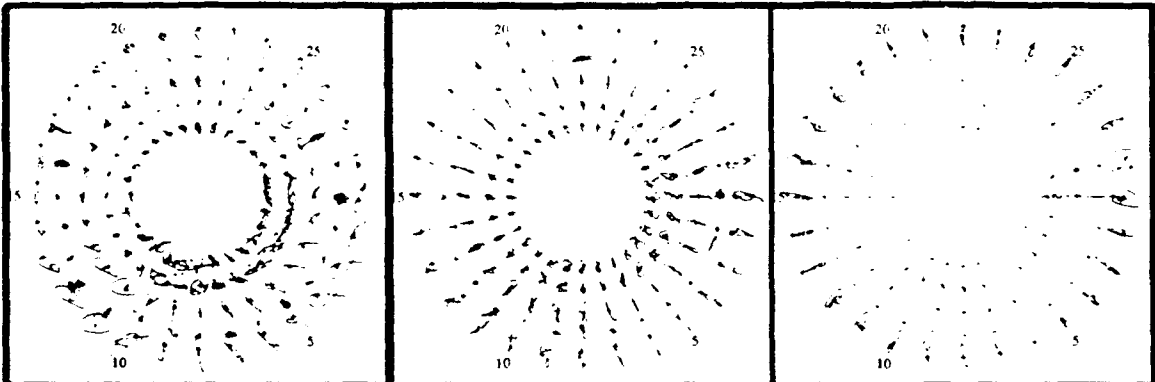
The arrow produces strong transverse energy with almost equal radial energy. The wavelet is more complex than simple hammer blows.

The caged plank produces strong shear energy of sufficient strength to image the reflector. However, deployment is slow, since a vehicle must be positioned atop the source. The source is easily repeated in either direction.

Table 3 Descriptions of Figure 8.

	Strike Plate	USGS Hammer	Buffalo Gun
Sources	The strike plate is a tractional hammer driven source consisting of a welded metal platform which is coupled to the ground with 6 inch spikes on the bottom and the weight of the operator who stands atop the platform. The operator forces the system with a 20 lb. hammer blow which can be applied to either end of the strike plate.	The USGS hammer is a truck mounted rotational trip hammer which is ground coupled by the weight of the vehicle in which it is installed. Extensive hydraulics are used to deploy and rotate the hammers. Once a given rotational speed is achieved, the hammers are tripped generating an impact type source in either a vertical or horizontal configuration. For this experiment, only the vertical source was recorded.	The buffalo gun is a 10 gauge blank shotgun shell which is installed in a side ported pipe assembly. The assembly is placed in a shallow, augured hole and detonated with an extended firing pin. This was proposed as a directional shear source, but proved to produce dominantly P waves.
Time Series	The strike plate produces the least complex wavelet of all sources tested and exhibits the bipolar character of tractional sources. Transverse amplitudes dominate in directions perpendicular to the source activation while radial amplitudes dominate parallel to the source. Anomalous amplitudes are evident in the right and lower quadrants.	The USGS hamer was the least energetic compressional source tested, but adequate power was transmitted from a single shot. The hammer produces a dominantly radial wave field as evidenced by the cyan nature of the time series. Large amplitude late arrivals are evident on both radial and transverse elements. Anomalous amps on rt and lower quad.	The buffalo gun produced time series dominated by radial power. Anomalous radial amplitudes are evident in the right quadrant approximately perpendicular to the port side of the downhole assembly. Transverse amplitudes are anomalously high, as for all compressional sources, in the right and lower quadrants.
Radiation	The strike plate produces bipolar transverse radiation with fair development of nodal structure in the direction of activation. Radial radiation is enhanced in the direction of activation an anomalous radiation sub parallel to the radial nodal plane is evident.	The USGS hammer produces an approximately isotropic radial radiation pattern and little transverse radiation. The radial radiation is enhanced in the right and lower quadrants more than other compressional sources. Transverse radiation is comparable in distribution to other compressional sources.	The buffalo gun produces a more isotropic radial radiation pattern than does the USGS hammer. The large radial amplitude at station 1 corresponds to the largest transverse amplitude observed. The scattered power exhibited on the transverse radiation pattern is similar to that of the 50 caliber gun and dynamite. There is no indication of the buffalo gun being a shear source.
Reflections	The strikeplate provides the first source powerful enough to generate a coherent reflected arrival at 300 ms. While small in amplitude, the Sh component (cyan) is apparently coherent throughout the array at 300 ms. Stacking multiple shots would be necessary for reflector definition.	The USGS hammer does not produce recognizable reflected events, possibly due to a complex source function leading to high amplitude post cursors in the wave field. While no P reflectors are evident for any compressional source studied, none of the remaining sources exhibited the late arriving wave train produced by the USGS hammer.	The buffalo gun produces no discernible reflected energy, however none of the compressional sources were capable of producing coherent reflected power within the 400 ms window.

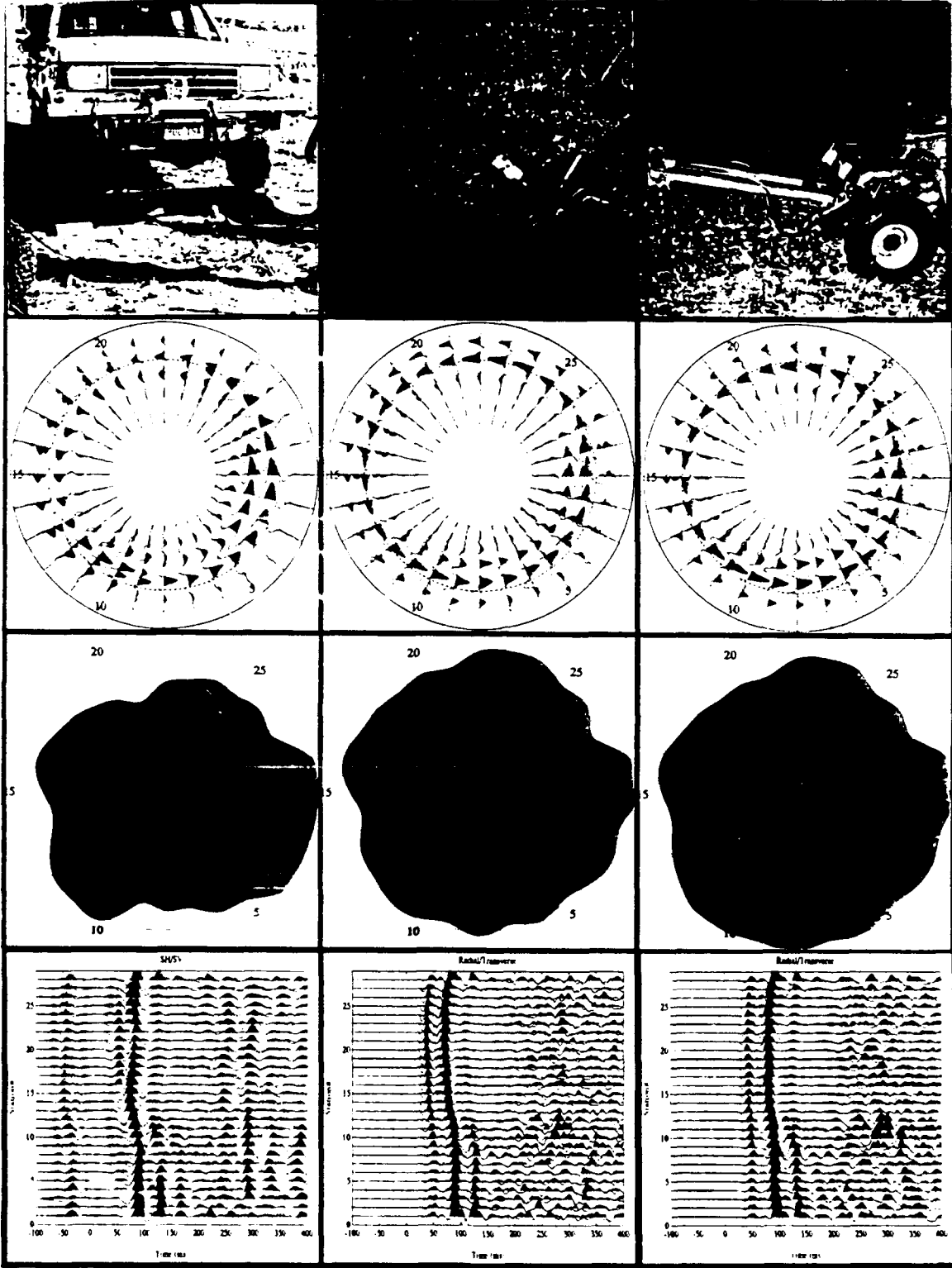




$10^{-2.0}$
 $10^{-2.5}$
 $10^{-3.0}$
 $10^{-3.5}$
 $10^{-4.0}$
 $10^{-4.5}$
 $10^{-5.0}$
 $10^{-5.5}$
 $10^{-6.0}$

Table 5 Descriptions of Figure 10.

	Swig	Fifty Caliber	Dynamite
Sources	The SWIG is a tractional source consisting of pneumatically driven, mechanically coupled, pair of 220 lb. hammers accelerated at approx. 125 ft/sec ² into a base plate anvil which is coupled to the ground by the weight of a vehicle. The source can be activated in either of two opposite directions.	The 50 caliber gun is a single shot 50 caliber rifle modified to muffle the air blast. The gun is fired vertically into a dry 1 m hole.	1/12 pound of dynamite in a 1 m tamped dry hole was detonated electrically.
Time Series	The SWIG time series exhibit the expected bipolar character of tractional sources. Transverse amplitudes dominate in directions perpendicular to the source activation while radial amplitudes dominate parallel to the source direction. Anomalous transverse amplitudes are evident centered about stations 1 and 11.	The 50 caliber gun produces time series dominated by radial power which is almost identical in nature to the dynamite and buffalo gun sources. Anomalous high scattered transverse power corresponds to the direction of higher amplitude radial power in the right and lower quadrants.	The dynamite source was the most powerful source tested and produces time series dominated by radial power. The waveforms are similar to those of the 50 caliber and buffalo guns. Anomalous high scattered transverse power corresponds to the direction of higher amplitude radial power in the right and lower quadrants.
Radiation	The SWIG produces well developed bipolar transverse radiation with almost complete extinction of power on the nodal plane. The radial radiation is not as powerful or well developed due to anomalous radiation sub parallels to the radial nodal plane.	The 50 caliber gun produces near isotropic radial radiation similar in form to all compressional sources. The radial radiation is slightly enhanced in the direction of stations 24 and 1. Scattered transverse radiation is similar to that of the buffalo gun.	Radial radiation for the dynamite source is near isotropic and similar in form to the radial radiation of all compressional sources. Scattered transverse radiation is similar to the USGS hammer.
Reflections	A single activation of the SWIG is adequate to produce a coherent shear reflections (cyan) at ~ 295 ms. The components have been rotated into Sh/Sv components. The precursor signal generated by activation of the source is evident on the AGC traces at ~ -50 to 0 ms.	As with all compressional sources, the 50 caliber does not produce a coherent reflection arrival within 400 ms. The 50 caliber section is similar to that of the dynamite, the components are not rotated due to the isotropic nature of the source.	No coherent reflected power is evident within the 400 ms window, as is the case for all compressional sources tested. The dynamite section is similar to that of the 50 caliber. Components are not rotated due to the isotropic nature of the source.



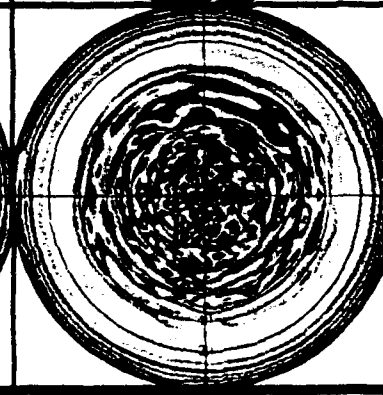
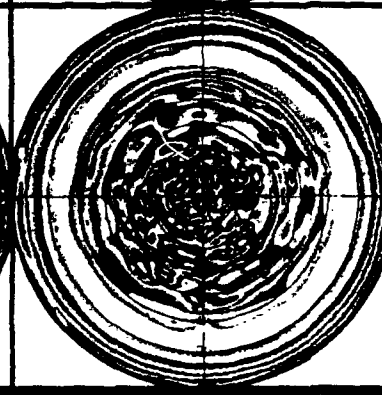
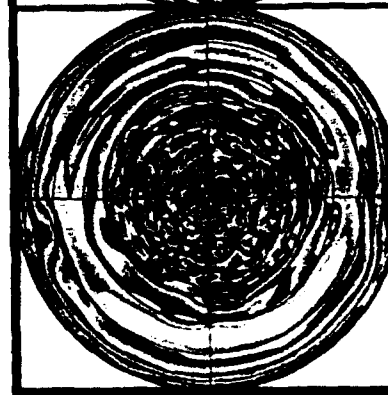
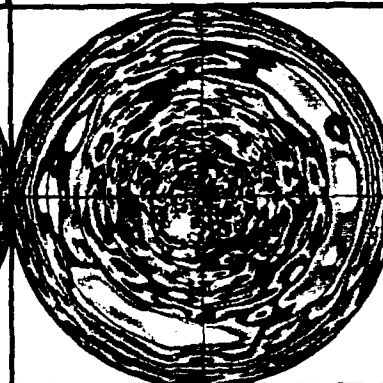
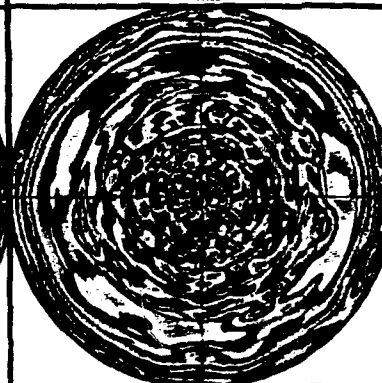
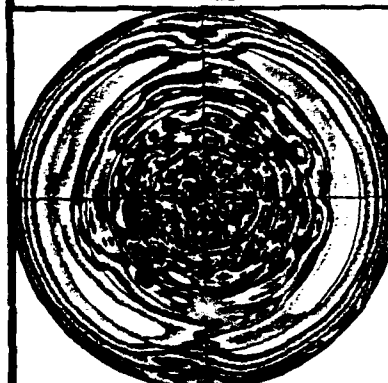
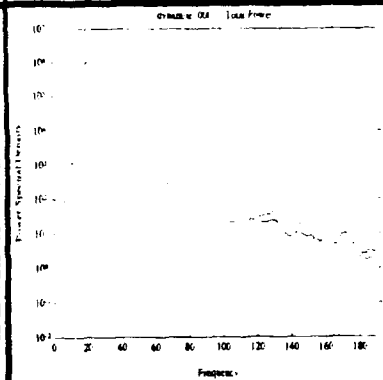
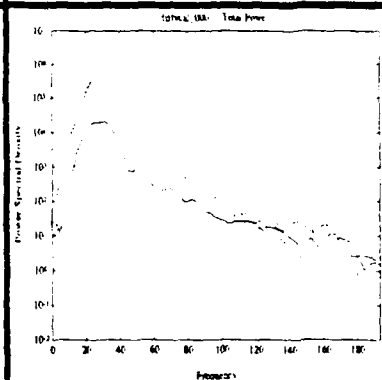
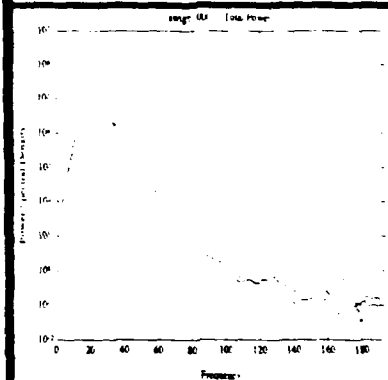
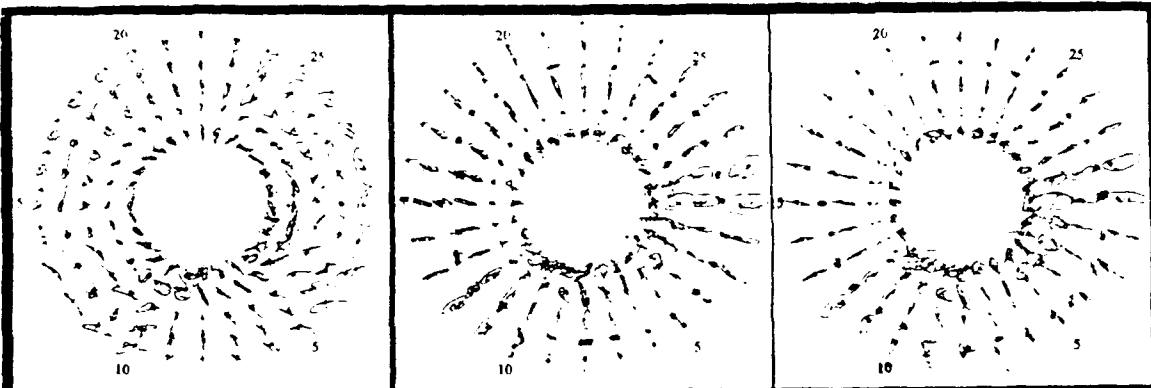


Table 6 Descriptions of Figure 11.

	Swig	Fifty Caliber	Dynamite
P a r t i c l e M o t i o n	The SWIG particle motion is most highly polarized radially on the transverse nodal plane due to the well developed transverse node. The more poorly developed radial node leads to degradation of the polarization of the transverse maximum.	The 50 caliber produces well polarized particle motion radial to the source. Linearly polarized stations dominate over elliptically polarized stations such as station 1. The 50 caliber polarization is similar to but less well developed than dynamite.	Dynamite produces the highest degree of linear polarization of all compressional sources. Major anomalies are evident with some elliptical particle motions and linearly polarized motions rotated relative to radial directions from source.
M e a n S p e c t r a	As is observed for all shear sources, the SWIG mean spectra are \approx equal in radial and transverse power at all frequencies up to 110 Hz. The variance of both component spectra is the least for all shear sources tested.	The 50 caliber spectra dominate power in the radial component to 110 Hz with \approx equal power in radial and transverse components from 110 to 200 Hz. Variance is more pronounced in the scattered transverse spectrum. Appears slightly broader band than dynamite.	The dynamite spectra are predominately radial to 100 Hz and \approx equal in radial and transverse power from 110 to 200 Hz. The variance of the radial spectrum is the least of all tested compressional source while transverse spectral variance is similar for all compressional sources.
T r a n s v e r s e S p e c t r a	The SWIG produces well developed nodal structure in the transverse spectra between 5 and 55 Hz. The north node is best developed and less complicated than the south node which is slightly obscured by high amplitude power levels.	The fifty caliber transverse spectra are comparable in form to those of the buffalo gun, though with greater power level.	Dynamite transverse spectra are similar in form to both the 50 caliber and buffalo gun at the highest power levels.
R a d i a l S p e c t r a	The radial spectra do not exhibit well developed nodal structure and are dominated by power in the southern quadrant. Radial power is confined to frequencies between 5 and 60 Hz.	The fifty caliber produces isotropic radial power spectra between 5 Hz and 45 Hz. Lesser degree of isotropy is seen from 45 to 80 Hz.	Dynamite produces isotropic radial power spectra from 5 to 60 Hz with anomalous power levels in the east and south quadrants.

S u m m a r y

The SWIG produces the simplest wavelet of all the shear sources. It shows the cleanest radiation pattern, clearly illuminates the reflector, and is the highest shear power source tested. Deployment is slow due to the necessity of a vehicle for movement and coupling, and an air supply is required, however, once deployed, many shots can be quickly taken.

The fifty caliber gun produces energetic radial energy comparable to the dynamite source. The source is easily deployed and repeated. Repeated firing in a dry hole causes the hole to change shape and significant changes in the source function.

Dynamite is the highest energy source used with most of the energy concentrated on the radial component. Azimuthal variation is partitioning of energy is indicative of the first order effect imposed by the test bed on source characterization studies.

Figure Captions

Figure 1. Location map of the test site south of Rosenberg, Texas on the Caldwell Executive Golf Course (the most modern golf course between Beasley and Needville).

Figure 2. Reconnaissance Survey. The near offset and group interval are both 0.5 m. The far offset is 36 m. The compressional section (2a) shows an obvious reflection at 75 ms, but noise wave interference makes it difficult to detect in the field at trace spacings beyond about 1.5 m. The shear section (2b) shows a clear reflection at approximately 180 ms, but the refraction breaks are obscured by the direct P arrival and air wave.

Figure 3. Geologic Model. The P and S velocity model is derived from combined refraction and reflection interpretation of the reconnaissance section.

Figure 4. Plan view of Array Layout. Each of the 28 stations is composed of 2 horizontal components (radial and transverse to shot point) at a range of 10 m. The station numbers are shown on the perimeter of the array. All sources were located within 1/2 m of the center of the array. Receiver orientations were checked at the start and finish of the experiment to confirm they were within a few degrees of radial and tangential directions.

Figure 5. Total Relative Horizontal Received Power. The observed received power spans two orders of magnitude at amazingly equal increments. For all sources of one type (P or S) the proportion of radial to transverse power is nearly constant. Shear sources have slightly more power in the transverse than in the radial, while for P sources, the transverse power is only 1/10 of the radial.

Figure 6.

Figure 7.

Figure 8.

Figure 9.

Figure 10.

Figure 11.

Figure 12. The received power for each component at station 8 is plotted vs. the total power for each source. Shear sources are labeled in magenta and P sources in blue. Total relative received power spans 2 orders of magnitude at almost equal increments throughout the total power scale.

Figure 13. Reflected power for each of the sources. Shear sources are labeled in magenta and P sources in blue. In general, the larger difference in S_v and S_h power correlates with a more visible shear reflection. The large offset for the USGS hammer is an indication that the energy is part of a complex source function rather than reflected energy.

References

- Arnold, M. E. 1977, Beam forming with vibrator arrays: *Geophysics* 42:1321-1338.
- Birkelo, B.A., Steeples, D. W., Miller, R. D. and Sophocleous, M., 1987, Seismic reflection study of a shallow aquifer during a pumping test: *Ground Water*, 25, 703-709.
- Brown, G. L., 1966, Seismic torsional wave generators. U. S. Patent 3, 280, 935.
- Cherry, J. T., 1962, The azimuthal and polar radiation patterns obtained from a horizontal stress applied at the surface of an elastic half-space. *BSSA* 53:27-36.
- Dorn, Geoffrey A., 1984, Radiation patterns of torsionally vibrating seismic sources. *Geophysics*, 49(8):1213-1222.
- Edelmann, H. A. K., 1985, Shear-wave energy sources *in* Seismic shear waves Part B: Applications p 135-177.
- Goforth, T. and Hayward, C. T., 1992, Shear wave profiling of a bedrock surface buried under alluvium: *Geophysics*, 57, xxxx-xxxx
- Knapp, Ralph W., and Steeples, Don W. (1986) High-resolution common-depth-point reflection profiling: Field acquisition parameter design. *Geophysics* 51(2):283-294.
- Kobayashi, N., 1959. A method of determining the underground structure by means of SH wavers, *Zisin* 12:19-24.
- Hasbrouck, Wilfred P., 1983, Sketches of a hammer-impact spiked-base, shear-wave source. USGS Open File Report 83-917.
- Hasbrouck, W. P., 1986, Shallow shear-wave reflections within the Panoche Fan area, central San Joaquin Valley, California: in *Proceedings of the Surface and Borehole Geophysical Methods and Ground Water Conference and Exposition*, Oct. 15-17, 1986, Denver, Colorado, p.437-450.
- Hasbrouck, W. P., 1988, Five shallow feasibility surveys: in *Expanded Abstracts of the Technical Program with Authors' Biographies*, v. 1: SEG 58th Annual International Meeting & Exposition, 286-289.
- Heelan, P. A., 1953, Radiation for a cylindrical source of finite length: *Geophysics* 18:685-696.
- Hirona, T., 1948 Mathematical theory on shallow earthquake: *The Geophysical Magazine*, 18:1-116.

- Hunter, J. A., Pullan, S. E., Burns, R. A. Gagne, R. M. and Good, R. S. 1984, Shallow seismic-reflection mapping of the overburden-bedrock interface with the engineering seismograph - some simple techniques: *Geophysics*, 49, 1381-1385.
- Jongorius, P., and Helbig, K., 1988, On-shore high-resolution seismic profiling applied to sedimentology: *Geophysics*, 53, 1276-1283
- Kahler S., and Meissner, R., 1983, Radiation and receiver pattern of shear and compressional waves as a function of Poisson's ratio. *Geophysical Prospecting* 31: 421-435.
- Liu, Hsi-Ping, Warrick, Richard E., Westerlund, Robert E., Fletcher, Jon B. and Maxwell, Gary L., 1985. An air-powered impulsive shear-wave source with repeatable signals. *Bulletin of the Seismological Society of America* 78(1):355-369.
- Lynn
- Miller, G. F., and Pursey, H. 1954, The field and radiation impedance of mechanical radiators on the free surface of a semi-infinite isotropic solid: *Proc. Roy. Soc. Lond. Ser. A*, 223:521-541.
- Miller, G. F. and Pursey, H., 1956, On the partition of energy between elastic waves in a semi-finite solid. *Proc. Roy. Soc. A* 233:55-69.
- Miller, R. D., Pullan, E. E., Waldner, J. S. and Haeni, F. P., 1986, Field comparison of shallow seismic sources: *Geophysics*, 51, 2067-2092.
- Miller, R.D., Pullan, S.E., Steeples, D.W., and Hunter, J. A., 1989, Field comparison of shallow seismic sources near Chino, California: 59th Ann. Internat. Mtg., Soc. Explo. Geophys., Expanded Abstracts, 262-265.
- Miller, R.D., Pullan, S.E., Steeples, D.W., and Hunter, J. A., 1989, Filed Comparison of shallow seismic sources near Chino, California: *Kansas Geol. Surv. Open-file Rep.* 89-38.
- Miller, R.D., et. al., 199x What ever the title is. What ever the publications
- Miller, R. D., Pullan, S. F., Steeples, D. W., and Hunter, J. A., 1992, Field Comparison of shallow seismic sources near Chino, California: *Geophysics*, 57, 693-709.
- Murphy, V. J., 1977, Method for generating and detecting seismic shear-wave energy in the earth. U.S. Patent 4,038,631.
- Pullan, S. E., and MacAulay, H. A., 1987, An in-hole shotgun source for engineering seismic surveys: *Geophysics*, 52, 985-996.

Robertson, J. D., Corrigan, D. 1983, Radiation patterns of a shear-wave vibrator in near surface shale: *Geophysics* 48:19-26.

Ruskey, F., 1981, High-resolution seismic methods for hard-rock mining: Information Circular 8891, U.S. Bureau of Mines, 4-28.

Schepers, R. 1975, A seismic-reflection method for solving engineering problems: *J. Geophys.*, 41, 367-384.

Steeple, D. W. and Miller, R. D., 1990, Seismic-reflection methods applied to engineering, environmental, and ground-water problems, *in* S. Ward, E., *Investigations in geophysics, No. 5, Review and tutorial, Vol. 1: Soc, Expl. Geophys.*, 1-30.

Stumpel, H., Kahler, Meissner, R. and Milkereit, B. (1984), The use of seismic shear waves and compressional waves fro lithological problems of shallow sediments. *Geophysical Prospecting* 32:662-675.

**CHARACTERIZATION OF THE SHALLOW
WEATHERED ZONE WITH COMPLETE
SEISMOGRAMS**

Mark A. Bogaards
Brian W. Stump
Department of Geological Sciences
Southern Methodist University
Dallas, Texas 75275-0395

INTRODUCTION

Seismic observations made at the earth's surface propagate through the shallow weathered zone. Only in the case of borehole instrumentation recording waves from sources at depth can these effects be minimized. The spatial variability of the weathered layer leads to a degradation of waveform coherence as estimated by closely spaced instruments at the earth's surface as a result of both amplitude and phase changes between isolated receivers. In the case of exploration seismology and in particular reflection seismology, the effect is to reduce the consistency of high frequency or short wavelength data and in turn decrease the subsurface resolution of the geological structure. Near source, regional and teleseismic wave propagation and source studies also suffer from these effects as the shallow weathered layers in some cases prevent deterministic interpretation of the data to high frequencies that are important in discriminating one model from another. A third area of impact is in quantification of strong ground motion from both earthquake and explosion sources. The spatial coherence of the wavefield can contribute to the extent of ground motion damage to large engineering structures. The three problems noted include both horizontally and vertically propagating energy in these near surface layers and thus both body and surface wave components.

The general approach to this problem is one that separates stochastic and deterministic wave propagation effects. The stochastic component is interpreted in terms of a scattering model. Figure 1 summarizes the division by a number of researchers of stochastic and deterministic propagation effects in frequency and receiver offset space. McLaughlin et al. (1983) quantify the station to station coherence for complete waveforms observed at 6 km from a contained nuclear explosion at Pahute Mesa, Nevada Test Site. The signals above 5 Hz at station spacing of 100 m are incoherent. Reinke and Stump (1988) analyzing ground motions at a variety of azimuths from 5 lb. explosions find large differences in waveforms above 35 Hz at a range of 10 m and above 25 Hz at 30 m. Vernon et al. (1985) report that the coherence of earthquake signals at station spacing of 50 m and observational distances of 10 to 50 km for P waves is good to 25-35 Hz and to 15 Hz for S waves. Menke et al. (1990) give additional regional observations at closely spaced stations in hard rock. These results from a large range of source-receiver offsets all show the importance of interstation spacing and thus the structure of the weathered zone around the receiver on the coherence of the observations.

These results motivate the development of shallow site characterization tools that divide the deterministic and stochastic components of the seismic waves

PREVIOUS WORK

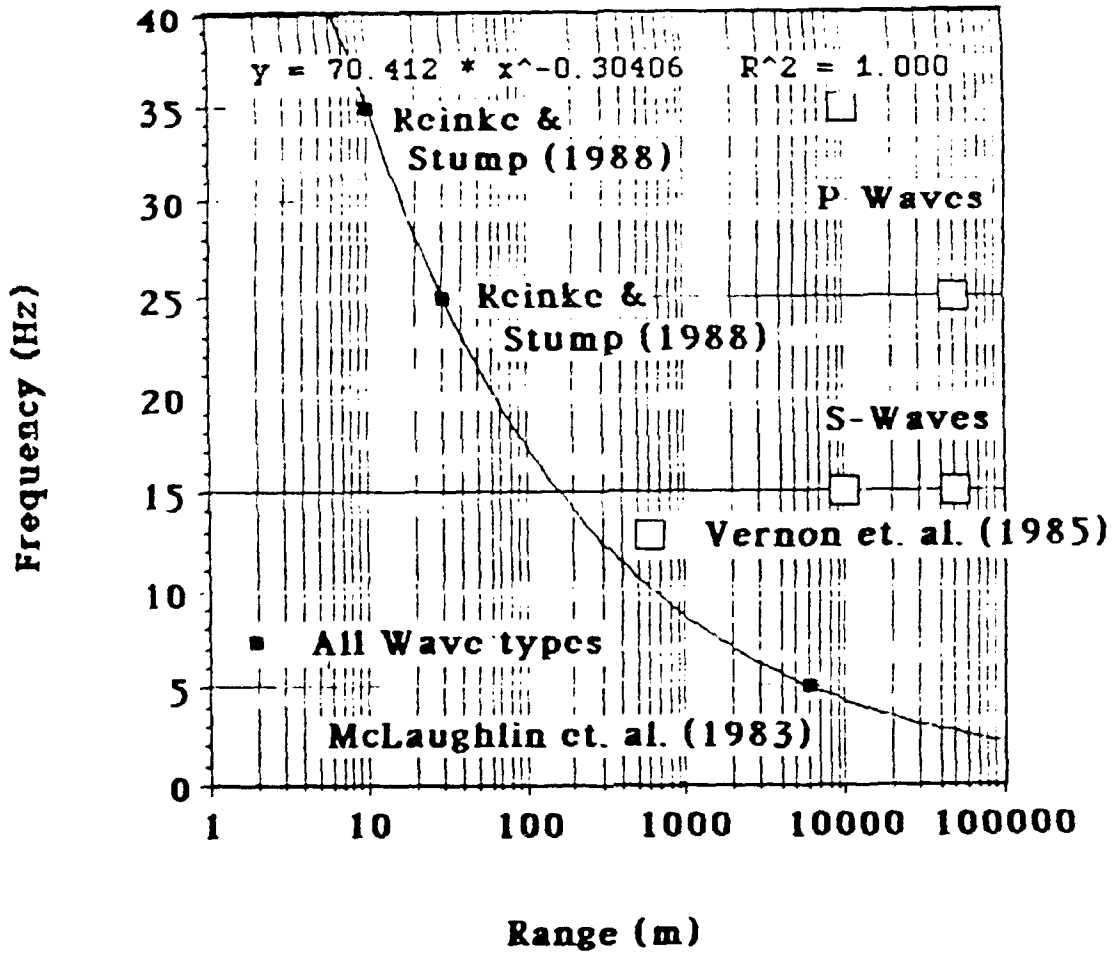
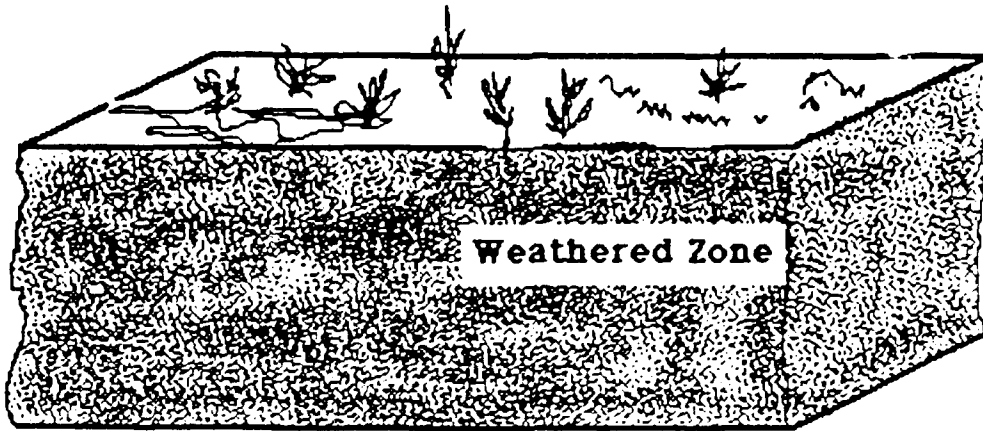


Figure 1: The maximum frequency and range at which observational data begins to show significant variations.

and in turn the geological model. Figure 2 describes the problem. The deterministic model is a simple representation of the local geology, possibly as simple as plane or dipping layers. Standard reflection and refraction imaging as well as surface wave inversion techniques determine this component of the model. The stochastic contribution constrains the scattering model with the amplitude and phase variations in the wavefield not accounted for by the deterministic model.

The unique aspect of this work is that it reports initial attempts for *experimentally* determining and separating these stochastic and deterministic wave propagation effects. These experimental techniques characterize a particular geological site and thus predict its performance as a location for a single station or a surface array. This information might be useful in regional or teleseismic array design, source studies and earthquake or explosion ground motion assessment. The components of this experimental approach include closely spaced instrumentation at the earth's surface excited by man-made, controlled sources. High resolution frequency-wavenumber estimators separate the wavefield components. The estimation procedure includes standard Fourier analysis for the time to frequency transform and a modeling technique for the space to wavenumber transform. The modeling procedure avoids common window effects and produces a high resolution wavenumber estimate with a minimum number of spatial samples. Once the wavefield components have been identified closely spaced circular arrays provide the statistical characterization of the wavefield. Azimuthal effects are characterized in the time and frequency domain through statistical measures. It is the combination of these different field and analysis techniques that provides the complete characterization of the material.

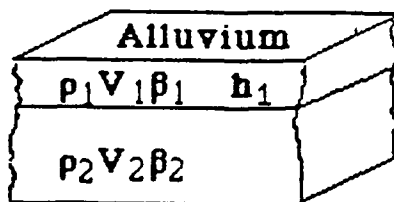
Problem



Source
Wave Field
Superposition

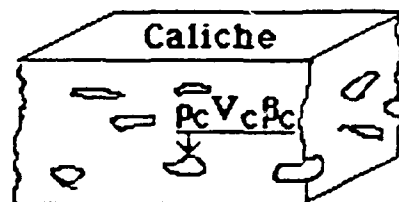
Deterministic Wave Field

Deterministic Seismic Models
Geological Layers
Geophysical Properties



Stochastic Wave Field

Statistical Characterization
Scattering Model
Inhomogeneity Properties



Wave Field Boundary

Time-Range ($t-x$) Domain
Frequency-Range ($f-x$) Domain
Wavelength-Range ($\lambda-x$) Domain
Frequency-Wavenumber ($f-k$) Domain

Figure 2: Schematic diagram which describes the separation of the wavefield into stochastic and deterministic components.

TEST SITE

The field location chosen to illustrate this new technique is McCormick Ranch south of Albuquerque, New Mexico (Figure 3). The site is in the Rio Grande Valley at the base of the Sandia Mountains. The subsurface geology consists of dry alluvium down to the water table at 75 m. Unconsolidated eolian sands, alluvium and lacustrine deposits extend to 15-30 m. Three to four hundred meters beneath this material are the Tertiary Santa Fe and Galisteo formations with a total thickness of 180-300m. This local area is part of a shallow basin which at one time contained a playa. As the limestone caps of the near-by Sandia Mountains eroded, they provided the ingredients necessary to cement shallow materials together forming isolated caliche deposits. These caliche lenses have been identified at the McCormick Ranch previously through trenching and subsurface excavation (Reinke and Stump, 1988 and 1991). The cementation process dramatically changes the elastic properties of the unconsolidated material with strong increases in both P and S velocities. The intermittent nature of these deposits in combination with the large velocity contrasts makes them a good source of scattered seismic waves.

McCormick Ranch is a good site to develop these characterization tools because of the simple plane layered geological structure with the superposition of intermittent caliche lenses as scatterers. Previous work analyzing strong ground motions from explosive sources (Reinke and Stump, 1988 and 1991; Stump and Reinke, 1988) provided initial information of waveform variability at the site. Characterization of the site with the new exploration tools will provide direct comparison of this exploration technique with waveforms generated by more energetic sources. Such a test of the procedures provides a validation of the exploration procedure with application to other sites where such control is not available.

GEOLOGY OF TEST SITE

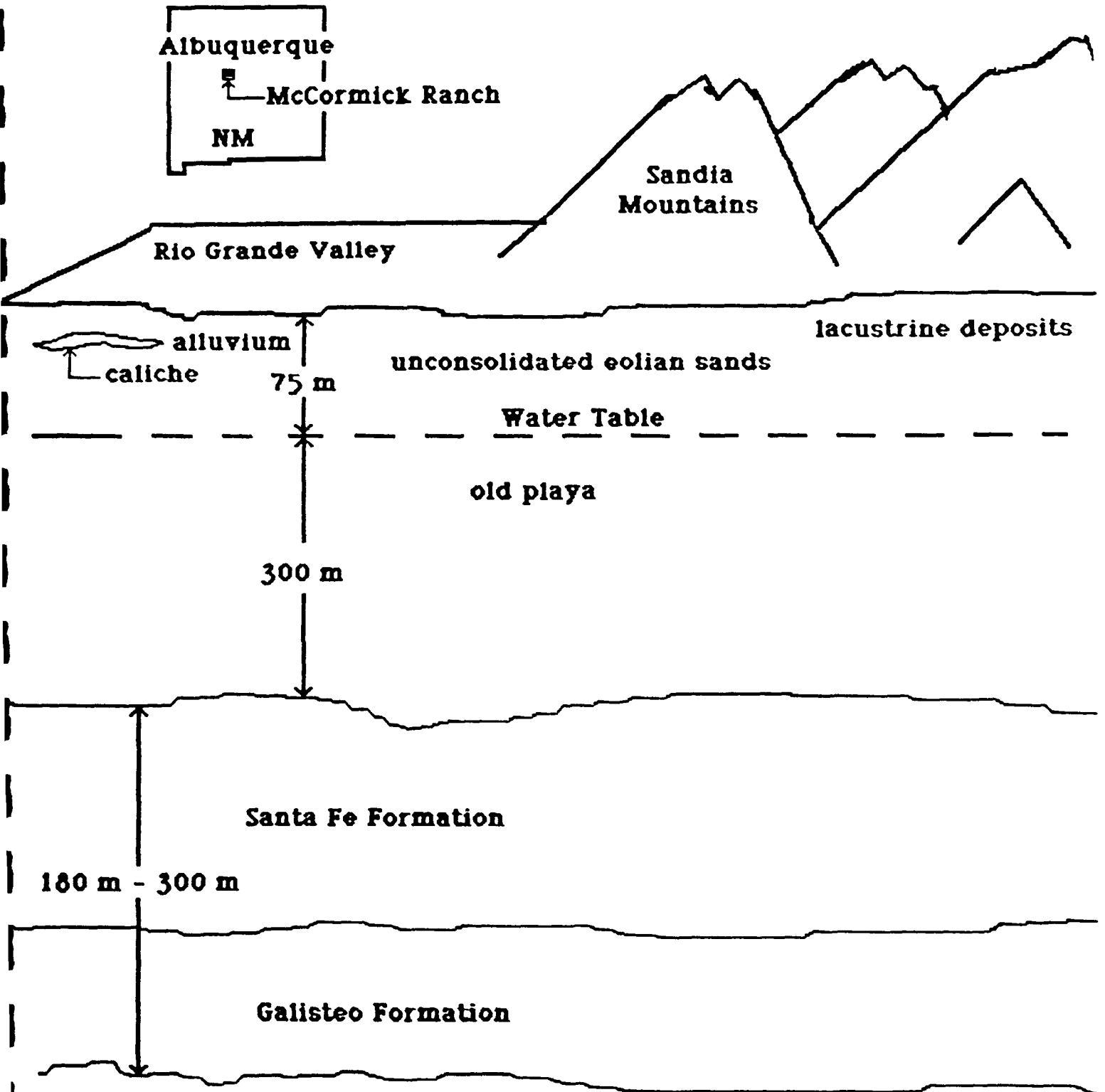


Figure 3: The geology of the McCormick Ranch Test Site.

EXPERIMENTAL DESIGN

The first step in the site characterization is the identification of the deterministic component of the wavefield through high resolution frequency-wavenumber analysis. These tools allow separation of the body and surface waves. Closely spaced linear arrays of instruments provide the data for this portion of the procedure. Multiple observations at the same range provide the data for the stochastic component of the model. These two types of requirements led to the spoked wheel geometry displayed in Figure 4. Individual spokes in the diagram are instrumented with 72 geophones at 1 m interstation spacing. Sources occupy the central point of each wheel as well as at the reversed end of a few spokes. A total of 1,152 receiver locations provide the necessary characterization data. The Nyquist wavenumber for each linear array is 0.5 cycles/m.

Geophones used in the study were 4.91 Hz Geo Space GS-11Ds deployed in the vertical mode. Each geophone was leveled in a shallow hole and then back filled with soil. The purpose of this emplacement technique was to enhance the geophone coupling and decrease the wind and surface noise (Krohn, 1984.). Data were recorded on an EG&G Model 2415f 24 channel seismograph with an 8 bit analog to digital converter. Amplifier gains were adjusted for each seismogram so that the entire 8 bits were used in characterizing the ground motions. The data was sampled every 0.25 msec and a 2 pole Bessel filter with a corner frequency of 500 Hz was applied as an antialias filter.

The primary source for these experiments was the Betsy Seisgun. This source is an eight gauge shotgun that fires either a lead or steel slug vertically into the ground. This slug produces a vertically oriented cylinder in the near surface materials and accounts for the radiation of P and Sv waves away from the source. Empirical work with the source indicates that the source signature changes little after this subsurface cylinder has been formed. Prior to any data acquisition the Betsy was fired several times to stabilize the source signature or repeatability. One disadvantage of the shotgun source is the amount of air blast that accompanies the detonation. This aspect of the source became problematic at the McCormick Ranch test site since P and especially the S velocities of the near surface layers were comparable to the acoustic velocity in air. The air blast was reduced by berming dirt around the base of the Betsy. Noise reductions of between 9 and 20 dB were observed with this berming procedure.

A huddle test was performed to investigate differences in receiver coupling as well as identify problems with the recording system. Twenty-four

Spoke Wheel Geometry

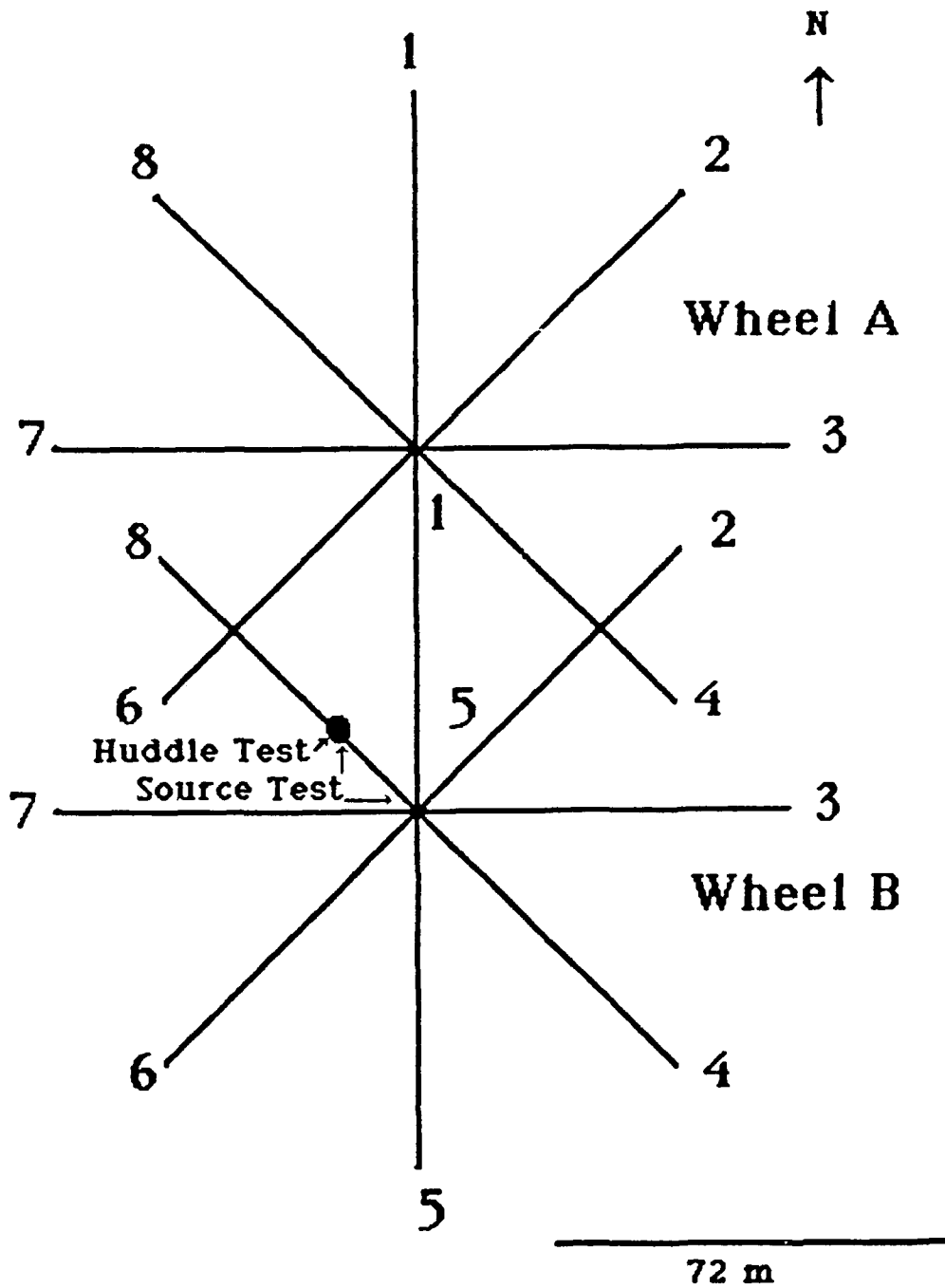


Figure 4: The spoked wheel geometry employed in the site characterization procedure.

geophones were emplaced in the same manner as in the rest of the experiment but at only 7 cm spacing. The location of the huddle test is indicated in Figure 4 and was 23 to 25 m from the Betsy source. Negligible instrument differences were found below 100 Hz for these tests. Variations above 100 Hz could be attributed to the 2 m span of the geophones in the huddle test.

Betsy source repeatability studies were conducted in a similar fashion with a linear array deployed between 1 and 24 m (Figure 4). Data were acquired after the source cavity had been formed and stabilized. Only minor inter shot spectral differences were identified above 175 Hz.

CHARACTERIZATION TOOLS

1. Travel Time Analysis:

The first step in this shallow site characterization study was the development of a simple deterministic model using the travel time data. The complete waveforms from one of the linear arrays of vertical geophones are given in Figure 5 where the various phases have been identified. The initial body waves are used in this deterministic characterization of the near surface layers. Arrival time data were recovered from all the spokes of the A and B wheels in Figure 4. Comparison of the reversed profile which consists of line 5 from wheel A and line 1 from wheel B are given in Figure 6. The two lines give arrival times which are on average separated by only 0.6 msec and support a plane layered interpretation for this portion of the test bed. Early arrivals from line 5-A in the first 10 m are probably due to slight variations in the very thin near surface layers. The variability in arrival times on 1-B between 10 and 20 m is a result of poor signal to noise ratios at first onset for these data. Interpretation of the observational data supports a top layer with a thickness between 5.5 and 5.9 m and a velocity between 500 and 520 m/s. The deeper material has a velocity of 670 m/s.

This arrival time interpretation was applied to all the data gathered in this study and was used to develop simple plane layered interpretations as a function of azimuth for the test site. The velocities of the top layer and the underlying material as a function of azimuth are given in Figure 7a with the layer thicknesses in Figure 7b. These representations indicate some azimuthal variation in the material properties at the test site which were not picked up in the simple reversed profile discussed earlier. The top material shows relatively small variations in velocity while the second material is consistently slow to the east and fast to west. Similarly the top layer thicknesses are thin to the east and thickens to the west. These results suggest that the local structure at this site dips to the west explaining the similarity in the reversed north-south refraction line.

Shear wave data at relatively large station spacing (5 m) was also recovered for a portion of the test site (Figure 8). The interpretation of this data supports a model in which the top layer has a velocity of 230 m/s and the second layer 360 m/s. The layer thickness from crossover estimates is 3.5 m although this estimate is relatively crude based on the large station spacing. This layer thickness estimate is not inconsistent with the P wave analysis.

2. High resolution frequency-wavenumber estimators:

WHEEL A LINE 8 U

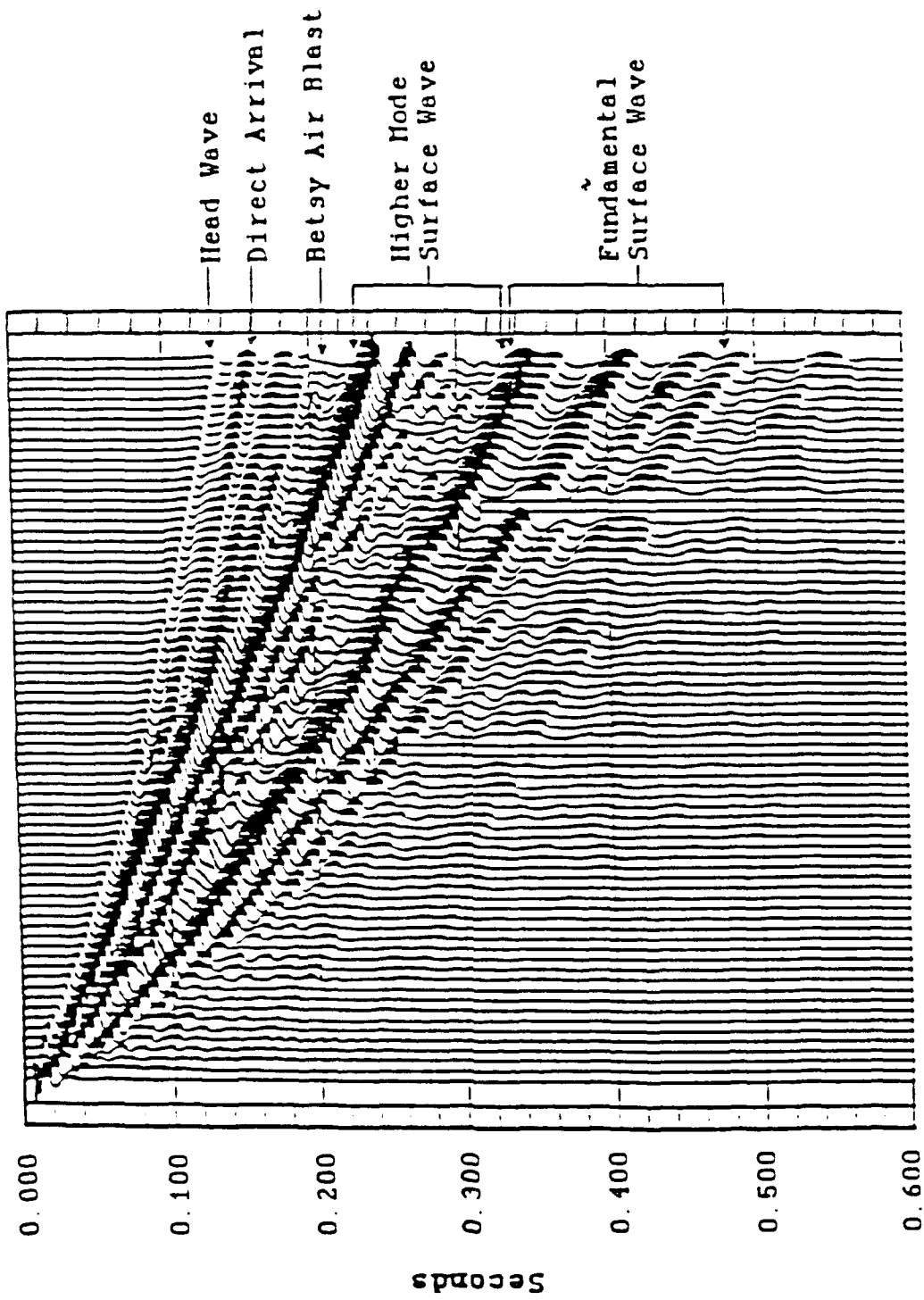


Figure 5: Wheel A, line 8 wiggle trace plot in the t-x domain. The range of the observations is from 1 to 72 m.

FORWARD & REVERSE REFRACTION LINES

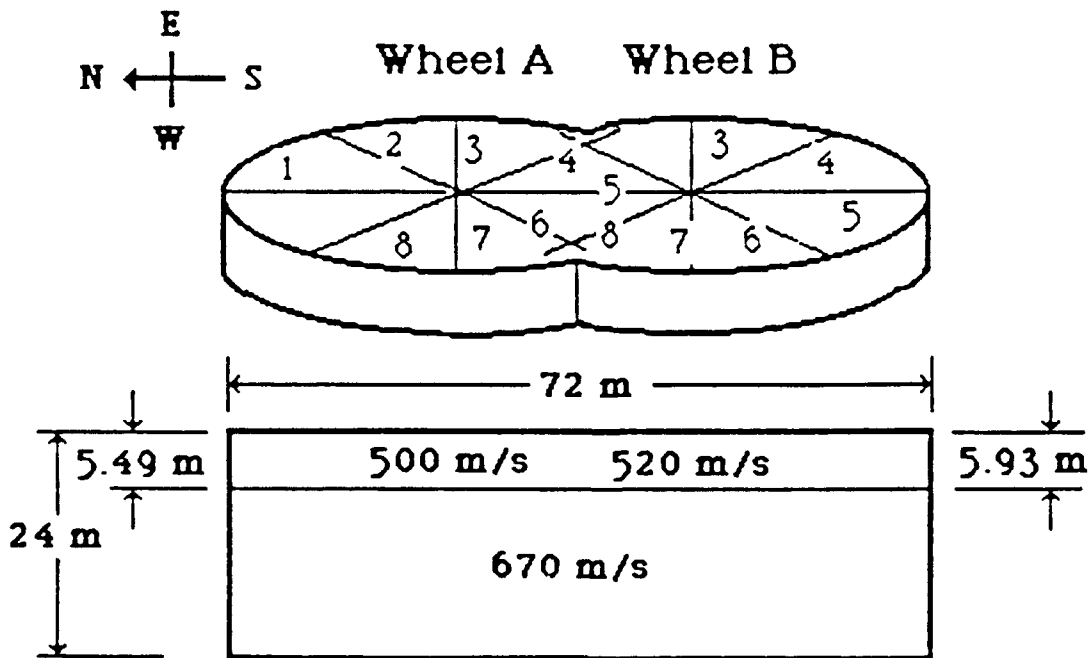
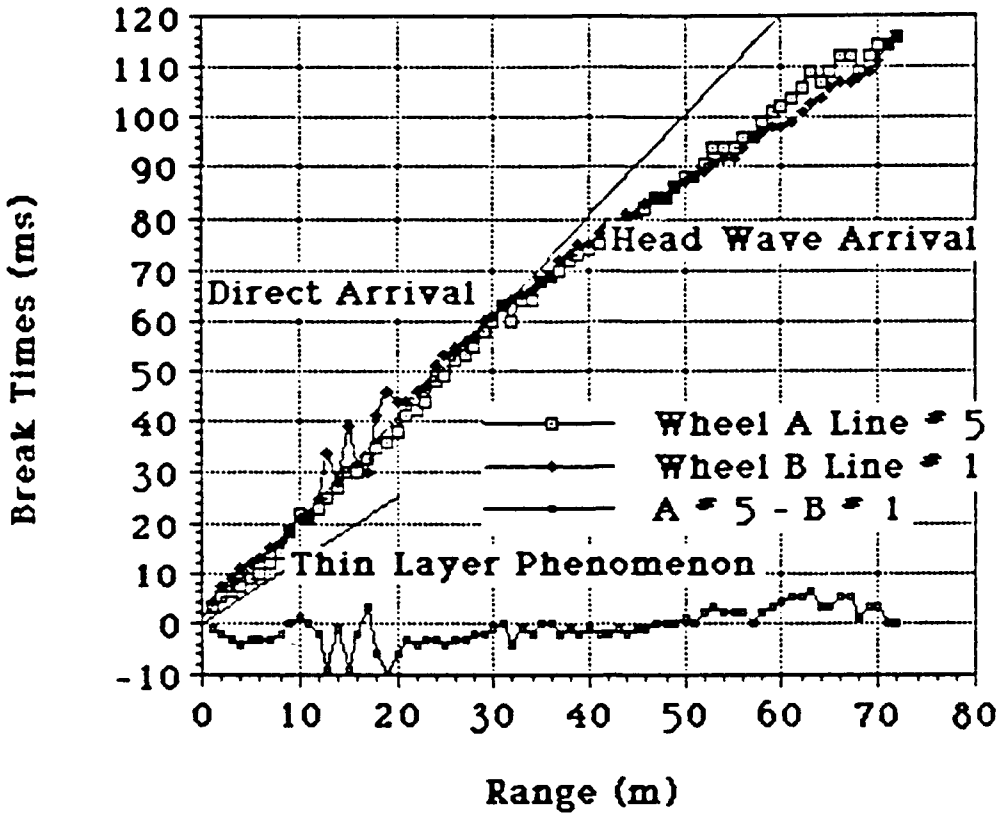


Figure 6: The travel time curves determined from line 5, wheel A and line 1, wheel B. The location of these lines is illustrated in the bottom half of the figure.

LAYER 1 & 2 P-VELOCITIES

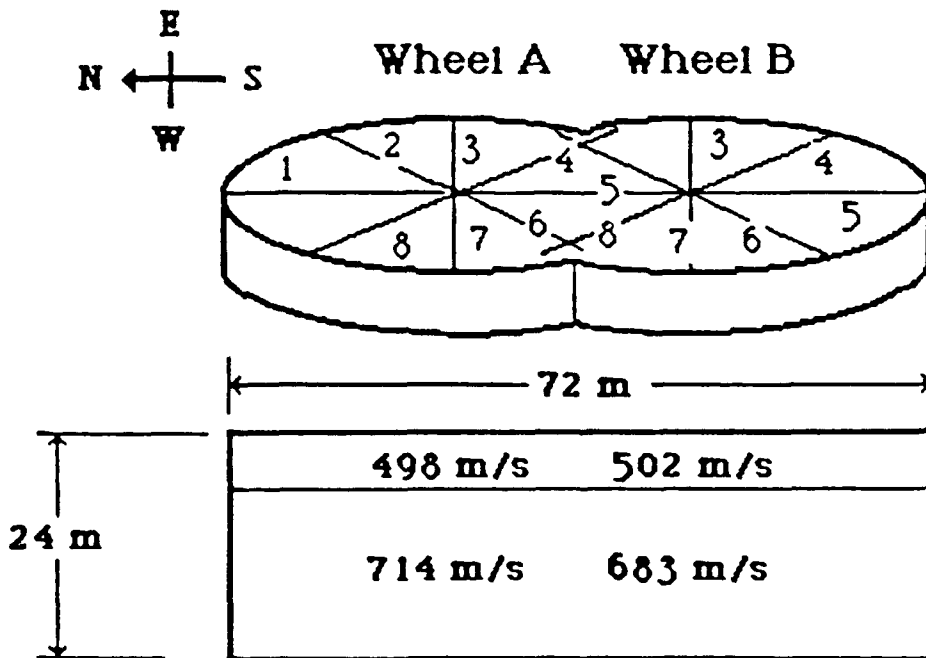
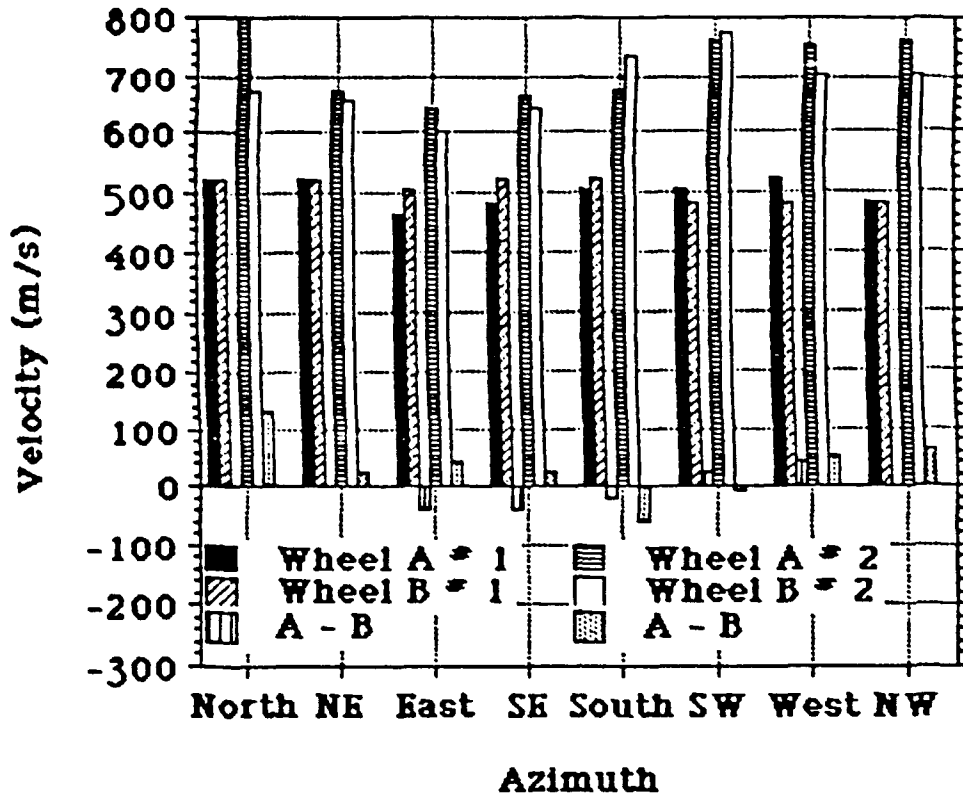


Figure 7a: The top (#1) and second (#2) layer velocities from both wheel A and B.

TOP LAYER THICKNESS

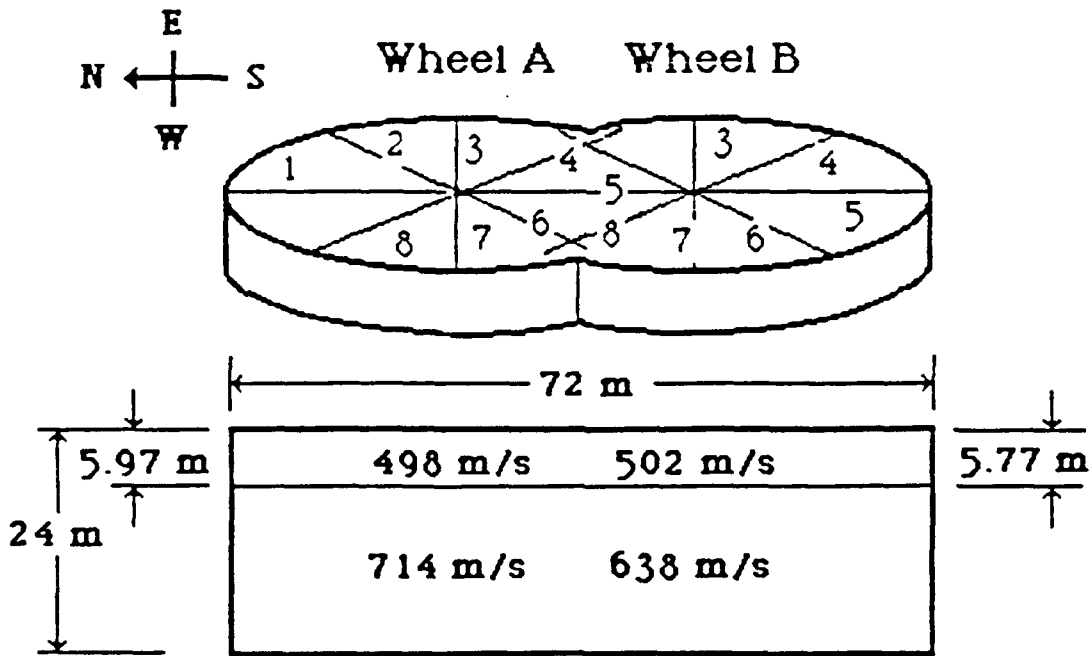
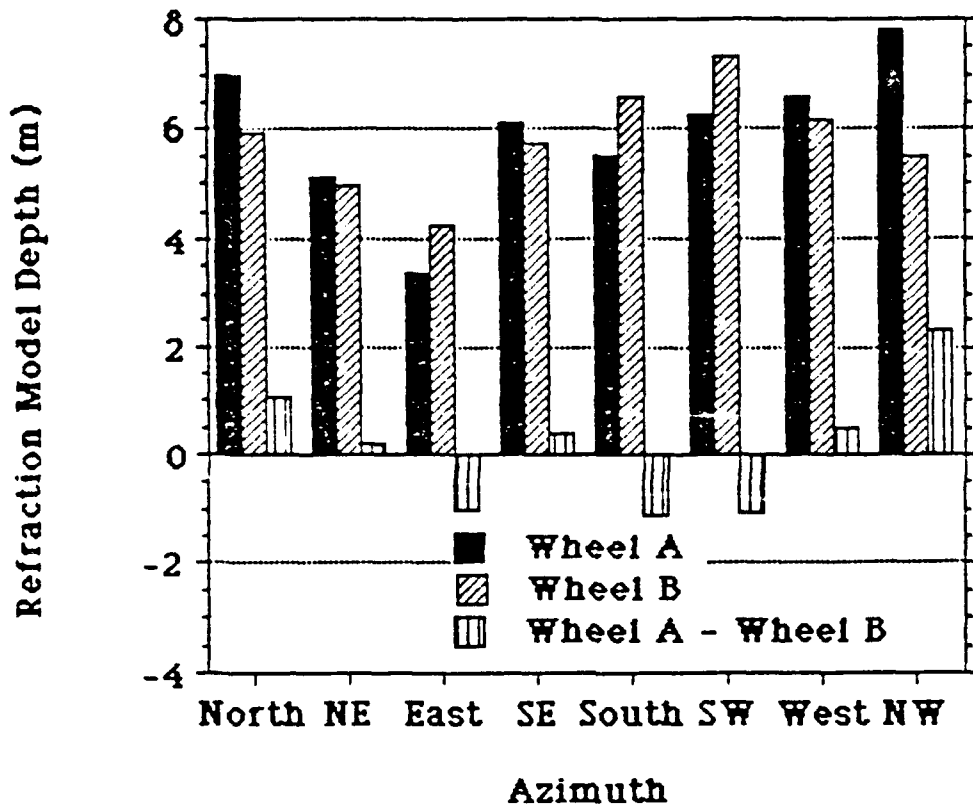


Figure 7b: The layer thickness determined from each spoke of wheel A and B.

SHEAR REFRACTION DATA

Wheel A Line # 4

$Dx = 5 \text{ m}$

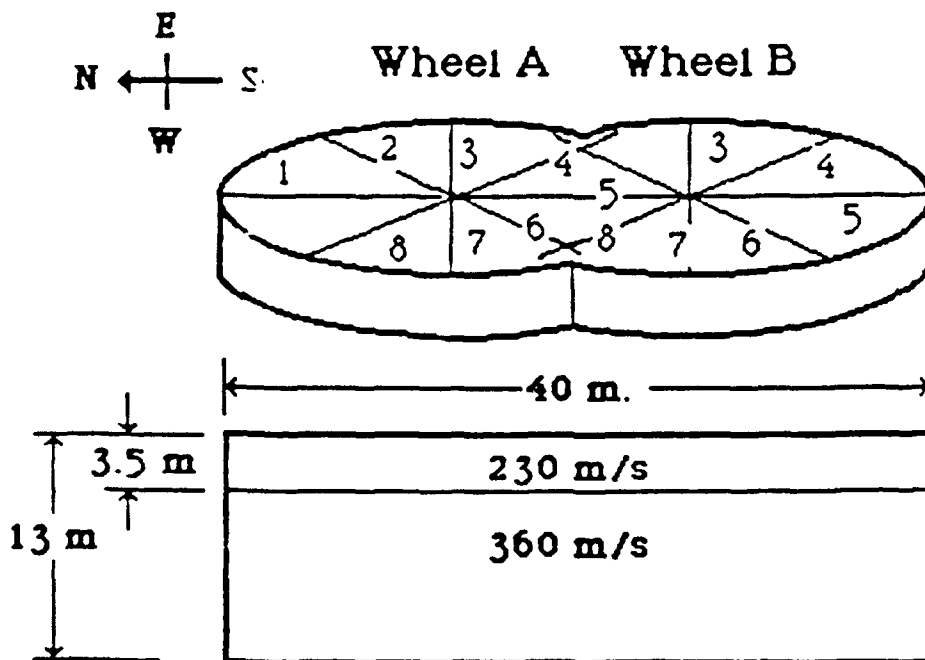
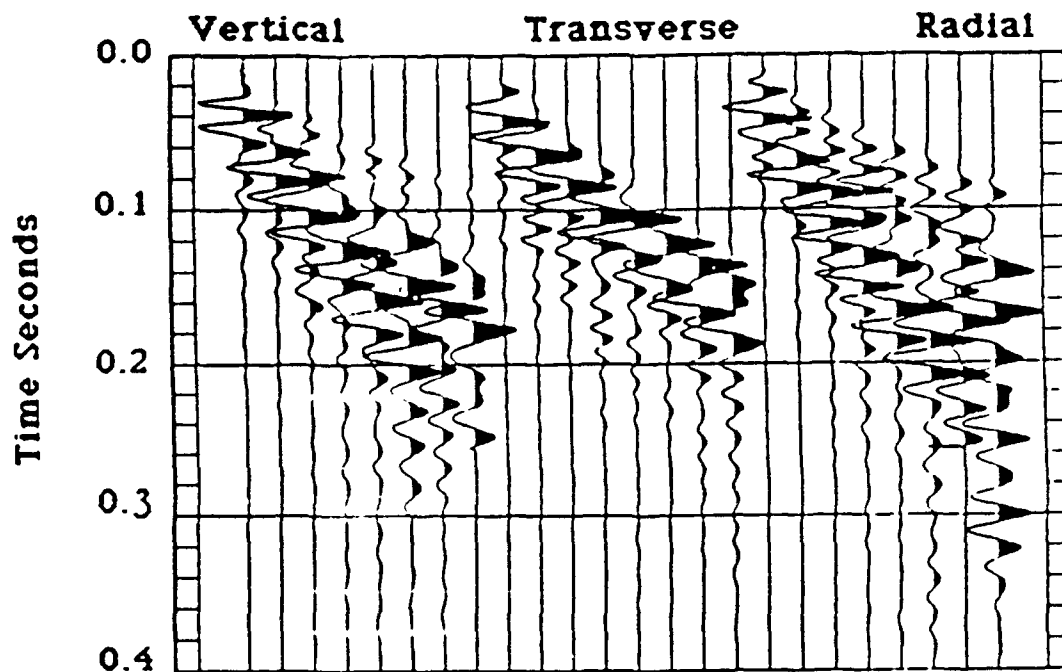


Figure 8: The three component data collected during the shear wave survey.

As indicated in the waveform data (Figure 5), the shallow exploration source generates a wide variety of arrivals that can be used in characterizing the subsurface. In the case of first arrival time data the identification of the important information is simple. The separation of the latter phases for the purposes of site characterization is a more complex task. The advantage of the array data collected in this series of tests is that frequency-wavenumber techniques can be applied to separate the different phases. The standard procedure for estimation of the f-k spectra is to use the periodogram method with the application of FFT to the data in the time and space domain. This technique applied to the McCormick Ranch data produces the results represented in Figure 9. This estimation technique has four advantages: (1) It is robust; (2) It is a relatively fast computation; (3) The resulting spectrum is a good estimate of power as a function of frequency and wavenumber; and (4) Filtering can be easily accomplished. Application of the periodogram technique assumes that the data are stationary, periodic and equally sampled in space and time. One major disadvantage of the technique is a degradation of the spectrum from spectral leakage when there are a small number of points in either the time or frequency domain. Tapers are applied to the data to control leakage and variance although the spectrum becomes biased. Smaller signals are often hidden in the spectral leakage from larger signals. These windowing effects are easily identified in Figure 9 where the primary surface and body wave arrivals are represented in red and the bias from the windowing spreads energy throughout the window into both positive and negative wavenumbers. Even when all 72 channels of vertical data are used in developing the f-k spectrum strong windowing effects remain.

A number of alternate high resolution methods have been developed for spectral estimation (Marple, 1987). These procedures are model based where the data are used to constrain model parameters which in turn are used to represent the spectrum. Time domain data typically has many points so that normal Fourier techniques can be used to make frequency domain estimates. Generally spatial sampling of the data is not as robust and thus suffers more from these windowing effects. Bogaards (1989) along with others (Shirley et. al., 1987; Burg, 1987; Mavko and Burg, 1987) have suggested that these high resolution modeling techniques are applicable to wavenumber estimates when the number of spatial observations is limited. These procedures offer the added advantage that they can be applied to selected portions of the spatial wavefield to document local estimates of the wavefield which might be more coherent.

Bogaards (1989) reports the testing of a number of these model based spectral estimate routines. This analysis tests the different methods discussed by Marple (1987) with both synthetic and observational seismograms. Included in the testing are the autoregressive (AR), moving

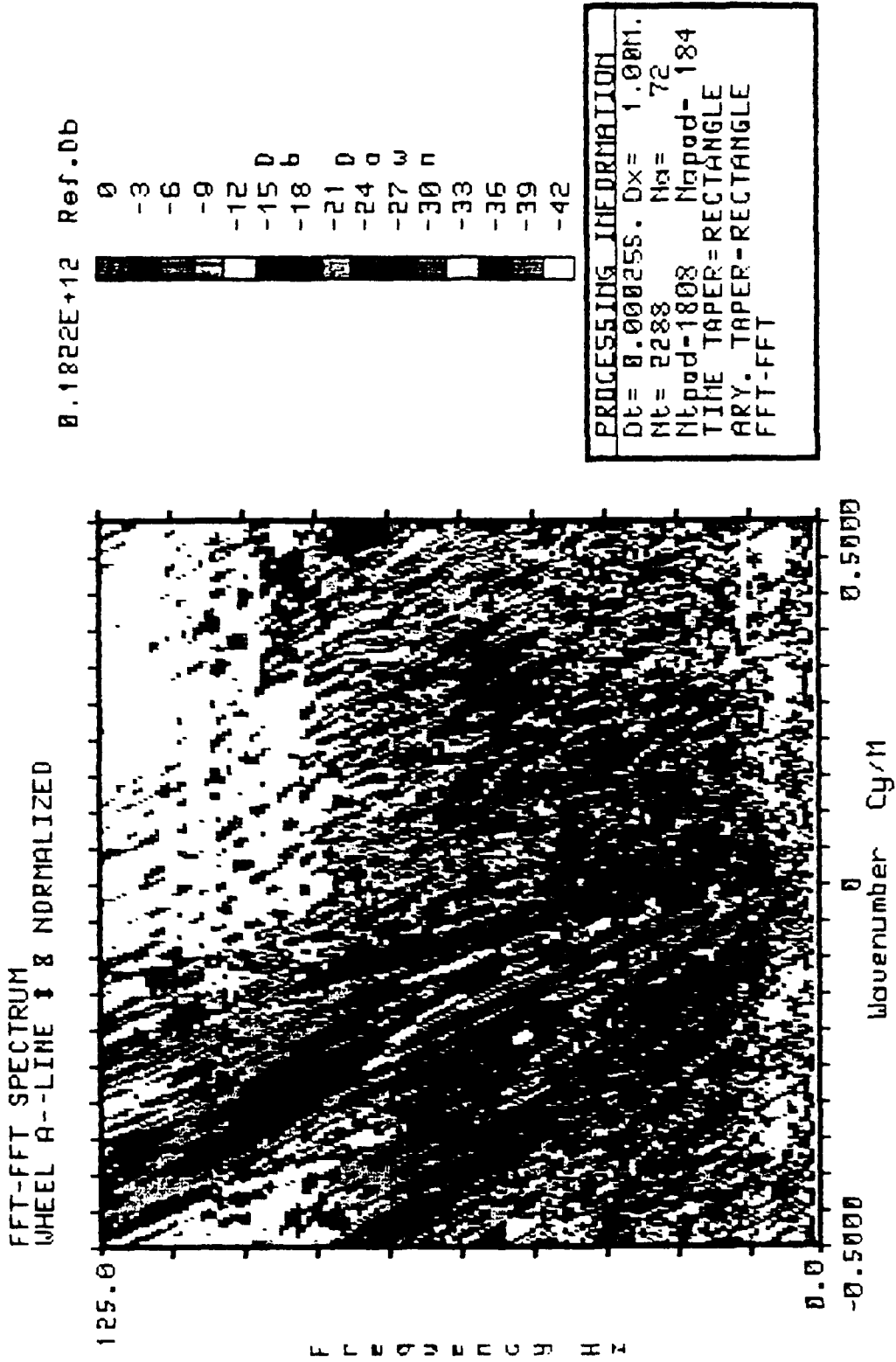


Figure 9: The FFT-FFT f-k spectra of wheel A, line 8.

average (MA), autoregressive moving average (ARMA), Prony and eigenanalysis models. Wavenumber estimates using these techniques were used to quantify the ability to separate overlapping signals, the resolution of single events and the effects of signal to noise ratio. AR wavenumber estimates using the Burg algorithm gave stable k estimates with no spectral leakage. It also produced good wavenumber estimates with a small number of spatial points and could separate the signal from nonstationary noise. The other methods all gave improved estimates over standard Fourier techniques and in some cases better than the AR-Burg spectra. All the other techniques suffered from problems of stability and thus were rejected as not providing a robust procedure that could be applied to a wide variety of data sets.

The autoregressive parametric model states that previous spatial points can be used to predict future ones, a good approximation for many wave propagation problems:

$$x(n) = \sum_{j=1}^p a(j) x(n-j) + u(n)$$

where p order of AR model
 $x(n)$ complex number in array position n
 $a(j)$ complex coefficient
 $u(n)$ complex white noise sequence

The power spectrum for this model is:

$$P_{\text{spec}}(k) = \frac{\widehat{\sigma^2} \Delta x}{\left(1 + \sum_{n=1}^p \widehat{a}_n e^{i2\pi kn \Delta x}\right)^2}$$

where $P_{\text{spec}}(k)$ power spectrum
 $\widehat{\sigma^2}$ variance of white noise
 Δx spatial sample interval

The AR parametric model represents the spectrum as a series of poles. The number of poles in the spectrum is equal to the number of coefficients in the recursion relation. This representation may be appropriate for wavenumber estimates as one would expect a finite number of arrivals from a plane layered velocity structure. Spectral estimation reduces to determining the number of poles or autoregressive coefficients and determining these coefficients. The order of the model, p , can be no greater than half the

number of array elements. Tests with synthetic data indicate that the choice of order depends on both the number of arrivals and the number of array elements. A single arrival was well characterized with 8 array elements, two different arrivals were separated with 12 array positions and three arrivals were separated with 24 elements.

The AR spectrum has three advantages. The spectral contour is quite sharp around the locations of the poles. When the number of array points is small the resolution is much greater than that produced by the periodogram. Finally the spectral detail can be controlled by the model order with the higher orders producing the greater detail already noted. The methodology has two disadvantages. The power cannot be directly estimated from the spectrum. High order models can produce spurious detail in the resulting spectra.

A number of methods for estimating the AR coefficients were investigated by Bogaards (1989). As a result of these tests, the algorithm suggested by Burg (1975), was chosen. This selection was made primarily on the stability of the procedure. A backward and forward prediction error is introduced. The autoregressive coefficients are determined by minimizing the sum of the squares of the forward and backward prediction errors using the Levinson recursion algorithm.

The frequency-wavenumber estimates using the new hybrid technique are reproduced in Figure 10. In this case the frequency estimates are made with simple Fourier analysis since the time windows contain a large number of points. The wavenumber estimates are made with the autoregressive technique and the Burg algorithm. In this example all 72 spatial samples are used and the model order is 30. Comparison of Figures 9 and 10 identify the merits of the AR wavenumber estimates. The individual arrivals are much more peaked in the AR estimates and thus can be more easily separated at the low frequencies. The individual phases that include the direct P arrival, head wave, shear wave/higher mode surface wave and fundamental surface wave are identified in the f-k spectrum. There is clear indication of the dispersive nature of the surface wave in this representation. The other phases show little or no dispersion.

The window effects in the spatial domain are quite apparent in Figure 9 where significant energy is found for both negative (away from the source) and positive (towards the source) wavenumbers. Since we are trying to separate stochastic and deterministic wave propagation effects one might interpret the positive wavenumber energy in terms of a scattering process. Comparison with the model based estimates shows that much of the positive wavenumber energy in the FFT-FFT estimate is eliminated and thus must be

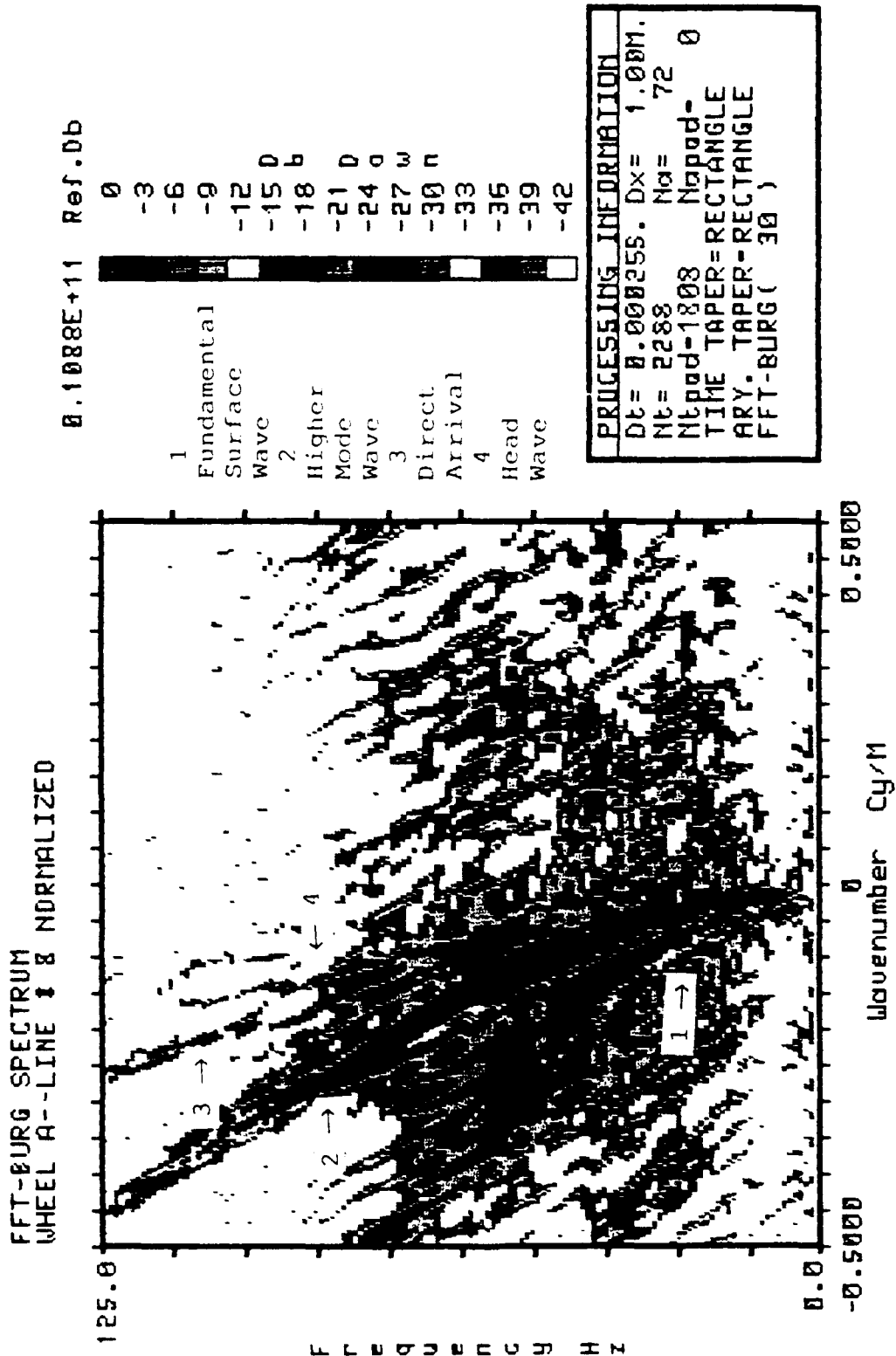


Figure 10: The FFT-AR Burg spectra of wheel A, line 8. The Burg order is 30.

attributed to the windowing effects. Some positive wavenumber energy remains in the model results and warrants further investigation.

As noted in the introduction to the hybrid f-k estimators, they can be applied to a small number of spatial samples and thus the development of the waveforms documented across the array. Twenty-two vertical seismograms between 35 and 56 m were used to estimate the f-k spectra in Figure 11 with a model order of 10. The four individual arrivals are again quite easy to identify with little contribution from other waves. The surface waves begin to break up at around 50 Hz in this distance range although there is energy to beyond 60 Hz. The energy in the positive wavenumber domain appears at this 50 Hz frequency and has a velocity estimate of 210 m/s. This result suggests that the scattered energy is traveling as S waves in the top layer.

The fundamental mode surface wave is the dominant arrival observed in the waveforms (Figure 5). As demonstrated in the f-k spectra (Figure 11), the waveform begins to degrade above 50 Hz which is representative of a wavelength between 4 to 5 meters. These high frequency surface waves traveling primarily in the near-surface layer are interacting with the intermittent caliche lenses resulting in scattering. The energy in the positive wavenumbers represents this scattered energy.

The f-k spectra from wheel A line 8 (Figure 4) were interpreted in terms of a direct arrival, refracted arrival, higher mode surface wave and fundamental surface wave (Figure 12). Linear fits to the direct and head wave arrivals give velocities of 480 and 760 m/s. The direct arrival estimates are consistent with the time domain measurements while the relative fast refraction velocity is high but is in the fast direction (NW) identified by the arrival time in the azimuthal study (Figure 7a). This result shows that these high resolution f-k estimators can be used to identify subtle azimuthal effects in these shallow geologic environments.

The fundamental and higher mode surface waves can also be interpreted in terms of a dispersive model with the determination of both phase and group velocities. Since the dispersion curves have been so well defined with this technique, a third order polynomial was fit to the f-k estimates for the surface waves. The phase velocity for the media is determined by taking the derivative of this function:

$$v(k) = 256 - 980k + 1683k^2$$

The group velocity is calculated from the phase velocity:

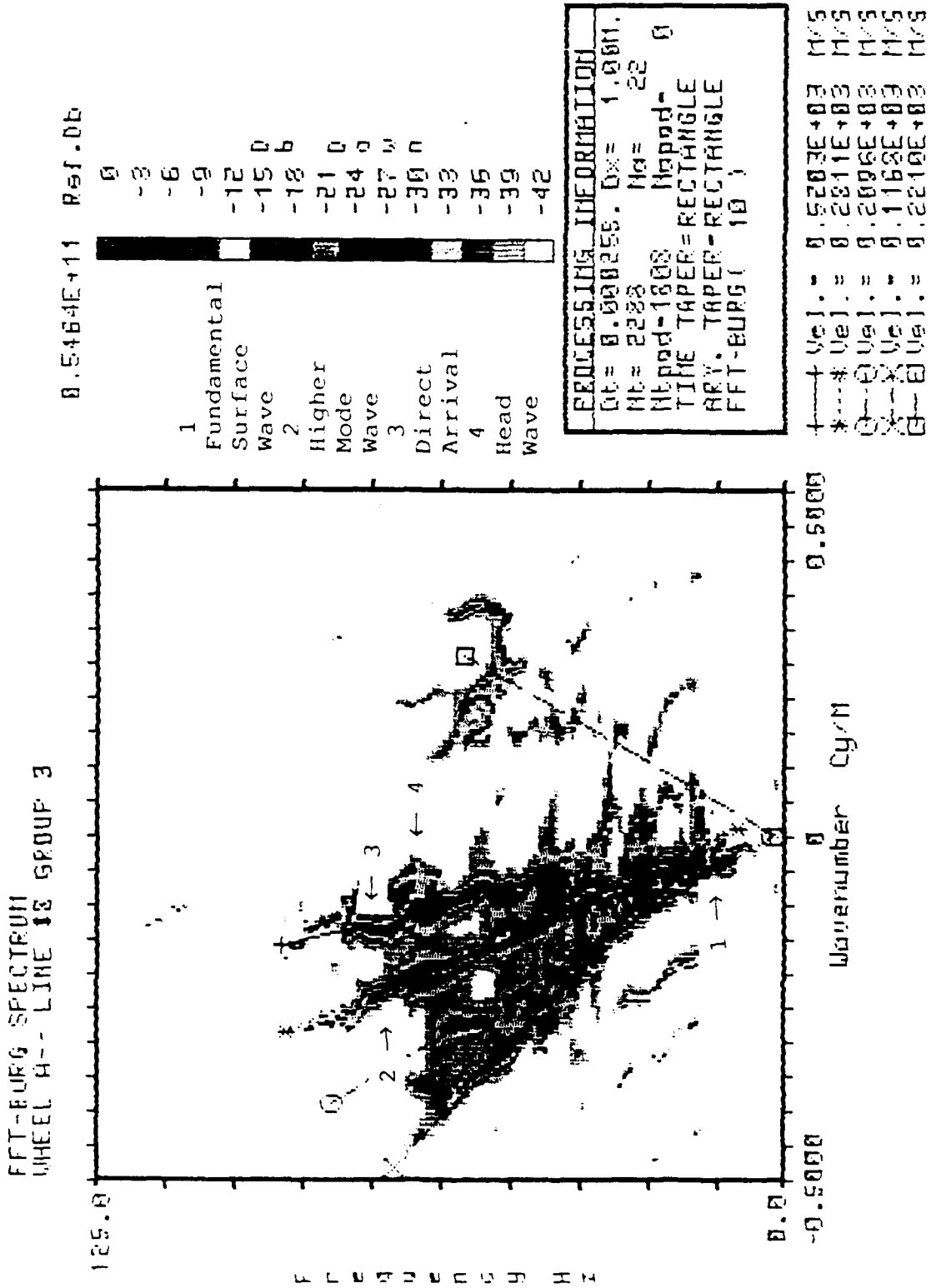


Figure 11: The FFT-AR Burg spectra of wheel A, line 8. Data between the distance ranges of 35 to 56 m. The Burg order is 10.

WHEEL A LINE • 8

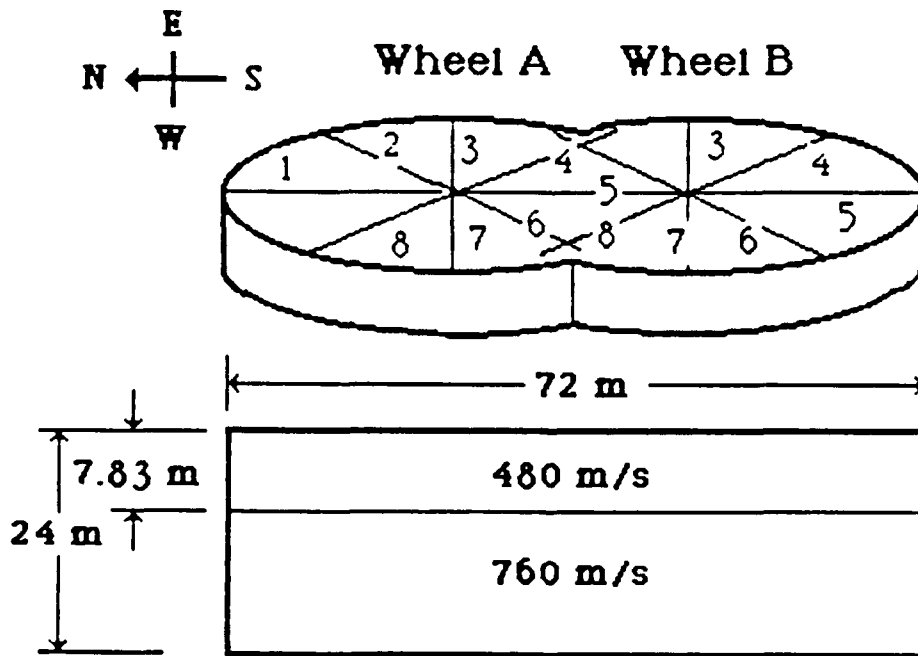
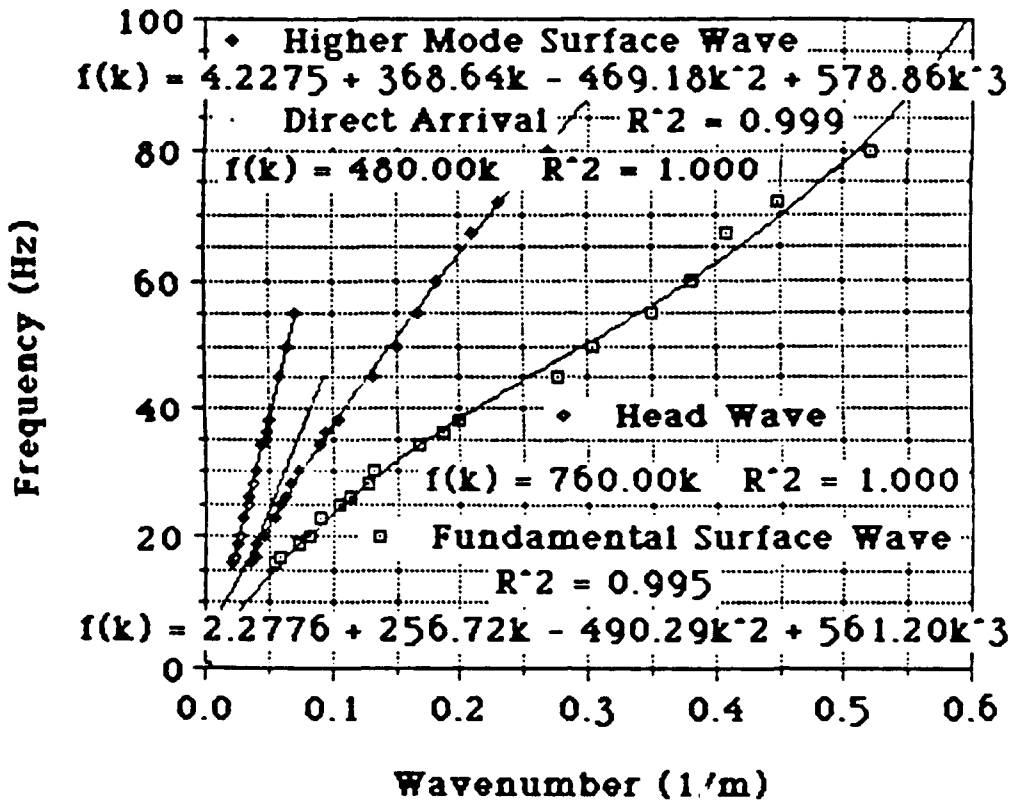


Figure 12: The interpretation of f-k spectra in terms of direct arrival (line), head wave (open diamonds), higher mode surface wave (solid diamonds) and fundamental mode surface waves (open squares).

$$U(k) = V(k) + k \frac{dV(k)}{dk}$$

The resulting phase velocity for the site becomes:

$$U(k) = 256 - 1961k + 5051k^2$$

The results of this analysis for both the fundamental and higher mode are summarized in Figure 13. Extension to short wavelengths is difficult due to the scattering effects already noted.

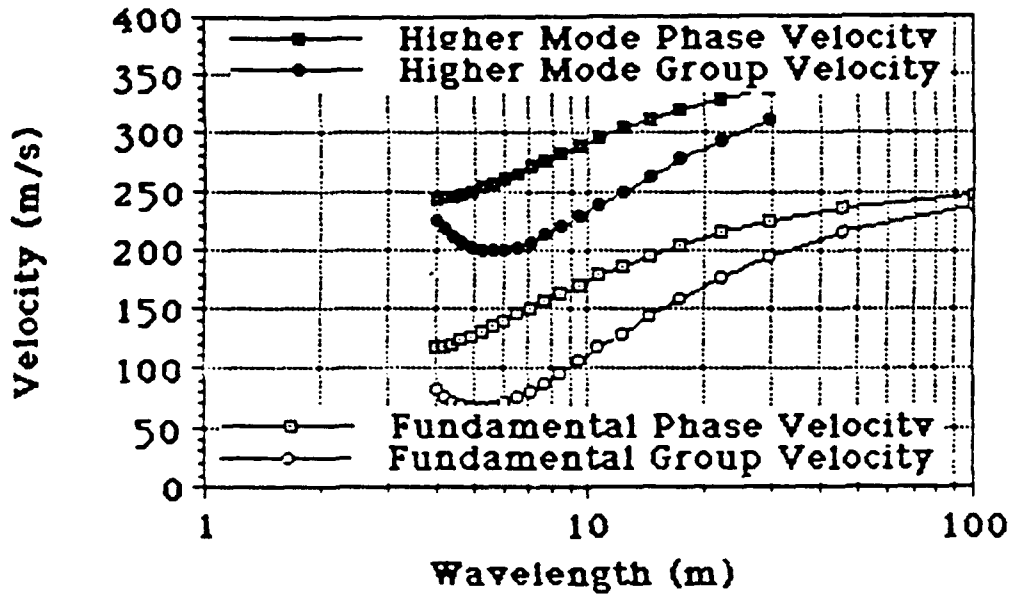
3. Statistical Characterization:

The experimental plan was designed to constrain both the deterministic and stochastic portions of the wavefield. The arrival time and f-k analysis are used primarily in the deterministic model. They provide secondary information such as the wavelengths at which f-k estimates degrade and the existence of energy traveling down the array towards the source attributable to the scattering process. The circular arrays that are described in Figure 4 were designed to quantify the azimuthal variations in the wavefield that can be attributed to scattering.

The first step in this characterization is the calculation of a mean seismogram for each range at which data were recovered. There are eight seismograms at each range that contribute to this calculation. The mean seismograms for the entire array are reproduced in Figure 14. First arrival time picks from the mean data are consistent with single station results yielding a top layer velocity of 463 m/s and a velocity for the deeper material of 699 m/s. As in the single station data, there is a hint of a relatively slow, very shallow layer. This layer is so thin that it is difficult to resolve with the existing data set. Careful inspection of the individual waveforms in Figure 14 indicates that the stacking procedure has decreased the frequency content of the latter arriving phases as well as improved the apparent coherence among adjacent records. The first arriving waves are less degraded in this stacking procedure.

The time domain stacking process takes into account both the phase and amplitude differences that are observed in the data. An alternate characterization of the media is to complete the stacking in the frequency domain. If the phase information is of secondary importance and energy is of primary interest then stacking of the modulus in the frequency domain as a function of range is appropriate. Following the work of Reinke and Stump (1988) each seismogram is Fourier transformed and the modulus computed.

WHEEL A LINE # 8 -SURFACE WAVES



$$U(k) = v(k) + k \frac{dv(k)}{dk}$$

WHEEL A LINE # 8 -SURFACE WAVES

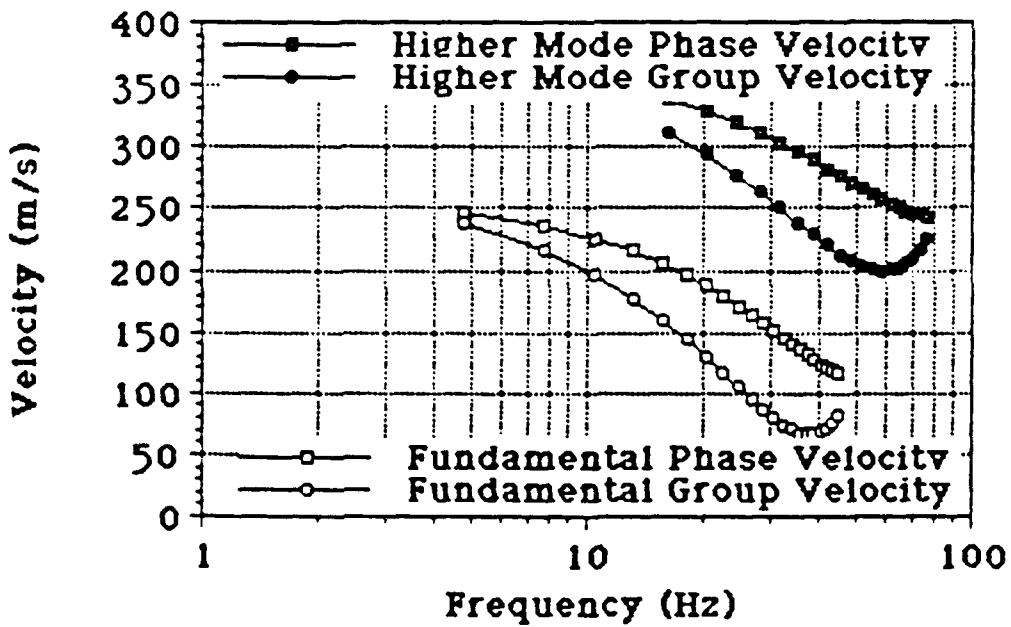
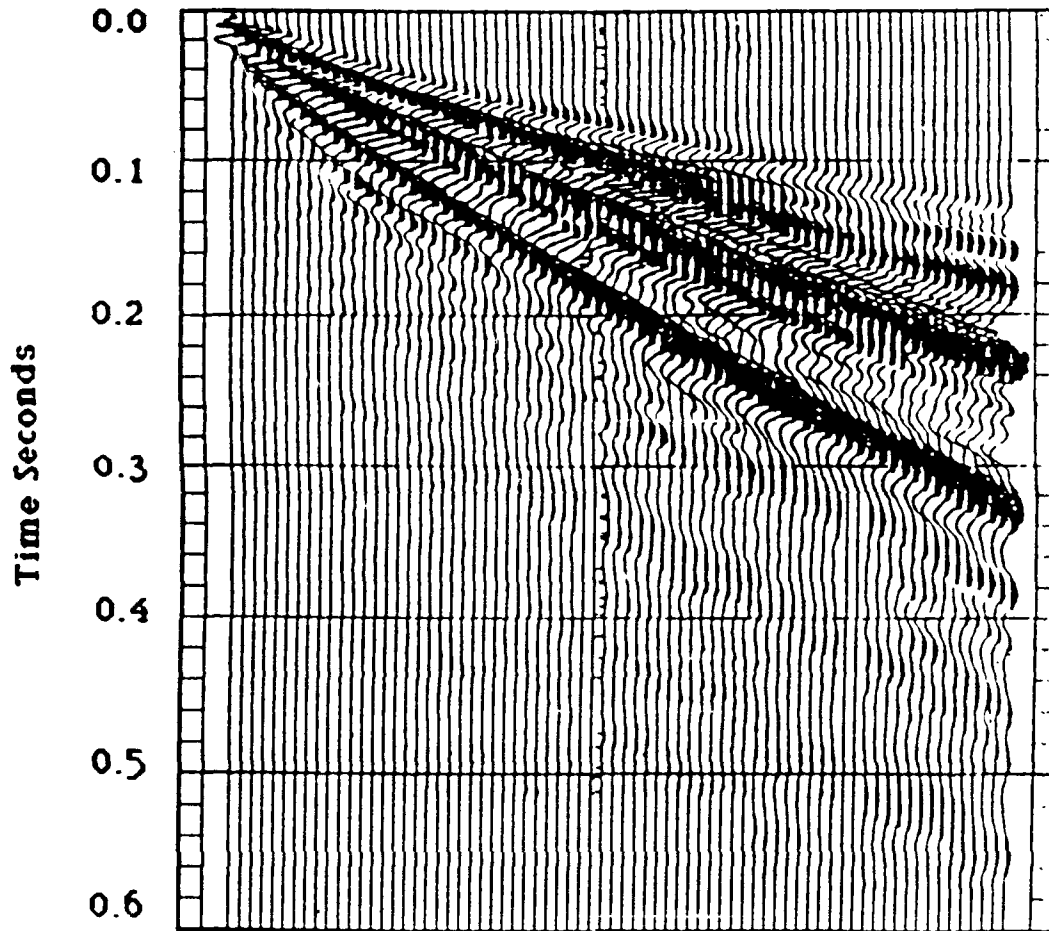


Figure 13: Phase and group velocities for the surface waves characterized in the f-k estimates. The velocities are plotted against wavelength (top) and frequency (bottom).

WHEEL A MEAN LINE

$Dx = 1 \text{ m}$ $Dt = 0.25 \text{ ms}$



WHEEL A LINE # 8

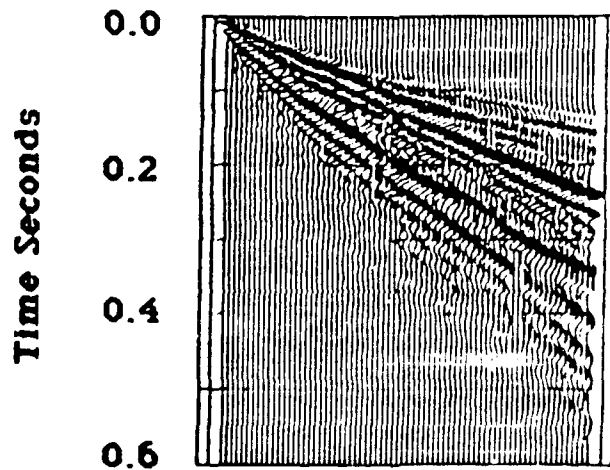


Figure 14: The mean seismograms for wheel A calculated from the data observed at all azimuths. The seismograms span the distance range of 1 to 72 m.

A mean spectral level as well as a variance is computed for each frequency at each range. A relative measure of variability known as the coefficient of variation (CV) is introduced following Bethea et al. (1983) in order to compare the variation in one frequency band with that found in another. The coefficient of variation is the standard deviation of the spectral estimate normalized by the mean:

$$CV(f,r) = \frac{\hat{s}(f,r)}{\hat{\mu}_M(f,r)}$$

where $\hat{s}(f,r)$ is the standard deviation of the mean modulus estimate at frequency f and range r

$\hat{\mu}_M(f,r)$ is the mean modulus at frequency f and range r

The advantage of this estimate of data variability is that all records at a particular range (eight for our experimental design) are combined into a single number. The CV value as a function of range and frequency for wheel A is reproduced in Figure 15. It is easy to identify the increasing variability in the wavefield as the waves propagate away from the source. At small source-receiver distances the CV values are quite small (<0.3) to high frequencies (70 Hz at a few meters). The location of this boundary decreases with increasing source-receiver distance in an exponential fashion reaching a transition below 20 Hz at a source-receiver offset of 72 m. Reinke and Stump (1991) report similar CV values from strong motion records of explosive sources at the same location as the site characterization data reported here. The site characterization data using the Betsy source is low stress but yet it gives CV values which are in agreement with those observed in the strong motion data. This comparison validates the site characterization technique for explosive motion fields and indicates the importance of scattering in these environments.

The mean spectra resulting from Fourier transforming all eight seismograms at each range and calculating the modulus are given in Figure 16. In this case phase differences between the individual arrivals are not taken into account. The spectra decay rapidly with range reflective of geometric spreading and attenuation. These spectra support the same decrease in signal bandwidth documented in the coefficient of variation plot. At the farthest range there is energy above background noise at high frequencies but it is the high amplitude energy at the long periods which have the smallest coefficient of variation and thus the most similarity across the test

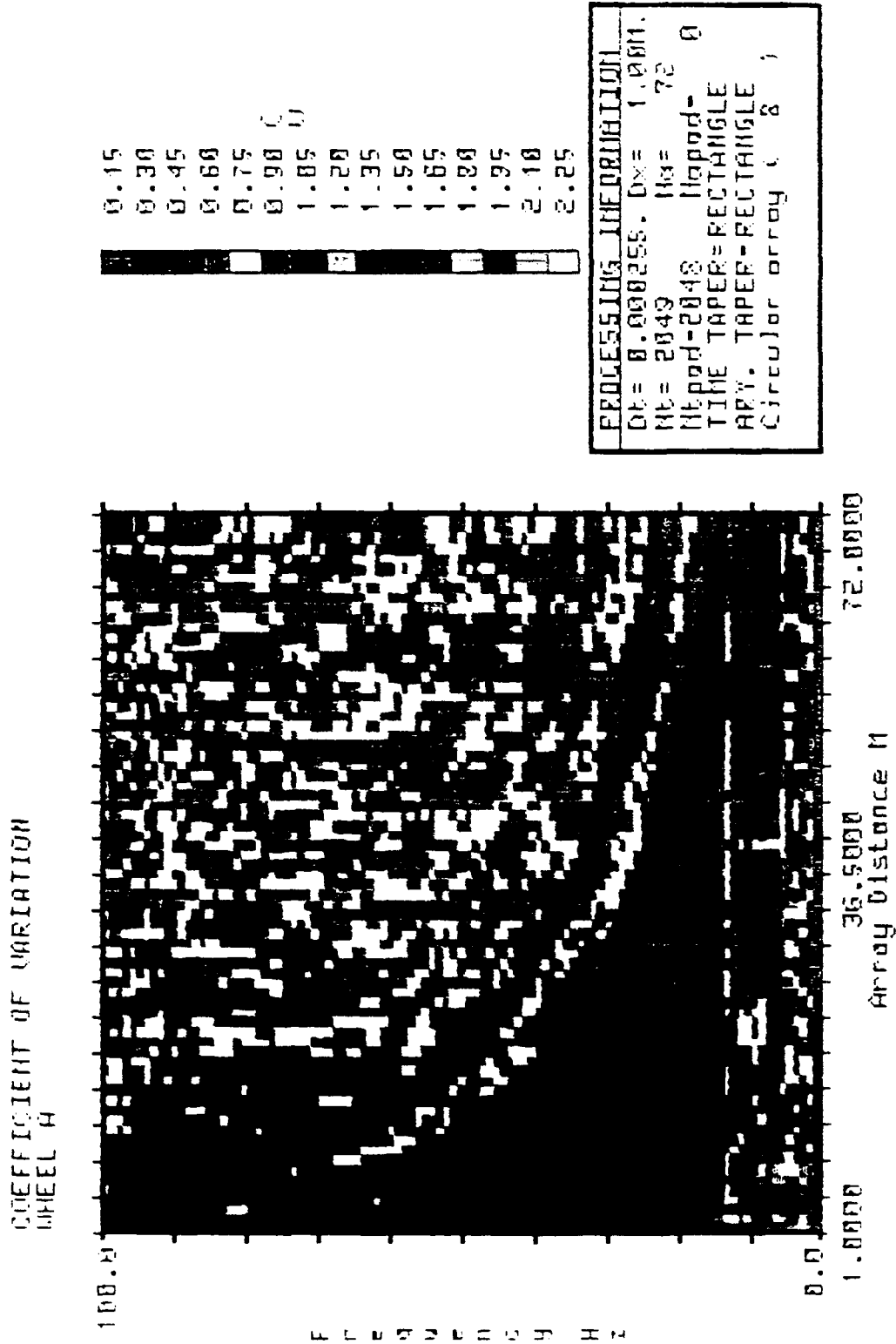


Figure 15: The coefficient of variation (CV) calculated from the modulus for wheel A. The CV is a function of frequency and range with the color in the plot representative of the amplitude.

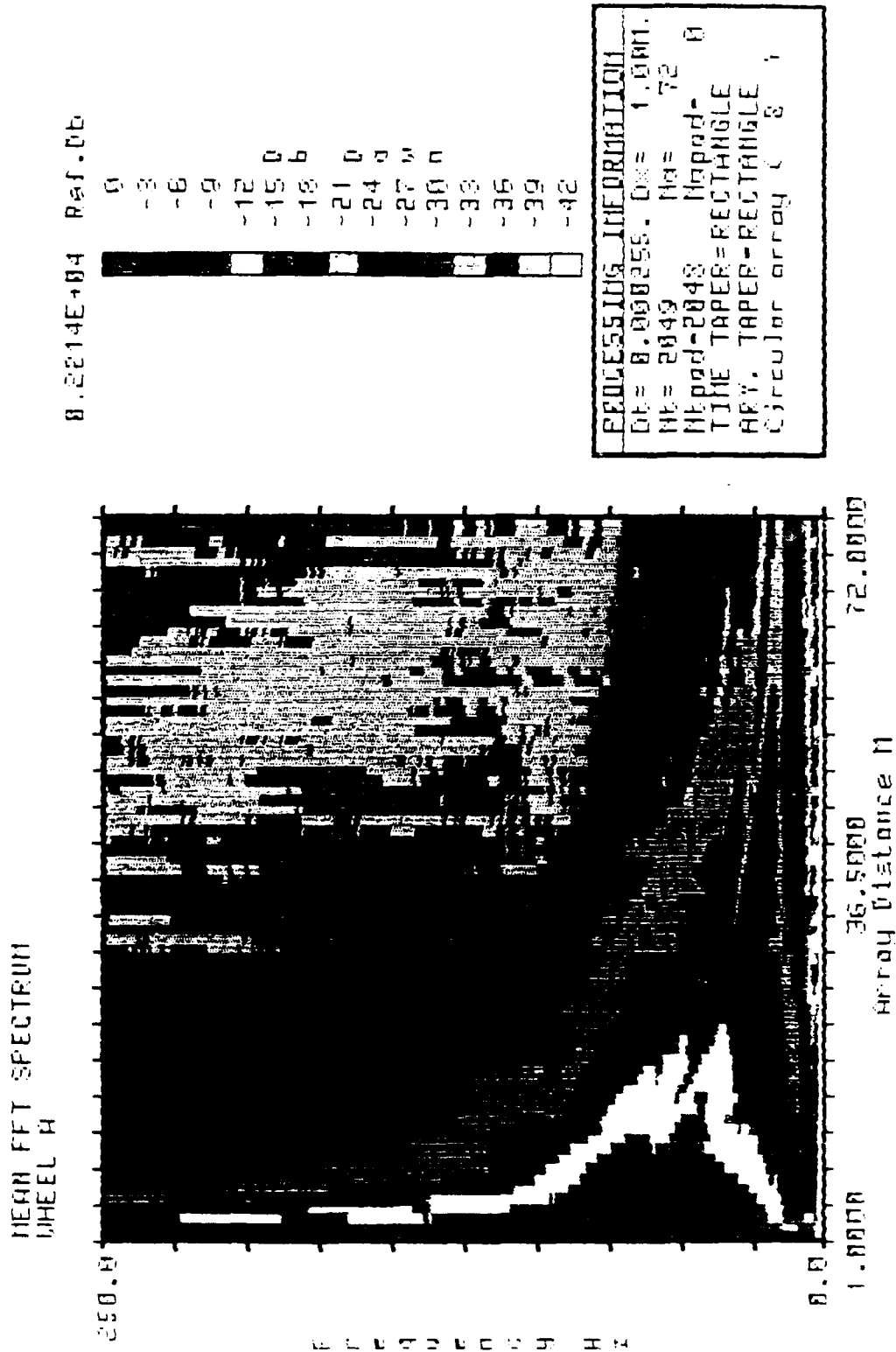


Figure 16: The mean of the different spectra calculated at each range for wheel A.

site. The mean spectra decreases rapidly above 20 Hz at the same frequency where the CV value increases.

The effect of the stacking procedure is further illustrated in the frequency-wavenumber domain. The hybrid f-k spectra for line 8, wheel A are given in Figure 17 for a relatively low order Burg model of 16. In this representation the fundamental and higher mode surface waves are well developed along with the body waves. There is significant energy in the right hand quadrant of the plot representing energy traveling towards the source. The mean time domain data from all of wheel 8 (Figure 14) was used to create a second f-k estimate reproduced in Figure 18. Comparison of the two estimates first indicates the existence of a strong airblast arrival on the mean line estimate. The dirt berming procedure to eliminate the air blast from the Betsy was only begun on line 8 of wheel A and thus the rest of the radial arms in wheel A have a strong airblast arrival, fortunately at relatively high frequencies. The second and more important difference between the two f-k spectra is the elimination of most all of the energy at positive wavenumbers in the mean data. This result supports the contention that this energy is scattered which would be reduced in the computation of mean seismograms.

The computation of wavefield energy in combination with a separation of deterministic and stochastic effects can be used to separate intrinsic attenuation from scattering effects. The energy can be calculated in either the time or frequency domain with Parseval's Theorem;

$$\int (v(t))^2 dt = \frac{1}{2\pi} \int (V(\omega))^2 d\omega$$

Flynn and Stump (1988) used the above relationships to quantify the energy in distinct waves in the frequency domain. These tools will be used in this study to quantify the percent of total energy contained in the variable part of the wavefield. Rather than calculate total energy the energy flux at the seismometer was computed as:

$$F = \rho C_0 \int (v(t))^2 dt$$

Application of Parseval's Theorem allows the calculation to be completed in the frequency domain. The energy flux representations that follow were all calculated in the frequency domain with the energy summation beginning at the high frequencies and integrating to the low frequencies. The energy associated with CV values larger than 0.3 is compared to energy for waves with CV values less than or equal to 0.3. The CV value of 0.3 was taken as

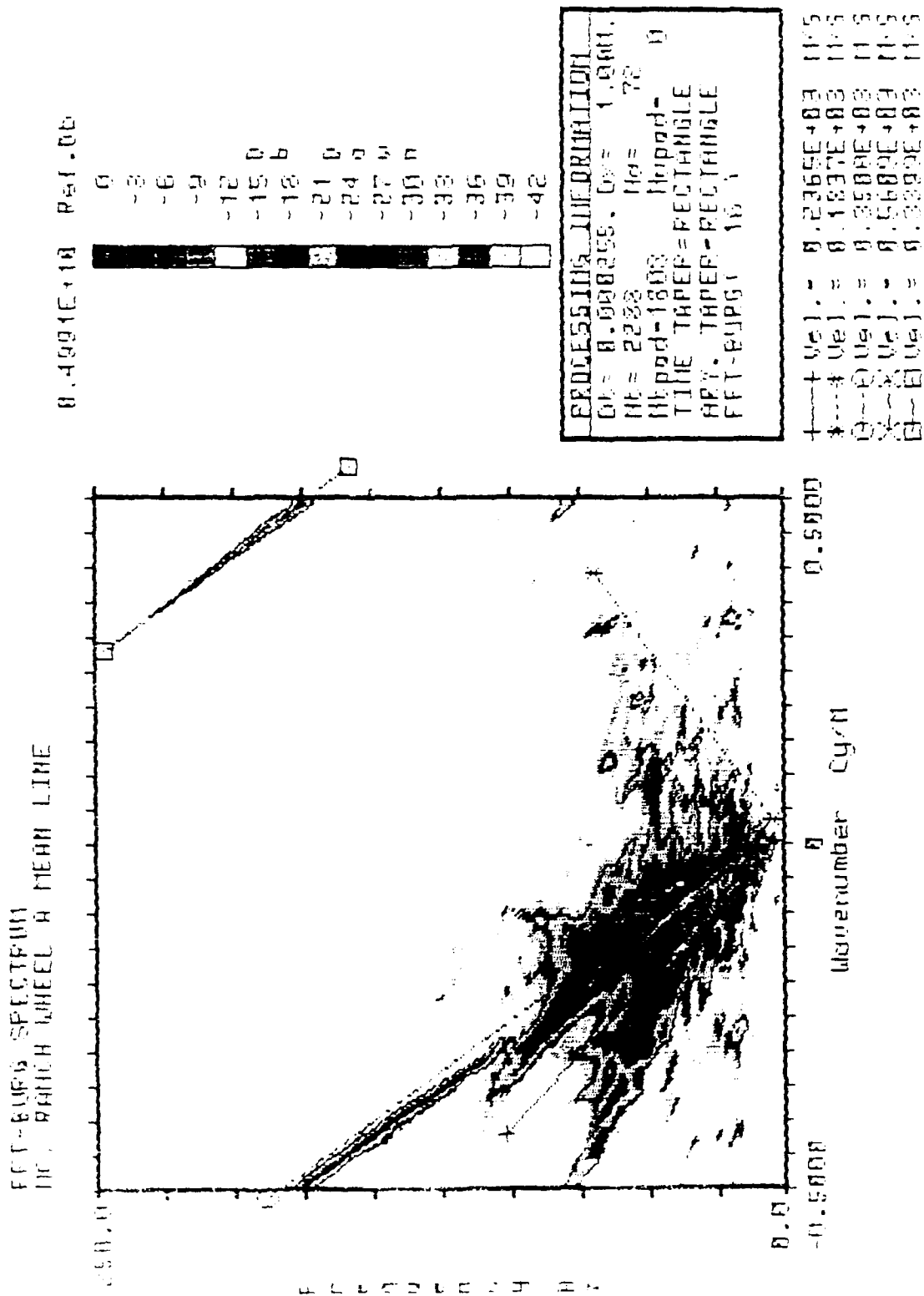


Figure 17: The FFT-AR Burg f-k spectra for the mean seismograms (Figure 14) from wheel A. The Burg order is 16.

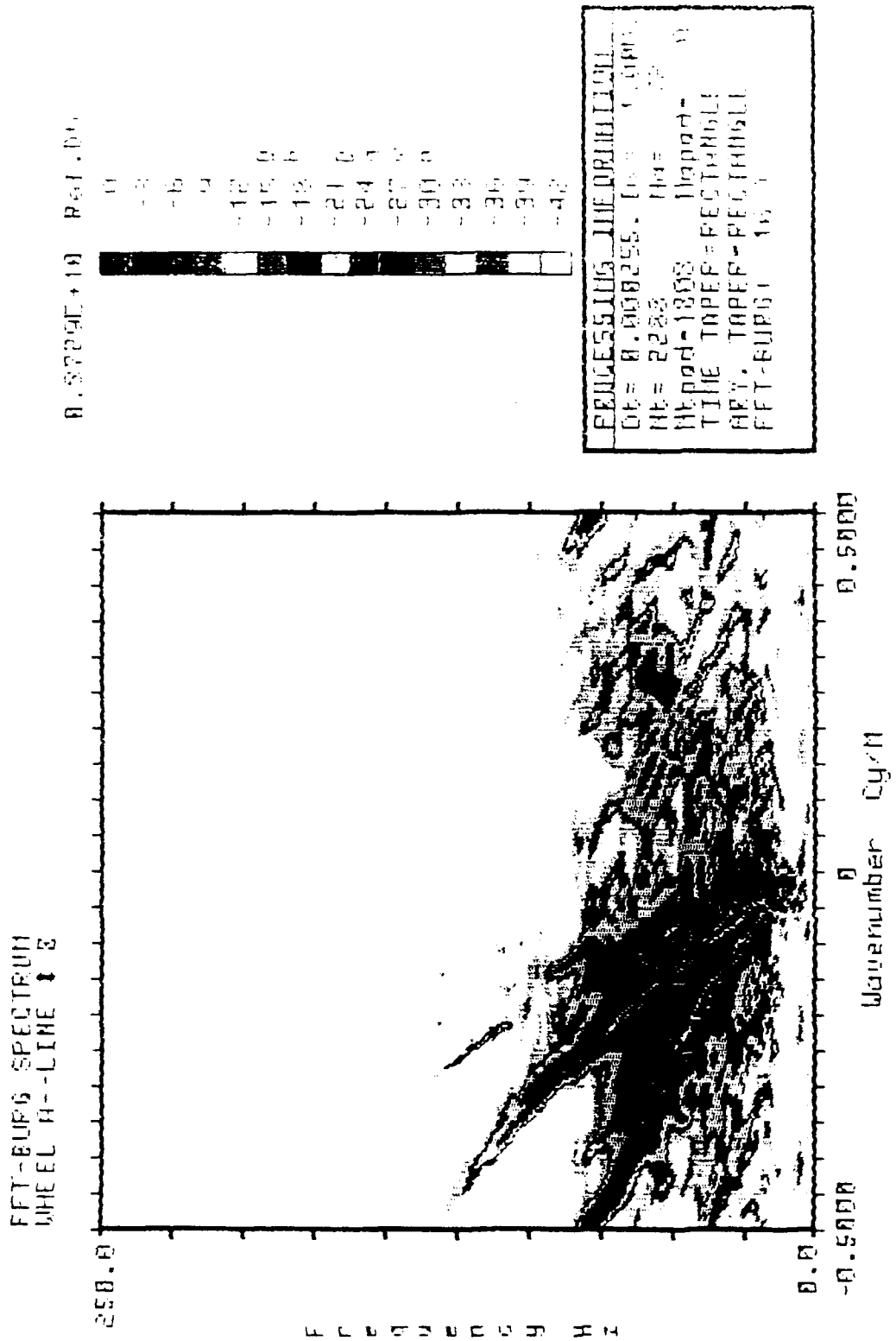


Figure 18: The FFT-AR Burg f-k spectra for line 8 of wheel A. The Burg order is 16.

the separation between deterministic and stochastic wave propagation effects. CV values in Figure 15 were used in the wavefield separation. The source repeatability test analysis shows that only 0.25% of the energy was attributable to CV values in excess of 0.3. This results supports the Betsy source as quite repeatable to frequencies as high as 175 Hz.

The normalized energy plot for the data from line 8, wheel A is given in Figure 19 where the total energy down to a particular frequency is given as a percentage of the total energy with the integral beginning at high frequencies and progressing to low frequencies. These energy contours indicate the strong role that the high frequencies play in the total energy with the 90% energy contour represented by the transition from -1 to 0 dB. This transition occurs at approximately 45 Hz at the closest source-receiver range and near 20 Hz at the farthest range.

For comparison the energy contours for the mean line from wheel A are reproduced in Figure 20. Superimposed on the figure are the CV values of 0.3 (open squares) taken from Figure 15. It is interesting to note that this CV boundary tracks closely the energy boundary where 40% of energy is associated with $CV < 0.3$ and the rest of the energy above this value.

The difference in energy between line 8, wheel A and the mean line further accentuates the effect of scattering as documented in line 8 and averaged out in the mean line. Figure 21 quantifies the difference between the two energy calculations. Wheel 8 is found to be more energetic as frequency and range increases which is consistent with a scattering model. The lower boundary which identifies a 40% difference between the mean energy spectra and the wheel 8 energy spectra follows the $CV=0.3$ contour approximately. This representation corroborates the $CV=0.3$ contour as an upper bound for separating deterministic and stochastic effects. It is an upper bound since much of the higher frequency energy may still be deterministic but it is well mixed with stochastic effects.

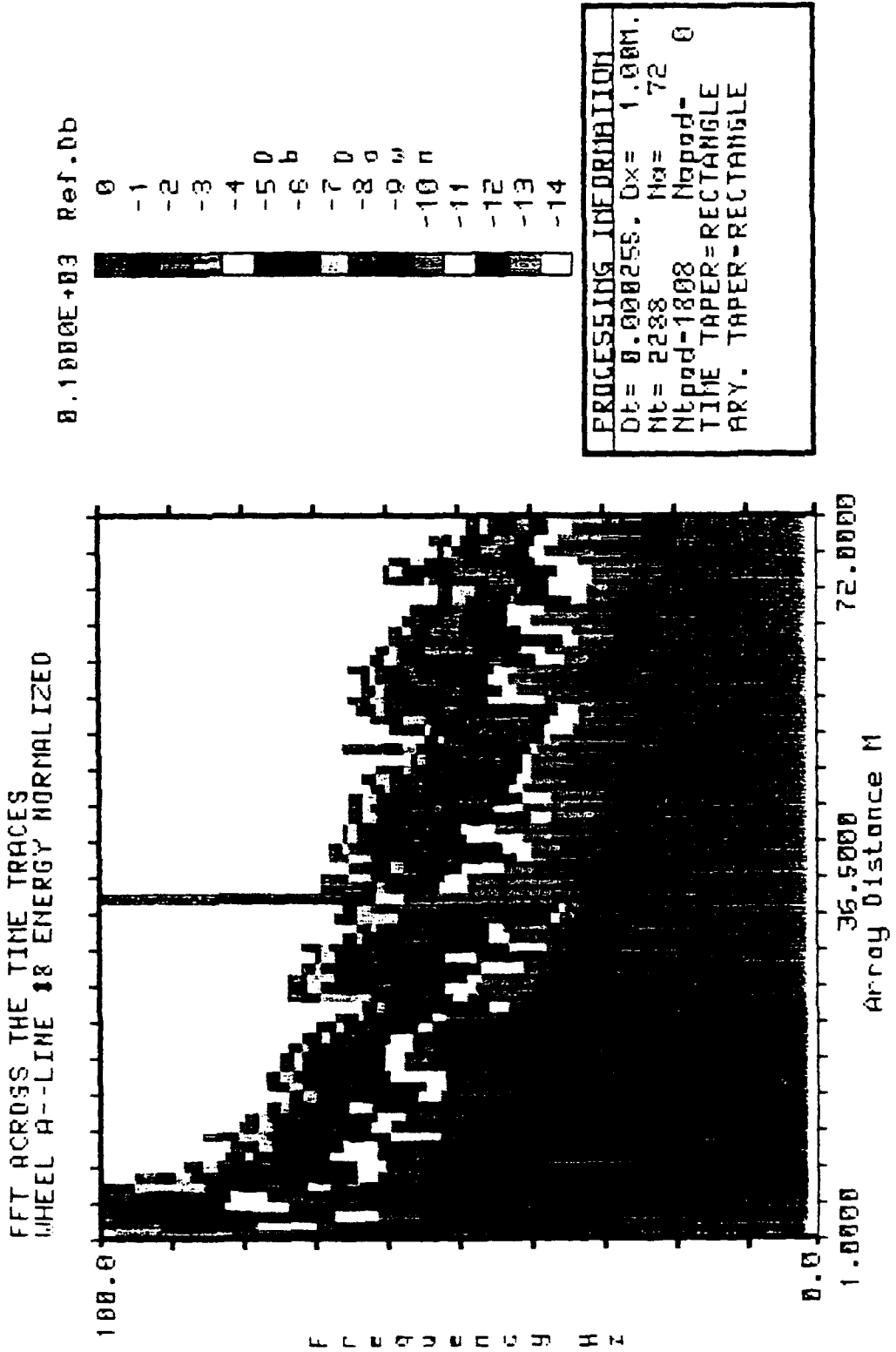


Figure 19: The normalized energy flux from wheel A, line 8 displayed as a function of frequency and range. The energy is integrated from high frequency to low.

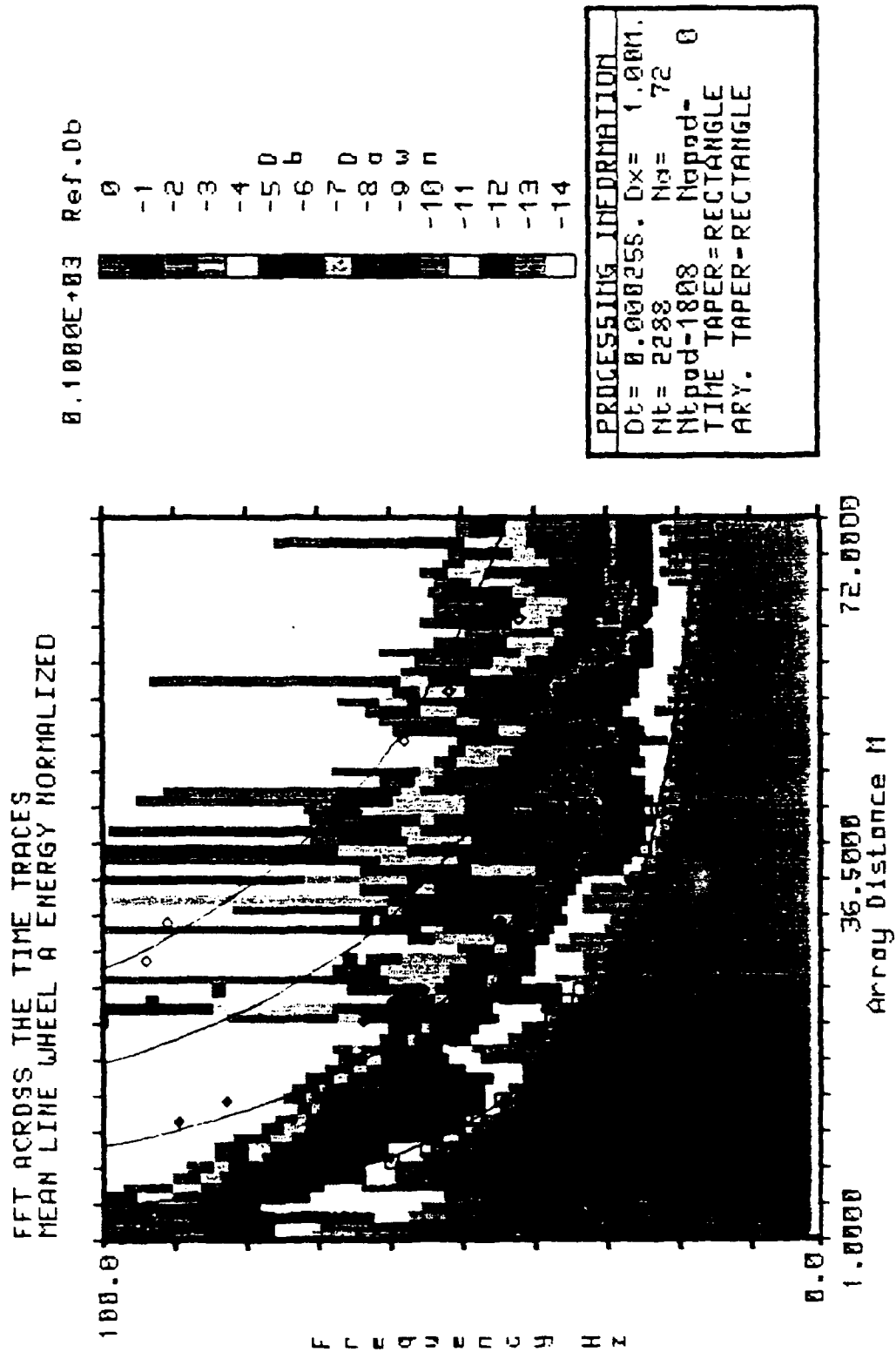


Figure 20: The normalized energy flux from the mean line of wheel A. The energy is integrated from high frequency to low.

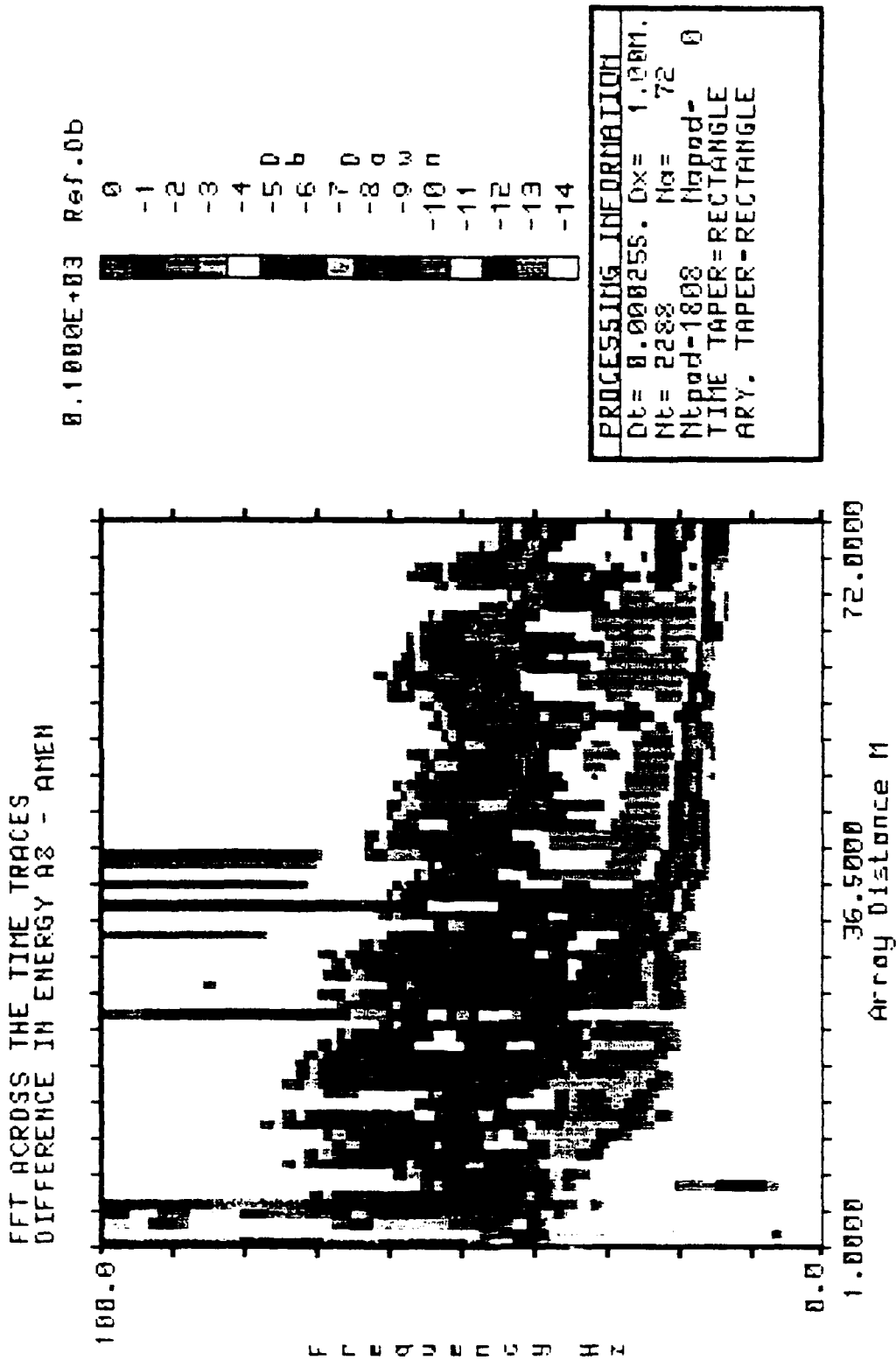


Figure 21: The difference between the normalized energy flux in line 8, wheel A and the mean line, wheel A.

IMPLICATIONS

A site characterization procedure that involves both a new experimental procedure and a number of techniques for separating stochastic and deterministic wave propagation effects has been applied to the determination of attributes of the shallowed weathered zone. A two layer model is indicated by the travel time data. The surface material has an average velocity near 500 m/s. The station spacing was such that a very thin surface layer (<1m) might go undetected in the survey. Second layer velocities ranged from 650 to 750 m/s. Variation in the top layer thickness between 4 and 6 m is consistent with these second layer velocity differences. The data supports a moderate dip to the west .

High resolution frequency-wavenumber estimates utilizing a hybrid FFT and AR-Burg routine separated the direct, refracted and surface waves. This information was used to further constrain the site characterization now with complete waveforms. Direct arrival velocity was found to be 480 m/s and the refracted arrival traveled at 760 m/s which was in agreement with the velocity determined from first arrivals for line 8, wheel A. These high resolution f-k estimates provided the opportunity to separate not only the direct and refracted P waves but also the fundamental and higher mode surface waves. Phase and group velocities were recovered from the surface wave data. Comparison of standard f-k estimates using the Fourier Transform to make the k estimate with the new modeling results demonstrate how side lobes from the windowing process can not only obscure closely spaced arrivals but also put energy in the positive wavenumber quadrant characteristic of energy traveling towards the source (back scattering). The hybrid f-k estimates eliminate this windowing effect although some energy remains in the positive wavenumber quadrant. When mean time domain seismograms are computed from the azimuthal array around the sources these scattering effects are averaged out and the f-k spectra show no evidence of the scattered energy.

The coefficient of variation was found to be a useful tool for quantifying the azimuthal variation in the waveforms at the test site. This mean normalized variance can be applied in either the time or frequency domain but was primarily used in the frequency domain in this study. Ultimately the variability is to be mapped into wavenumber so the frequency domain characterization was chosen. Previous investigations with synthetic data sets (Bogaards, 1989), analysis of the source repeatability studies and the huddle tests suggest that a threshold value for the CV of 0.3 could be taken as a conservative boundary separating stochastic and deterministic effects. At the McCormick Ranch Test Site this boundary was found to be range dependent and best modeled as an exponential function of range. The

boundary is 80 Hz at 5 m and decays to 20 Hz at 80 m. This transition frequency was also identified by comparing the spectra of a single line (line 8, wheel A) with the spectra from the mean line for all of wheel A as well as an energy boundary (Figure 22).

The last step in the data analysis is the linking of the stochastic characterization of the test site with the wavefield separation in the f-k estimates. If scattering is the dominant mechanism leading to the variations observed then the effect should be wavelength dependent. The phase velocity determinations provide the necessary information through f to map the stochastic results into the wavelength domain. Figure 23 is the mapping of the CV boundary into wavelength and distance space for the fundamental and higher mode surface waves. These results indicate that at a range of 20 m that the fundamental mode surface waves with wavelengths greater than 5 m show little variability. At a range of 72 m the wavelengths longer than 18 m are the ones that show little variation. If the stochastic effects are truly wavelength dependent then the stochastic boundary identified in Figure 23 is conservative for the other phases. Using the phase velocity results for the other phases, wavefield boundaries separating stochastic and deterministic effects for the other arrivals are given in Figure 24. These curves are superimposed on the mean line spectra in Figure 20 and seem to coincide with increases in deterministic energy in this representation.

WAVE FIELD BOUNDARY

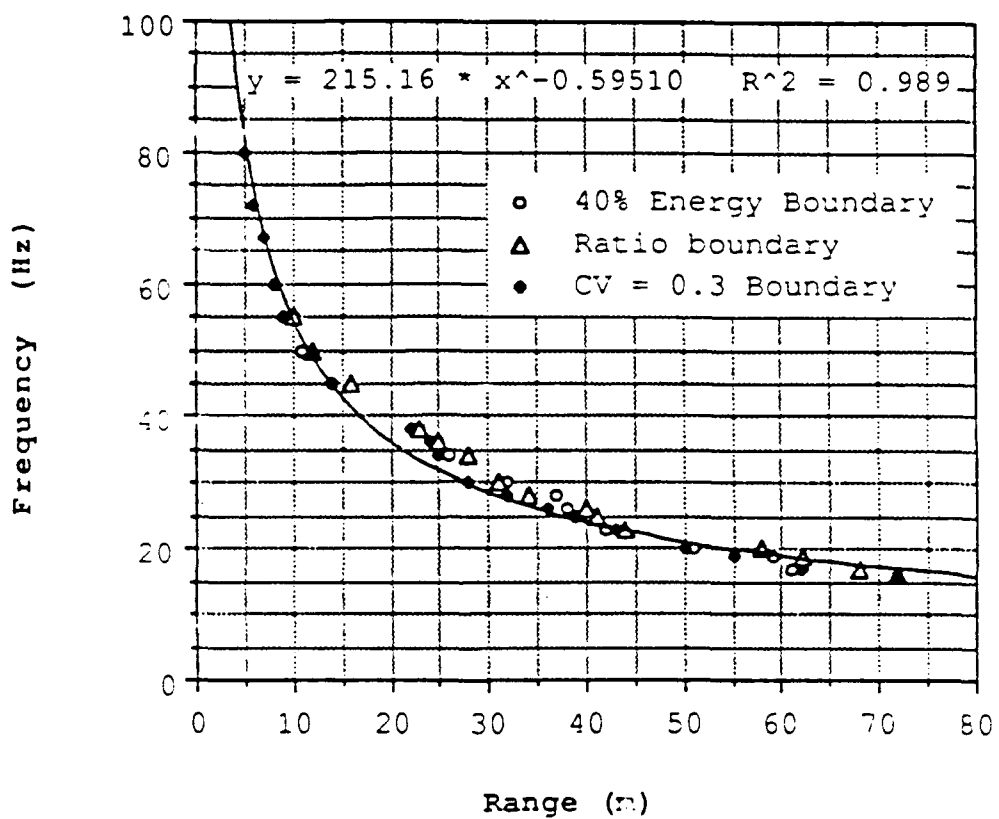


Figure 22: The frequency-offset representation of the Coefficient of Variation boundary (CV=0.3).

CV BOUNDARY WHEEL A

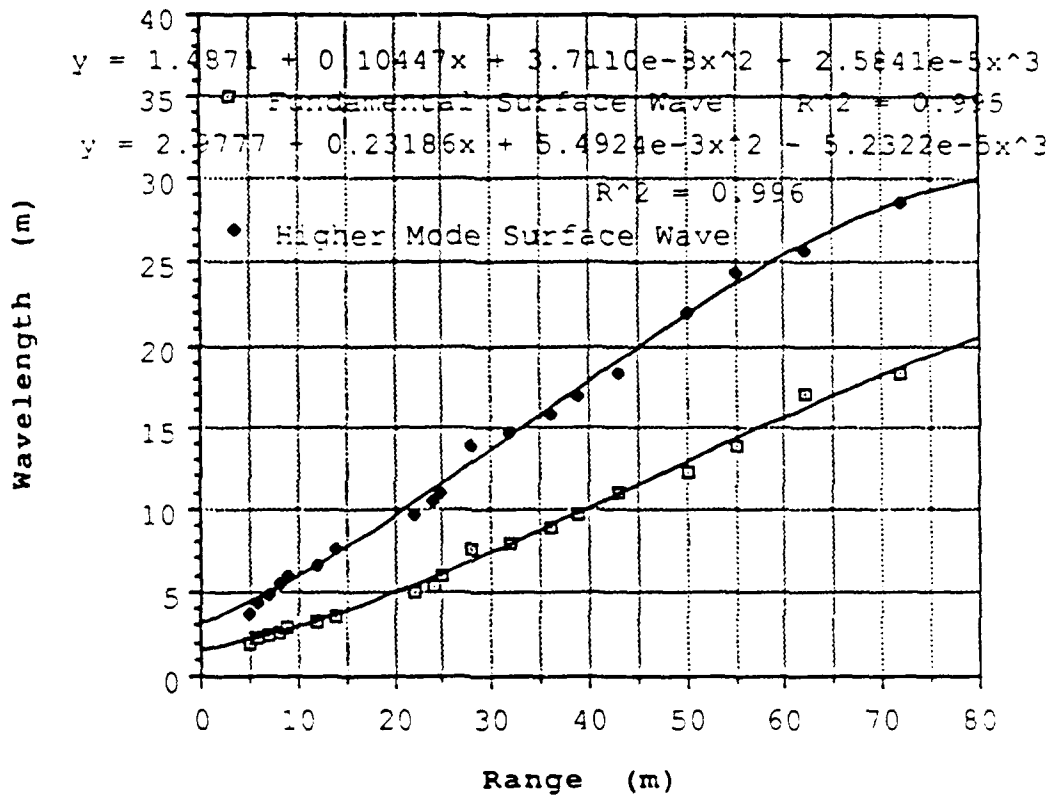


Figure 23: Wavelength boundary for the fundamental mode surface wave (open squares) and higher mode surface wave (solid diamonds) established from the CV=0.3 boundary. The CV frequency boundary is mapped to wavelength using the f-k estimates.

WAVE FIELD BOUNDARY

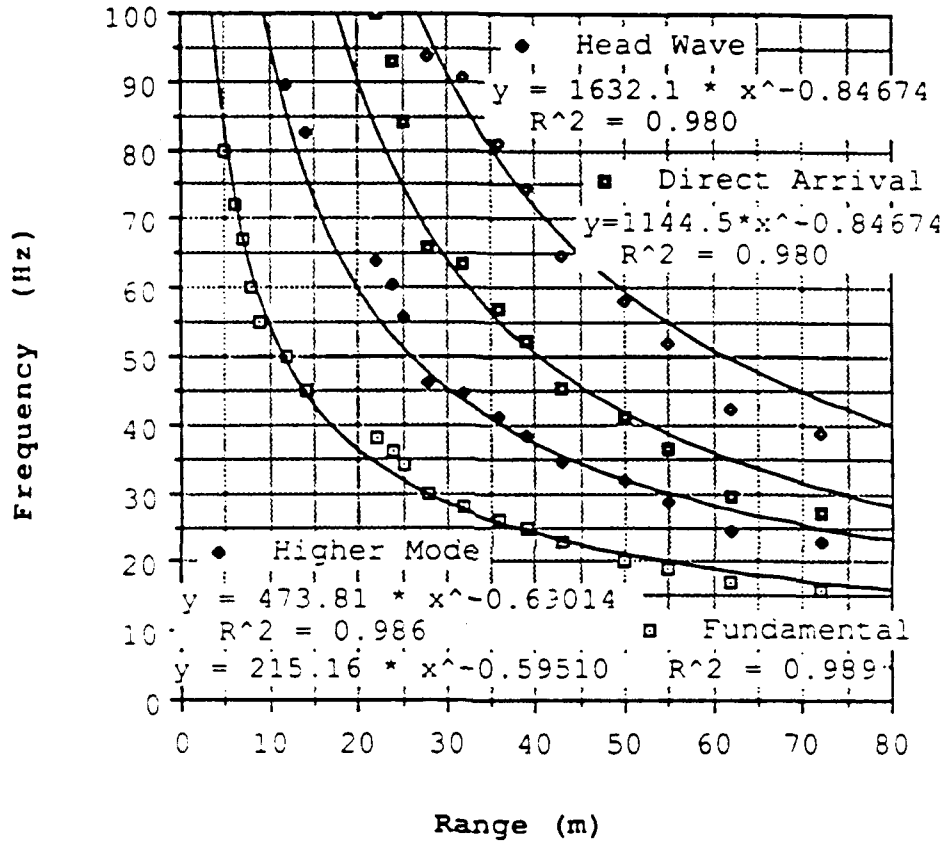


Figure 24: The wavefield boundary defined by $CV=0.3$ is mapped from the fundamental surface wave to the other arrivals identified through travel time analysis and $f-k$ estimates. The plot assumes that scattering is wavelength dependent and that the slowest wave is affected at the lowest frequency.

SCATTERING MODELS

The last step in this study is to use the characterization of the deterministic and stochastic wavefield in constraining the scattering model. Following Aki and Richards (1980) the velocity of perturbation in the media is defined as:

$$\mu = \frac{\delta C}{C_0}$$

where μ = average of the velocity of perturbation

δC = average difference in P velocity

C_0 = average P velocity for scattering layer

From the refraction analysis C_0 is taken to be 500 m/s. Some evidence of a fast thin layer was found in the refraction data (Figure 6). A conservative velocity of 560 m/s was taken for this material giving a velocity perturbation of 12% to be included in the scattering model. Assuming single scattering and the Born approximation the following estimate of the strength of the scattering process can be made:

$$\frac{\delta I}{I} = \frac{8 \langle \mu^2 \rangle (2\pi k)^4 (a_s)^3 L}{1 + 4 (2\pi k)^2 (a_s)^2} \quad 2\pi k a_s < 1$$

where L = travel distance in m

a_s = scale length in m

k = wavenumber 1/m

$\delta I/I$ = ratio of energy loss to total energy

In analyzing this equation the wavefield boundaries displayed in Figure 24 are used for constraining k and L . Previous work at the McCormick Ranch Test Site that has included subsurface sampling (Reinke and Stump, 1991) and suggests a scale length between 0.5 and 1.0 m. The application of the above equation gave the scattered energy predictions reproduced in Figure 25. Estimates of energy scattered by both the direct and the head wave are made in this figure. Comparison of the spectra from the mean seismograms to the spectra from line 8, wheel A was made in Figure 21 and the difference in these two spectra was attributed to scattering. Using the wavefield boundaries for the scattered direct and refracted waves in Figure 24, one can

VELOCITY PERTURBATION SCATTERING MODEL

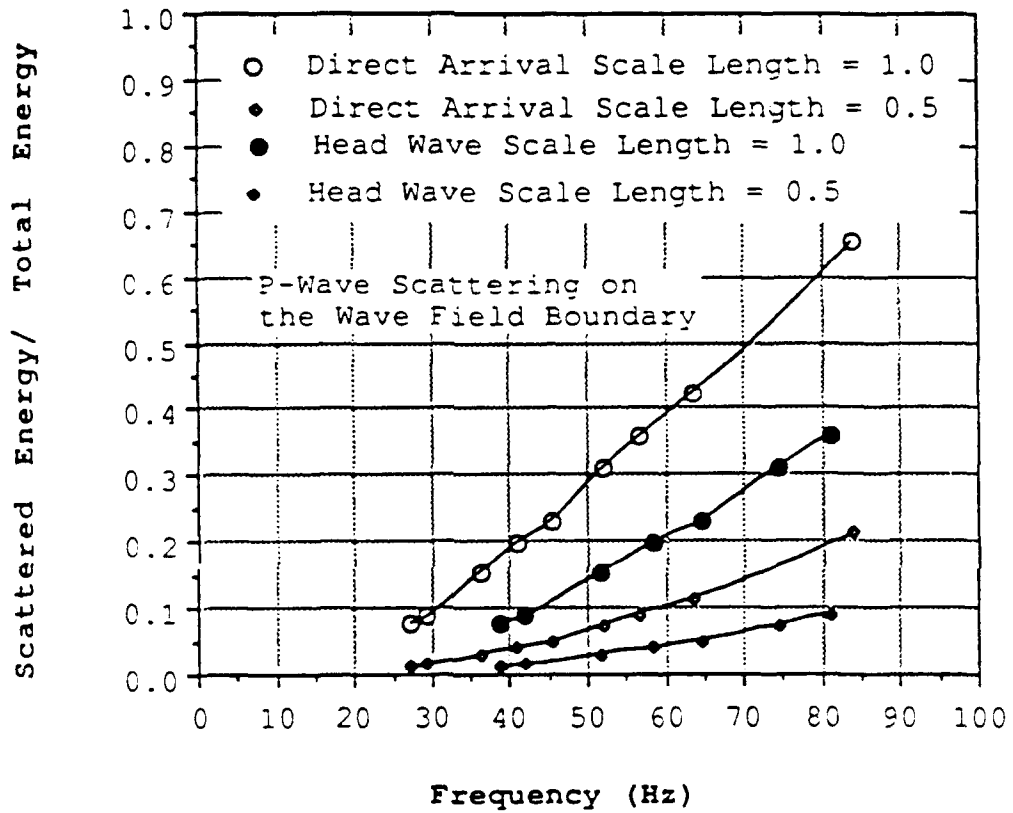


Figure 25: The scattered energy predictions for the direct and head waves in the McCormick Ranch material with scale lengths of 0.5 and 1.0 m.

place an upper bound on the energy in the scattered energy associated with each of these phases. The scattered energy calculations for the direct arrival from Figure 24 is less than 10% and for the refracted arrival less than 20 % for a scale length of 0.5 m. These numbers are consistent with the observational results in Figure 21 and support a scale length of less than 0.5 m in conjunction with the other characteristics determined in this study.

CONCLUSIONS

A procedure for separating the deterministic and stochastic components of the wavefield that have propagated in the shallow weathered layers has been designed and implemented. The key elements of the procedure are dependent upon the wheel design for instrumentation that allows both azimuthal and range effects in the wavefield to be quantified. The second major component of the characterization is the recovery of complete waveforms so that latter arrivals can be used in the site characterization.

Analysis begins with the development of a layered geological model from first arrival time analysis. This model can be azimuthally dependent as a result of the experimental configuration. The site characterization is extended to secondary arrivals through the implementation of a new high resolution hybrid f-k estimator. This procedure estimates the k part of the spectrum using a modeling algorithm which avoids windowing effects and gives very high resolution estimates so that closely spaced events can be separated. In this analysis an autoregressive algorithm is found to give the best resolution with model parameters determined using the Burg algorithm. The f-k spectra provided refined velocity estimates for the body wave phase and provided the information necessary to constrain dispersion relations for the surface waves.

The stochastic components of the wavefield is best characterized in the frequency domain with the determination of average spectra as a function of range which are compared to spectra from individual lines. This comparison between average and individual spectra is able to identify the frequencies and ranges at which variability becomes important. The coefficient of variation is found to be a good tool for representing this boundary.

These stochastic characterizations are combined with the f-k estimates to quantify the effects of scattering as a function of range on both the body and surface waves. These individual wave effects are finally compared to simple Born approximation scattering models. The results of this comparison suggest that a 10-20% velocity perturbation with a scale length close to 0.5 m is satisfactory to explain the data recovered in this site characterization process.

A technique for characterizing the shallow weathered layer has been suggested and implemented. It provides the opportunity to predict wave propagation effects in this media and thus will find use in a variety of seismology problems. Quite close to the site characterization an explosive tests was conducted. The purpose of this test (Stump and Reinke, 1991) was

CRAPS I CV 20m 0m Vel Vertical

— explosion
●— exploration

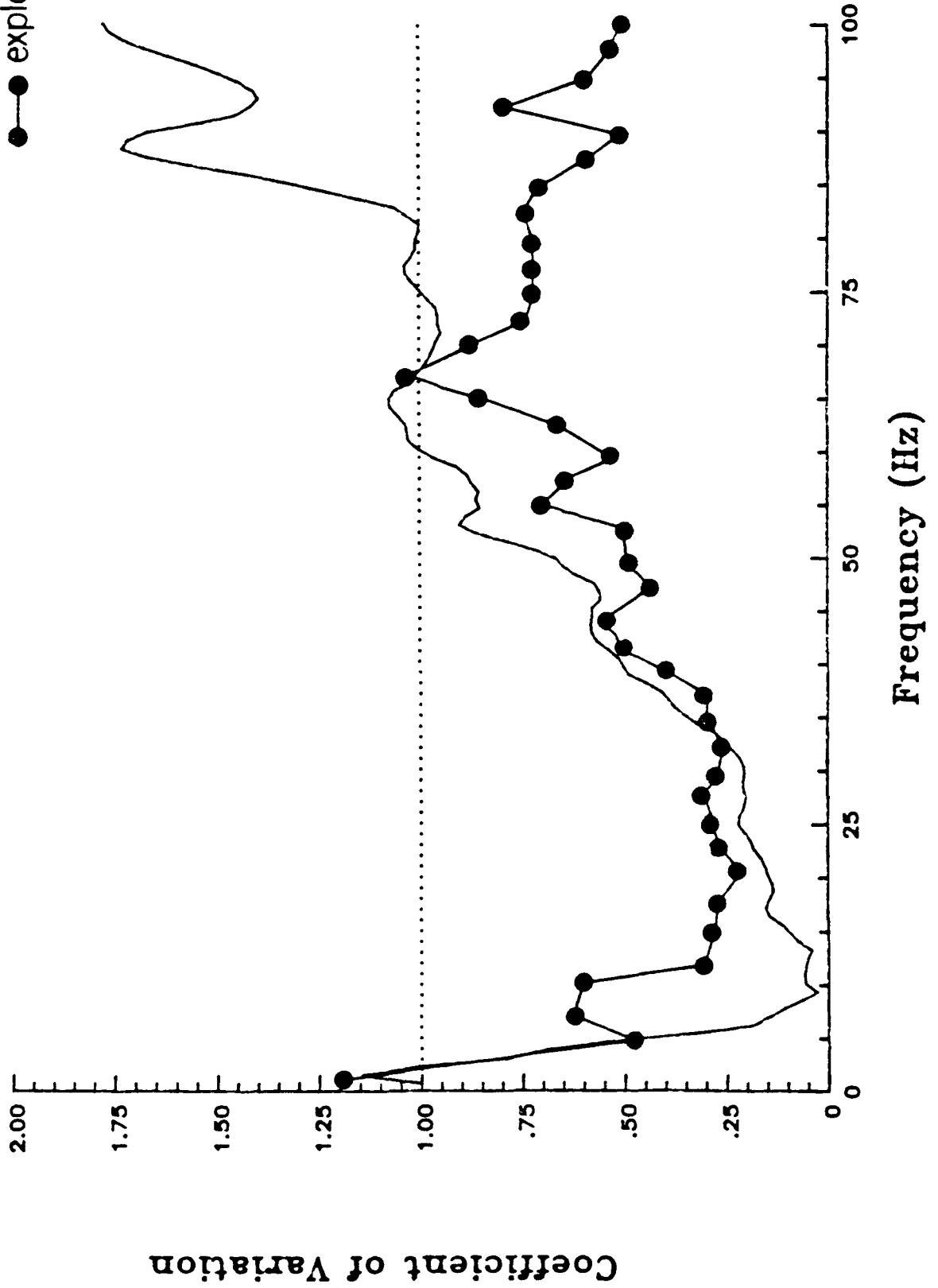


Figure 26: The coefficient of variation from exploration data (points) and explosion data both made at 20 m offset, McCormick Ranch.

to document explosive phenomenology at relatively high stresses. A number of azimuths were instrumented thus providing the opportunity to compare the results of the site characterization with explosively generated ground motions. Figure 26 compares the CV value from the site characterization with that determined from the explosive test. Despite small differences in the location of the explosive test and the site characterization the comparison is excellent. These results illustrate the utility of the procedures introduced in this paper.

The characterization of the McCormick Ranch Test Site in New Mexico has identified scattering in the near surface layers to be responsible for increased variation in waveforms with propagation distance. The effect is found to be wavelength or frequency dependent as constrained by the identification of individual phases in the waveform. At distances as close as 10 m the data shows little scatter to frequencies as high as 55 Hz. This boundary separating stochastic and deterministic effects decays to 17 Hz at 72 m. For the fundamental surface waves at the McCormick Ranch Test Site these boundaries are representative of wavelengths of 3 and 18 m respectively. An experimental procedure has been established for quantifying the effects of near surface variability in material properties with particular application to their effects on propagating waves.

REFERENCES

- Aki, K. and P. Richards, 1980. *Quantitative Seismology: Theory and Methods*, W. H. Freeman and Company, San Francisco, 2 volumes, 932 pp.
- Bethea, R., B. Duran and T. Boullian, 1983. *Statistical Methods for Engineers and Scientists*, Marcel Dekker, Inc., 698 pp.
- Burg, J. P., 1975. Maximum entropy spectral analysis, Ph.D. Thesis, Dept. of Geophysics, Stanford University, Stanford, California.
- Flynn, E. C. and B. W. Stump, 1988. Effects of source depth on near-source seismograms, *J. Geophys. Res.*, 93, 4820-4834.
- Krohn, C. E., 1984. Geophone ground coupling, *Geophysics*, 49, p. 722-731.
- Marple, S. L., 1987. *Digital Spectral Analysis with Applications*, Prentice-Hall, Inc., Englewood Cliffs, New Jersey, 492 pages.
- Mavko, G., and J. P. Burg, 1987. Two-dimensional maximum entropy spectral analysis, Society of Exploration Geophysicists, extended abstracts and bibliographies, 1987 Technical Program.
- McLaughlin, K., L. Johnson and T. McEvelly, 1983. Two-dimensional array measurements for near source ground accelerations, *Bull. Seismol. Soc. Am.*, 73, 349-376.
- Menke, W., A. Lerner-Lam, B. Dubendorff and J. Pachecho, 1990. Polarization and coherence of 5-30 Hz wavefields at a hard rock site and their relevance to velocity heterogeneities in the crust, *Bull. Seismol. Soc. Am.*, 73, 430-449.
- Reinke, R. and B. Stump, 1988. Stochastic geologic effects on near-field ground motions in alluvium, *Bull. Seismol. Soc. Am.*, 78, 1037-1058.
- Reinke, R. and B. Stump, 1991. Experimental studies of stochastic geological influences on near-source ground motions, in *Explosion Source Phenomenology, Geophysical Monograph 65, American Geophysical Union*, 63-72.

Shirley, T. E., S. J. Laster and R. E. Meek, 1987. Assessment of modern spectral analysis methods to improve wavenumber resolution of f-k spectra, Society of Exploration Geophysicists, expanded abstracts with bibliographies, 1987 Technical Program.

Smith, S. W., J. Ehrenbeg and E. Hernandez, 1982. Analysis of the El Centro differential array for the 1979 Imperial Valley Earthquake, *Bull. Seismol. Soc. Am.*, 72, 237-258.

Stump, B. and R. Reinke, 1988. Experimental confirmation of superposition from small-scale explosions, *Bull. Seismol. Soc. Am.*, 78, 1059-1073.

Vernon, F., J. Fletcher, L. Harr, T. Bolswick, E. Sembera and J. Brune, 1985. Spatial coherence of bodywaves from local earthquakes recorded on a small aperture array, *EOS Trans. Am. Geophys. Union*, 66, 954.

Progress report on MS thesis:
Shallow Shear Wave Velocity Determination
Using Surface Wave Dispersion
M.E. Craven

Several previous studies including Farrell et al (1980) have documented the need for shear velocity structure in characterizing areas in terms of nuclear hardness. Examples cited include the fact that deterministic techniques for predicting the crater geometry, free field ground shock effects and airblast induced ground motion from a nuclear surface burst require a site specific estimate of the shear wave velocity as a function of depth. Determination of this material property has historically been very difficult because of the lack of an adequate shear wave seismic source. One technique used in numerous studies including Cherry et al (1979), is to measure surface wave dispersion and invert for shear wave velocity structure. The current project entails surface wave techniques utilizing two sources and two types of surface waves. The study was conducted at McCormick Ranch. A previous, similar study was conducted at McCormick ranch by Simila (1982).

Simila (1982) used Rayleigh wave group velocities to model velocity structures in shallow (less than 25 meters) structures at McCormick Ranch. Simila utilized explosive sources to generate the Rayleigh waves. The dispersion analysis incorporated single phone processing at distances ranging from 6.55 to 228.6 meters. The processing included the moving window analysis technique for frequencies from 5 to 25 Hz for the fundamental mode and 25 to 50 Hz for the first higher mode. This thesis will extend Simila's work. New processing schemes are available to analyze arrays of data for both group and

phase velocity. New equipment is now available to make it more practical and economical to acquire an array of data, as opposed to the single phone acquisition used in the Simila study. A new shear source makes it possible to generate shear data and a resulting Love wave. The final extension of this work, as proposed by Simila, will be the use of inversion techniques, instead of relying on a trial and error forward modeling method.

A. Field Data Acquisition

The seismic data utilized in this study was acquired by Pearson and Stump of SMU. The acquisition system is fully documented in the report "SMU Portable Seismic Instrumentation Development" by Stump, Pearson and Thomason. The intent for this study was to generate two types of surface waves, both Rayleigh waves and Love waves. The seismic data was acquired in two parts with a different source in each case. The P-SV data set was acquired utilizing a commercially available source, the Betsy Seisgun.

The second source used in this study was the SMU fabricated SWIG, which stands for Shear Wave Impulsive Generator. The SWIG is a modification of a source described by Liu, et al(1988). The SWIG is a pneumatic ram mounted between channels that is weighed down by a pickup truck. The SWIG is oriented perpendicular to the source-receiver plane. One side of the piston is evacuated to the outside air. The high pressure side drives the mass horizontally until it impacts an anvil at the end of the SWIG. This impact produces a wavefield with particle motion perpendicular to the direction of propagation from the source to the geophones. The SWIG provides a very clean Sh wavefield. In the test site for this study, the source generated a very distinct Love wave along with the shear wavefield.

B. Data Processing For Surface Wave Dispersion

The data processing was done on a Sun 3/60 workstation in the SMU geophysics lab. The processing primarily utilized a system of programs developed as an ongoing project by Robert Herrmann of St. Louis University. This package contains interrelated programs which allowed the output from one program to be used as input to another. The software descriptions throughout this section will describe the Herrmann implementations of the various techniques.

The initial processing indicated that low frequency or long period data might yield some of the more useful information. Since the geophones used had a corner frequency of 10 Hz, an instrument response correction was applied to the data in order to expand the usable bandwidth of the data. A comparison of the spectrums at select distances both before and after instrument correction show that the only difference was a boosting of the amplitude below about 10 Hz. The seismic records after correction for instrument response were then processed to determine dispersion through various techniques. The most fundamental technique for determining group velocity dispersion utilized in this study was the multiple filter technique.

1. Multiple Filter Analysis

The Multiple Filter Analysis (MFA) technique was first proposed by Dzienwonski, et. al. (1969). The group velocity is determined by performing a narrow band filter on the data and searching for the maximum amplitude of the envelope function. This procedure is then repeated for each frequency over the band of interest. The group velocity, $U(\omega)$, can be related to the time, $t(\omega)$, for the peak of the envelope by the equation:

$$U(\omega) = D / t(\omega)$$

where D is the distance between the source and receiver. Some advantages of the MFA over the moving window analysis are documented by Dziewonski et al (1969). This includes better frequency resolution, no intrinsic period shift and less computer processing time required for the MFA.

The implementation of the MFA used for this project was the St. Louis University software provided by Herrmann(1987). Filtering is accomplished with a Gaussian filter which is set to zero outside a given bandwidth and is tapered inside this bandwidth from the center frequency. The range of center frequencies are selected by the user with the bandwidth controlled by one parameter α .

The usable bandwidth of the acquired data used in this study is approximately 10 to 30 Hz. Some effort was put into recovering quality data below 10 Hz, including correction for instrument responses. It appears that this was not efficacious because the major events were separated by less than 200 msec. at the source-receiver spacings utilized in this study. In order for this technique to work at these lower frequencies, it appears that data would have to be acquired at much further source-receiver offsets.

The group velocity determined from the seismic trace is an average over the spatial interval between the source and receiver. This implies that for any given receiver, say at 80 meters, the next receiver should have very similar results. In the processing it was found that group velocities determined at 80 and 85 meters are very similar, in spite of being relatively noisy. If the site were horizontally stratified and homogeneous, two receiver locations 0.5 meters apart should be extremely similar.

There exist two portions of the data set that are at approximately the same source-receiver spacing, but cover a different interval of ground. When the data was acquired, the source was moved back 30 meters at a time with the receivers left in the same 60 locations. Two stations covering about the same

range are analyzed at 34.5 and 35 meters, although the travel path for these two stations overlaps by only 5 meters. Differences between these two traces is most pronounced at the higher frequencies. The two data sets at 64.5 meters and 65 meters demonstrate more pronounced differences. The data set at 64.5 meters has almost 4 full cycles apparent on the raw trace of the Love wave. The 65 meter trace only shows about two cycles of Love wave. The two intervals imaged by the Love wave are geologically different. The dispersion results are very similar between 10 and 30 Hz. The high frequency components show the most variability over the entire data set.

The Love wave group velocity increases for each dispersion curve as the range increases from 5 to 34.5 meters. This result is consistent with Mari's (1984) statement that it would take an offset distance of 4 to 6 times the deepest layer imaged for the Love wave to stabilize. The velocity still shows some increase over the interval from 35 to 64.5 meters, but substantially less change than observed in the 5 meter data set. The Love wave is not fully stabilized by 35 meters, but is nearly so at 65 meters. The MFA interpreted dispersion curves from 65 to 94.5 meters almost overlay between 10 and 25 Hz. The Love wave appears stabilized and usable at these offsets for making geological interpretations.

2. Array Processing of Group Velocity

The Herrmann (1987) software package used in this study implements a technique from Barker (1988) to make use of an array of seismograms to determine group velocity. This technique uses the multiple filter algorithms previously documented. Each trace is bandpassed with a series of Gaussian filters. The envelope of each resulting bandpassed trace is then computed. The additional step involved in array processing is to stack the normalized envelopes along lines of constant velocities. As Herrmann notes, this is not a slant stack,

since only a single point results from stacking along each velocity. Up to four peaks of this stacked envelope function are selected to yield group velocities of up to four modes at this frequency. This is then followed by a more detailed analysis, in which each original envelope trace is searched around each of the four average velocities to get the individual group velocities which would generally differ from the initial estimate. The individual velocities are used to compute a mean group velocity and standard error. These velocities represent an average response of the material being imaged by the different source receiver pairs.

The results of this analysis show high frequency variability which indicates more geologic complexity in the shallowest environments than was expected at the start of this study. The consistencies at lower frequencies, or longer wavelengths, indicates that the deeper horizons are more geologically uniform than the shallowest environment.

The body wave portion of the wavefield in the MFA shows some variance in velocity versus frequency, but is centered around 200 meters/sec for the nearest data set. The body wave velocity increases with offset. This result is consistent with a normal refraction survey which would be expected to show an increase in velocity with depth for various layers.

The Betsy source data set is more complicated, but the basic results are similar. The Rayleigh data includes a fundamental mode and one higher mode. Both modes show more clearly defined dispersion and higher group velocities as the source is moved further away. This is consistent with the earlier observation that some time or distance had to elapse before the surface waves are fully developed. The 65 meter data set has a further complication in that the air blast at 300 m/sec couples to the higher mode data at high frequencies.

The energy for the three data sets fall into two distinct data groups. The faster, higher frequency band is the first higher mode Rayleigh wave data.

There also tends to be a less dispersive portion at 300 m/sec. This energy is generated by the air blast from the source. The 35 meter fundamental mode data set breaks up at about 25 meters and shows some sort of Aries phase at about 18 Hz. This is consistent with the results from Simila (1982). The 65 meter higher mode data appears to be strongly biased by the air blast above 45 Hz.

3. Phase Matched Filter

A complementary technique for calculating velocity dispersion is phase-matched filtering or PMF as documented by Herrin and Goforth (1977) and Goforth and Herrin (1979). The PMF procedure starts with an initial estimate of dispersion, generally from the multiple filter technique. An iterative technique is used to find and apply a filter that is phase-matched for extracting a particular mode or arrival of a surface wave. This phase-matched filter is then used to calculate the final dispersion curve. The results from this study show that this technique can be useful for separating events for use in processing, but that the dispersion results from a single phone are not markedly better than the Barker technique on an array of data. The Barker technique is much less sensitive to individual processing technique.

4. Array Processing of Phase Velocity

The phase velocity calculations on array data used for this thesis were computed from software by Herrmann (1987). The original concept was from McMechan and Yedlin (1981). This technique called for a slant stack or transform into the τ - p domain. This step was followed by a 1d transform or FFT along lines of constant slowness, converting the intercept dimension to frequency. Since slowness is the inverse of velocity, this effectively results in a direct representation of amplitude on phase velocity versus frequency. The maximum amplitudes should correspond to dispersion of various modes.

Mokhtar et al (1988) describe an alternate method of mapping into the p - ω domain without doing a slant stack. The procedure is described in detail in Herrmann (1982) program documentation for the p - ω stack procedure. The results of this processing showed very consistent phase velocity with range. This appears to have been a function of the acquisition geometry. The receivers were planted in the same spot for the entire survey and the source was moved to increase the source-receiver spacing. As a result, the phase velocity effectively imaged the same area of approximately 25 meters in length for the entire survey. The group velocity measurements were over different intervals and therefore showed variance with range.

C. Inversion For Velocity Structure

Most of the effort of this study has been devoted to deriving accurate dispersion analysis of the surface waves. These dispersion results were inverted to derive a velocity and Q model. As with any non-linear inversion technique, some sort of start model was necessary to constrain the computations. The starting model was provided by refraction analysis. Standard refraction techniques were utilized with both the compressional and shear data sets to generate layer thicknesses and velocities.

The results at this time indicate some inconsistencies between the refraction results and the dispersion inversion. The ongoing part of this project will focus on this aspect of the study.

Bibliography

- Barker, T. G. (1988). Array processing of Rayleigh waves for shallow shear wave velocity structure, abstract in *Seismological Research Letters*, Vol. 59 no. 1, January-March, 12.
- Cherry, J. T., W. E. Farrell, W. L. Rodi, H. J. Swanger and B. Shkoller (1979), Shear wave velocities in MX valleys estimated from an inversion of Rayleigh wave group velocities, Systems, Science and Software report SSS-R-80-4232, December.
- Dziewonski, A., S. Bloch, and M. Landisman (1969). A technique for the analysis of transient seismic signals, *Bull. Seism. Soc. Am.* 59, 427-444.
- Farrell, W. E., R. C. Goff, and J. Wang (1980). Shear Waves in MX valleys: Rayleigh wave and Love wave excitation by vertical and horizontal weight drop sources, Systems, Science and Software Report SSS-R-80-4363, February.
- Goforth, T. T., and E. Herrin (1979). Phase-matched filters: application to the study of Love waves, *Bulletin of the Seismological Society of America*, 69 no. 1, 27-44.
- Herrin, E. and T. T. Goforth (1977). Phase-matched filters: application to the study of Rayleigh waves, *Bulletin of the Seismological Society of America*, 67, 1259-1275.
- Herrmann, R. B. (1982). *Computer programs in seismology, Voi IV, .*
_____ (1987). *Computer programs in seismology, Vol II, .*
- Jackson, D.D. (1972). Interpretation of inaccurate, insufficient and inconsistent data, *Geophysical Journal of the R. astr. Soc.*, vol. 28, 97-109.
- Landisman, M., A. M. Dziewonski, and Y. Sato (1969). Recent improvements in the analysis of surface wave observations, *Geophysical Journal of the Royal Astronomical Society*, vol. 17, 369-403.

- Lankston, R. W. (1989). The seismic refraction method: A viable tool for mapping shallow targets into the 1990s, *Geophysics* 54, no. 12, 1535-1542.
- Liu, Hsi-Ping, R.E. Warrick, R.E. Westerlund, J.B. Fletcher, and G.L. Maxwell (1988). An air-powered impulsive shear wave source with repeatible signals, *Bulletin Seism. Soc. America* 78, 355-369.
- Mari, J. L. (1984). Estimation of static corrections for shear-wave profiling using the dispersion properties of Love waves, *Geophysics* 49, no. 8, 1169-1179.
- McMechan, G.A. and M. J. Yedlin (1981). Analysis of dispersive waves by wave field transformation, *Geophysics* 46, no. 6, 869-874.
- Menke, W. (1989). *Geophysical data analysis: Discrete inverse theory*, Academic Press.
- Mokhtar, T. A., R.B. Herrmann and D.R. Russell (1988). Seismic velocity and Q model for the shallow structure of the Arabian shield from short-period Rayleigh waves, *Geophysics* 53, no. 11, 1379-1387.
- Mooney, H. M. and B. A. Bolt (1966). Dispersive characteristics of the first three Rayleigh modes for a single surface layer, *Bulletin of the Seismological Society of America*, vol 56, no. 1, 43-67.
- Press, F. (1956). Determination of crustal structure from phase velocity of Rayleigh waves, *Bulletin of the geological society of America*, Vol. 67, 1647-1658.
- Simila, G. W. (1982). Shear wave velocity from Rayleigh wave dispersion analysis, report AFWL-TR-82-08, September, pp. 34.
- Stokoe, K. H. and S. Nazarian (1984). Seismic testing of two apron sections at Tyndall AFB using crosshole and surface wave methods, *Geotechnical Engineering Report GR84-3*, pp. 157.
- Waters, K. H. (1981). *Reflection Seismology*, J. Wiley & Sons, pp. 453.
- Wiggins, R.A. (1972). The general linear inverse problem: Implication of surface waves and free oscillations for earth structure., *Reviews of geophysics and space physics*, Vol 10, No. 1, 251-285.

EXPERIMENTAL STUDIES OF STOCHASTIC GEOLOGIC INFLUENCES ON NEAR-SOURCE GROUND MOTIONS

Robert E. Reinke

Geodynamics Section, Phillips Laboratory, Kirtland Air Force Base, Albuquerque, New Mexico 87117-6008

Brian W. Stump

Department of Geological Sciences, Southern Methodist University, Dallas, Texas 75275

Abstract. Analysis of accelerograms recorded at the same ranges but multiple azimuths from small-scale (5–100 lbs) high explosive experiments revealed wide (as large as 20 dB in the amplitude modulus of the Fourier transform) variations in response for frequencies higher than 30–40 Hz. Additional experiments were performed which ruled out source asymmetry or instrumental irregularity as the cause of these variations. The observations suggest that scattering by geologic inhomogeneity is responsible for the frequency-dependent spatial variability in ground motion. Modeling of the physical processes responsible for this variability requires a statistical description of the subsurface heterogeneity. One set of experiments was designed to accomplish this. Cone penetrometer testing was employed to directly probe the subsurface where a set of high explosive experiments was performed. High-resolution surface seismic surveys were performed at the site to characterize the deterministic and stochastic wave propagation effects. A statistical description of the subsurface is being developed from this data set and will be used in a simulation of wave propagation in random media. Although this paper deals specifically with travel paths a few tens of meters in length and random media scale lengths on the order of a fraction of a meter to a few meters in length, other examples in the literature suggest that random geologic variability exerts a significant influence on the complete spectrum of wave propagation from the near-field to teleseismic ranges and frequencies.

Introduction

Small, well-controlled, in situ explosive experiments provide an opportunity to isolate and study individual aspects of the source-propagation problem. Over the course of the past few years the Air Force Phillips Laboratory has conducted a number of small-scale high explosive experiments in an effort to better understand the physics involved in the generation of ground motions by explosive sources. One of the lessons learned from these ground motion experiments is that random geologic variations have a significant influence on experimental results and that any attempt to model these small explosive events must take into account these stochastic effects. The goal of these experiments is an increased understanding of the explosive source. This requires a separation of propagation path effects from source effects. Neglect of the effects of random spatial variability in propagation paths may lead one to draw incorrect conclusions regarding the results of experiments. Several of the tests, ranging in size from 5 to 100 pounds, were designed specifically to

study the effects of random geologic inhomogeneity upon small-scale spatial variability in ground motion. This paper will discuss the results of these tests, which were conducted in a dry alluvial geology, and the implications of random geologic variability for the interpretation of near-source ground motions.

This paper deals specifically with small explosive experiments, with travel paths a few tens of meters in length, and random media scale lengths on the order of a fraction of a meter to a few meters in length. Several recent discussions in the literature, however, suggest that random geologic variability exerts a significant influence on the complete spectrum of seismic wave propagation from the near-source to teleseismic ranges and frequencies. A quantitative understanding of the influence of geologic heterogeneity on wave propagation is necessary for users of seismic data in both the explosive source and earthquake communities.

Initial Experiments

One of the early experiments which we performed was the ARray Test Series (ARTS). The objective of these 5-pound tests was to study the ground motion effects of superposition of multiple charges in various spatial patterns [Stump and Reinke, 1988]. The plan was to analyze the data in a totally deterministic fashion—i.e., assume that the difference in waveforms from one azimuth to another would be relatively small. A single charge experiment, ART 2 (Figure 1), which included measurements at multiple azimuths at the same range, was performed as a test of this assumption. When the data were compared from one azimuth to another, variations as large as a factor of 10 were found at frequencies above 30 Hz (Figure 2). A "Huddle Test" in which the accelerometers were placed in a closely spaced group was conducted to verify that the instrumentation was not a problem. An additional set of experiments in which five 5-pound charges were detonated in sequence on the same test bed utilizing the same gage array provided convincing evidence that scattering by geologic heterogeneity and not source asymmetry was responsible for a significant portion of the variability [Reinke and Stump, 1988]. Analysis of data from these tests showed that the degree of variability in the ground motion data as a function of frequency was very similar for all five detonations, confirming that geologic heterogeneity was the source of the spatial variability in ground motion. Another experiment in the series was aimed at defining the dependence of variation in the seismic wavefield with range. This test included accelerometers at 10- and 30-m ranges. The results indicated an increase of variability with range [Reinke and Stump, 1988].

Craps Experiments

Additional tests were conducted to further constrain the relationship between stochastic variations in geologic material properties and ground

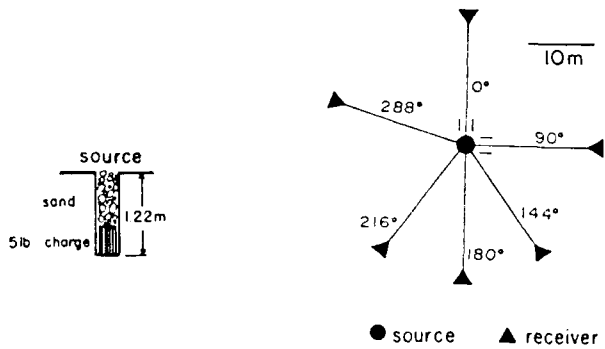


Fig. 1. Experimental layout for the ART 2 test event. A cross-sectional view of the explosive charge emplacement is shown at left. To the right is a plan view of the test bed.

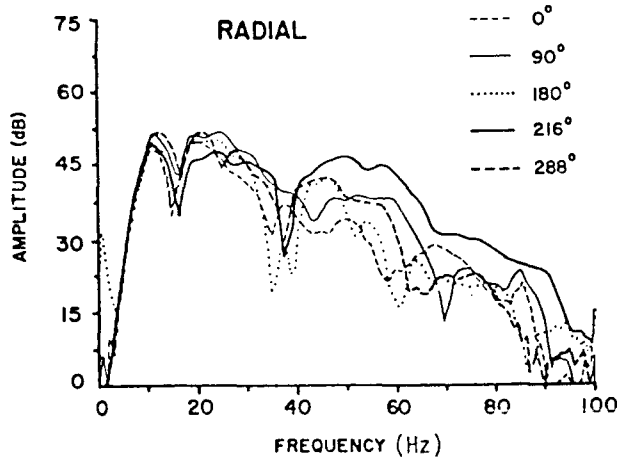
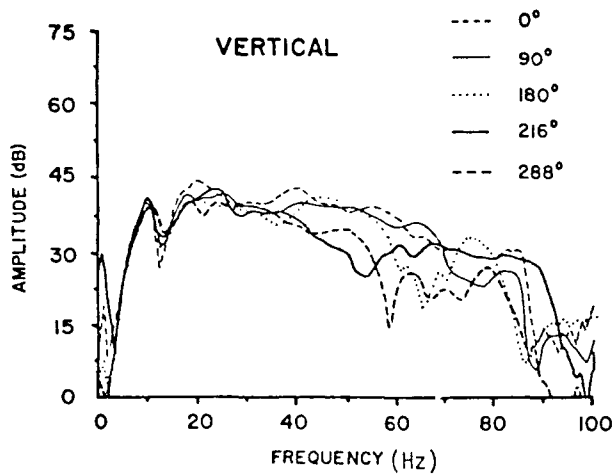


Fig. 2. Vertical and radial Fourier acceleration spectra for the records obtained on multiple azimuths for the ART 2 experiment.

motions. This test series, designated CRAPS for Coherence for Range and Array Parameters, consisted of four 100-pound detonations fired in sequence on the same test bed using the same gage array (Figure 3). In order to investigate the linkage between subsurface heterogeneity and spatial variability in ground motions, an extensive subsurface exploration effort was conducted in conjunction with this test series. This work included high-resolution seismic surveys, cone penetrometer testing, and drilling and sampling. In particular, the cone penetrometer investigation was designed to directly probe the subsurface material throughout the testbed. The site characterization effort, which will be discussed in more detail later, revealed extensive random spatial variability in material properties.

Ground motions from the CRAPS tests were recorded at ranges of 10, 20, and 30 m (Figure 3). A 100-pound explosive charge covered by a sand berm (the berm served to suppress the airblast) was detonated in a surface tangent configuration. The first charge was detonated on the surface of in situ material. The resulting crater was then excavated, leaving a pit which was filled with uniform sand for the remaining three detonations of the test series (Figure 4).

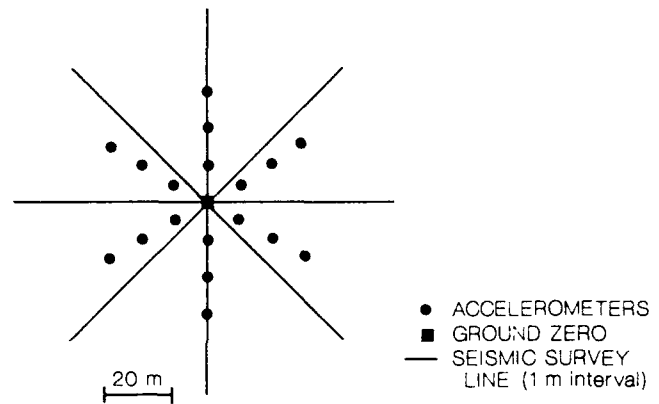


Fig. 3. Plan view of the CRAPS experiment. Each seismic refraction survey line was composed of 72 geophones spaced at 1-m intervals. The seismic source was located at the ground zero point.

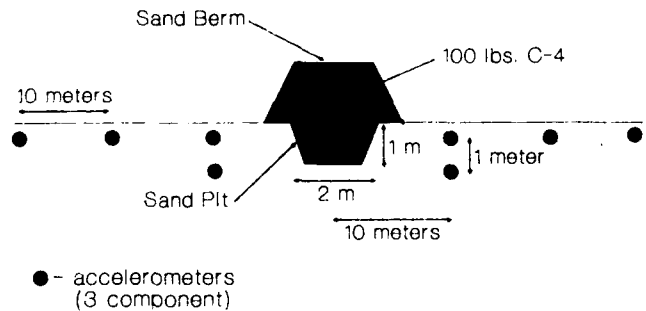


Fig. 4. Cross-sectional view of the CRAPS experimental layout. Accelerometers were located at 10-, 20-, and 30-m ranges.

Stochastic/Deterministic Ground Motion
Waveform Analysis

Figure 5 shows a set of vertical accelerograms from one of the early 5-pound experiments, ART 2. Waveform differences, both in amplitude and phasing, are easily identified, especially in the high-frequency data (>40 Hz). Techniques for quantifying these differences and relating them to the geology are needed. An elementary way of characterization, based upon

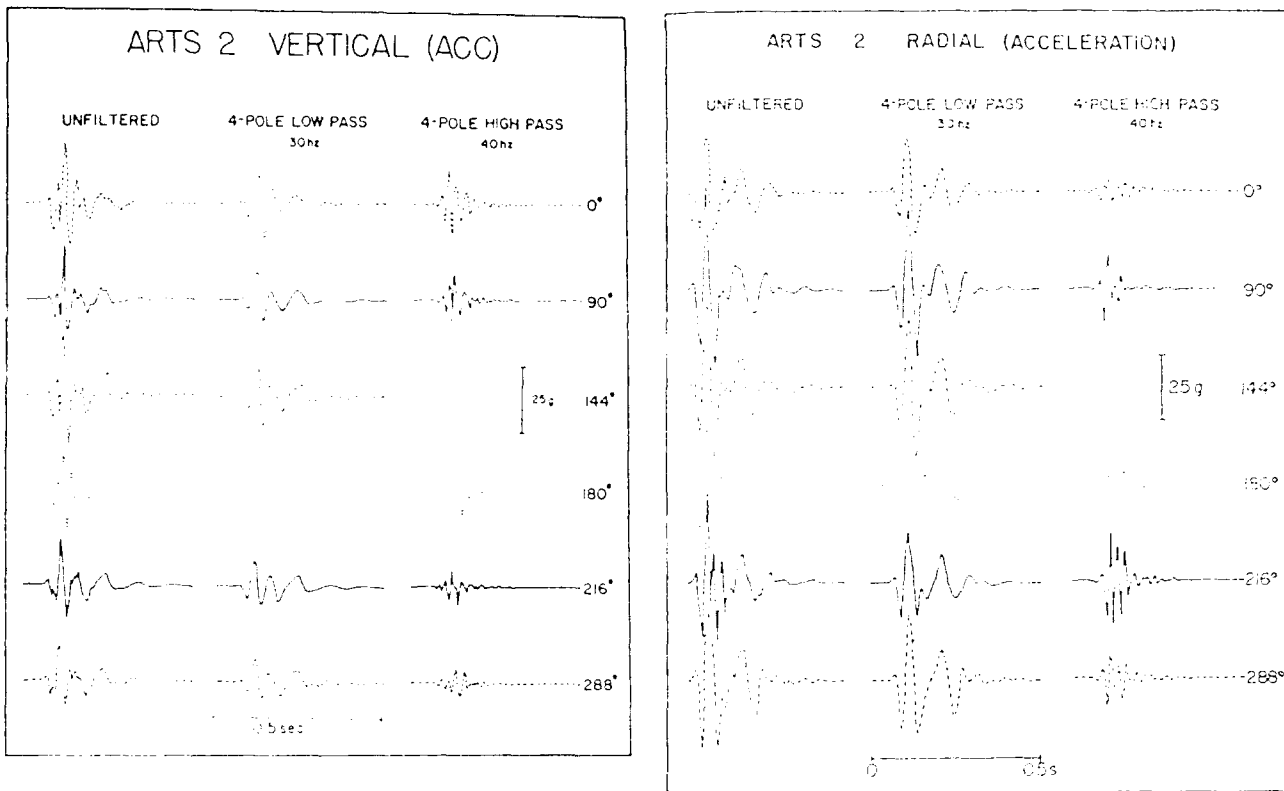


Fig. 5. Vertical and radial waveform sets from the various azimuths at the 20-m range. Low- and high-pass filtered waveforms are shown in addition to the unfiltered waveforms.

the observations such as those in Figure 5, is the computation of Fourier amplitudes for the set of waveforms. The amplitude spectra computed for the set of waveforms (Figure 5) are given in Figure 2. These spectra were computed using the complete waveforms shown in Figure 5 and a rectangular window. The individual spectra correlate well to frequencies as high as 30-40 Hz and diverge widely at higher frequencies. We can examine these data more quantitatively by treating the set of spectra as a statistical ensemble and computing the mean and standard deviation as a function of frequency. Figure 6 shows an example of such a representation for the set of spectra shown in Figure 2. The $\pm 1\sigma$ band is fairly narrow (2-3 dB) below 30 Hz, then widens rapidly for higher frequencies (20 dB). In doing this we have made the assumption that the spatial variation of spectral amplitudes at each frequency is described by a normal distribution. It should be noted, however, that a log-normal distribution may be more appropriate. The amplitude at a particular frequency may be considered to be the result of a number of scatterers acting on the signal along the travel path. The influence of each scatterer is likely to be proportional to the amplitude of the signal. Cramer [1961, p 220], suggests that in such cases the log of the function rather than the function itself is normally distributed. For our case, however, the scatter of the spectra in Figure 2 compares well with the $\pm 1\sigma$ bounds in Figure 6 computed assuming a normal distribution.

Another approach to quantifying the observed variation in waveforms is to compute the coherency between station pairs, thus quantifying phase differences. This method of characterization was employed by McLaughlin et al. [1983] for a set of small-scale-array data from a nuclear explosion at the Nevada Test Site. The coherency is defined by

$$\gamma_{xy}(\omega) = \frac{|\hat{\phi}_{xy}(\omega)|}{[\hat{\phi}_{xx}(\omega) \times \hat{\phi}_{yy}(\omega)]^{1/2}}$$

where $\hat{\phi}_{xy}(\omega)$ is the cross-power spectrum, $\hat{\phi}_{xx}(\omega)$, $\hat{\phi}_{yy}(\omega)$ are the power spectra of the two time series, and ω is the circular frequency. As is well known [Foster and Guinzy, 1967; Jenkins and Watts, 1968], smoothing must be applied to the spectra prior to estimation of the coherency in order to minimize variances at each frequency. For the coherency estimates computed here, a 4-point lag window was applied to the spectra prior to estimation of the coherency factors. The computed coherencies for the ART 2 station pairs are shown in Figure 7. The coherencies for the vertical and radial components are higher than might be intuitively expected after examination of the spectral plots in Figures 2 and 6.

Observed ground motion spectra from explosions are peaked and so absolute motions at different frequencies can vary by several orders of magnitude (Figures 2 and 5). In order to compare the variation in one frequency band to another a relative measure known as the coefficient of variation (CV) is introduced [Bethea et al., 1985]. The CV analysis is applied to spectra for all of the waveforms recorded at the same range. This technique has been employed to study the ground motions recorded on the CRAPS experiments. Amplitude spectra were computed at each range using the entire waveforms and rectangular windows. The set of spectra recorded at each range were treated as ensembles. The mean and standard deviation were computed as a function of frequency. The standard deviation was then normalized with respect to the mean ($CV = \sigma/\mu$) so that a CV value of 1 represents a standard deviation equal to the mean.

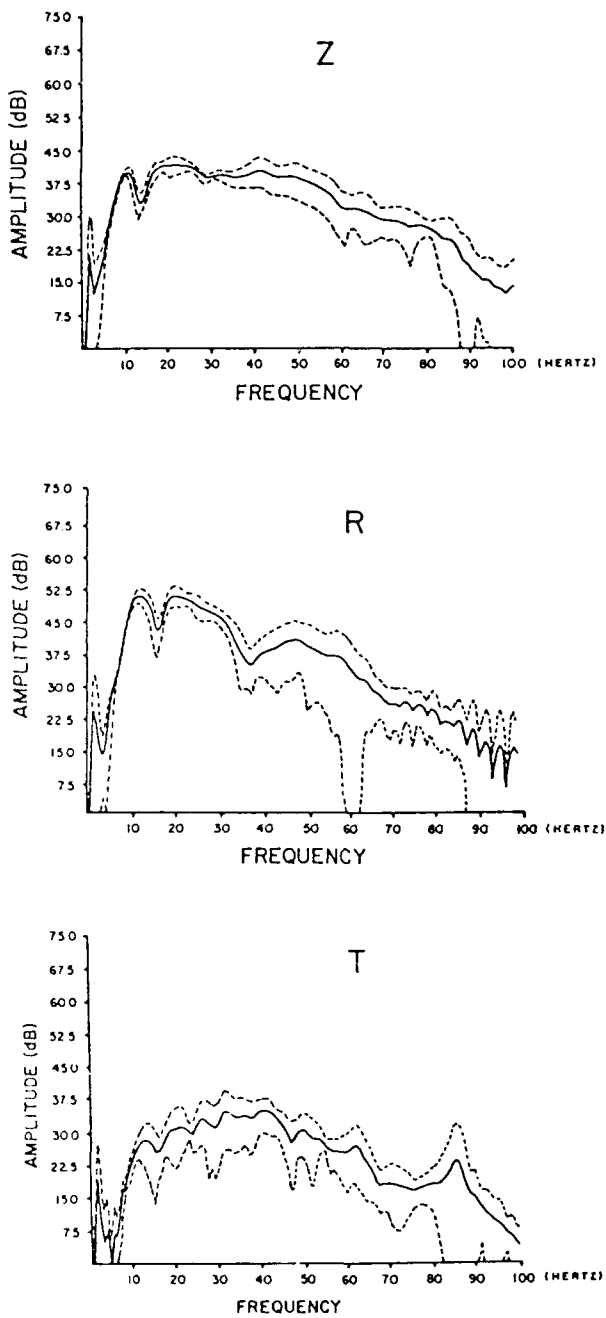


Fig. 6. Mean (solid lines) and standard deviation (dashed lines) of the ART 2 spectra.

Figure 8 is an example of the set of acceleration spectra from the 10-m range on the first CRAPS experiment. As in the ART experiment, the spectra correlate well to 30 Hz and then diverge widely. Figure 9 presents a comparison of the vertical spectral CVs for the first 3 (data from the fourth CRAPS test have not been included here since several gages did not operate successfully) CRAPS experiments as recorded at the 10-m range and 1-m depth. The CV values reflect the scatter seen in the spectral plots with small values from 5–40 Hz ($CV < 0.25$) then rising to values near 1

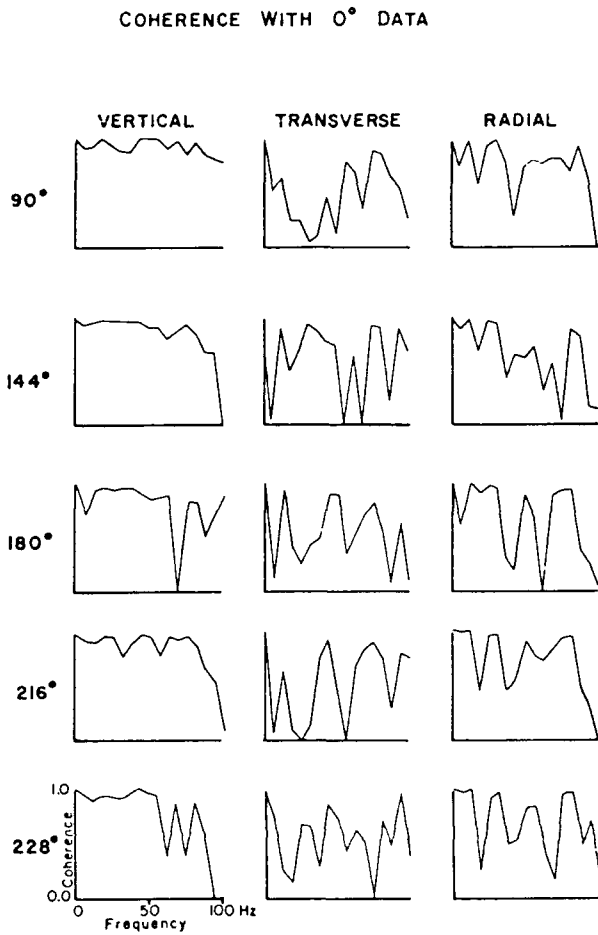


Fig. 7. Coherencies between the 0° waveforms and waveforms recorded at the other azimuths for the ART 2 experiment.

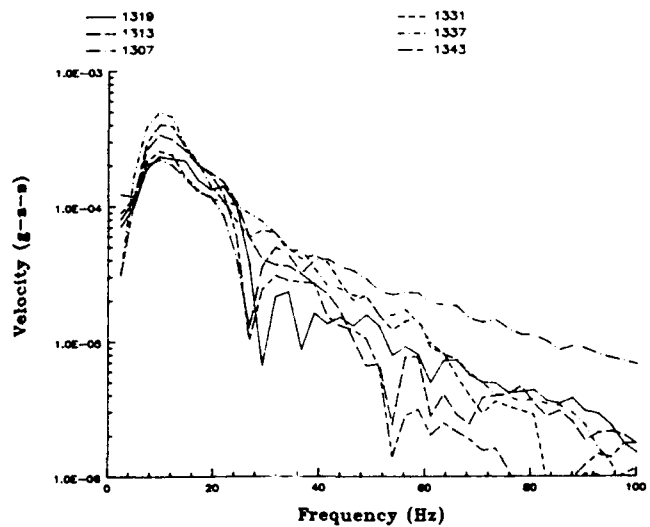


Fig. 8. Set of spectra for the six vertical velocity waveforms obtained at the 10-m range and 1-m depth for the CRAPS I experiment.

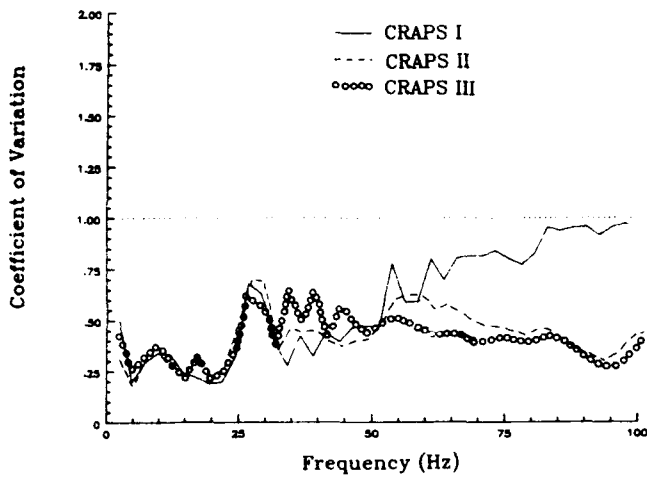


Fig. 9. Comparison of coefficient of variation curves for the CRAPS I, CRAPS II, and CRAPS III experiments. The curves shown here were obtained from the 10-m range, 1-m depth, vertical velocity spectra, and 1-m depth.

at 1 Hz. The CVs are remarkably similar for the three events although there are some high-frequency (>50 Hz) differences between the in situ experiment and the two following detonations which occurred on the surface of the backfill pit. This similarity in scatter for the three events supports the interpretation that random geologic heterogeneity and not some other influence is the dominant factor responsible for the observed azimuthal variability in ground motion spectra from the 10m range on the first CRAPS experiment.

After a glance at the data scatter in Figure 8 one might be led to the conclusion that it would be very difficult to learn anything about the source at frequencies higher than 20 to 30 Hz. In contrast, however, Figure 10 presents a comparison of the mean vertical acceleration spectra for the first three CRAPS experiments. These spectra are remarkably similar. Observed at the 10-m range there is less than a 20% variation for the two backfill shots out to frequencies of 400 Hz. Subtle variations do exist between the first test (detonated in situ material) and the following tests (fired in the backfilled crater pits). At the 10-m range, the first test has 40% higher amplitudes at the long (<20 Hz) periods. The high-(>20 Hz) frequency amplitudes for the in situ detonation are reduced by as much as a factor of 2 over the following tests. These differences may result from the in situ cratering process although the exact physical mechanisms remain to be identified. Overall, this spectral comparison shows that the variations in the mean spectra from shot to shot are much smaller than the azimuthal variability for a single shot which is as high as a factor of 5.

Site Characterization Tools

The ARTS and CRAPS experiments established that the observed scatter in ground motion data is the result of geologic inhomogeneity. A physical understanding of the observed spatial variation in ground motion requires a quantitative relationship between subsurface material properties and observed ground motion characteristics. Any ground motion model which incorporates scattering, whether it be the simple Born approximation [Aki and Richards, 1980, pp. 722-796; Reinke and Stump, 1988] or an elaborate finite difference simulation [Frankel and Clayton, 1986; Toksoz et al., 1989] requires a statistical description of subsurface material properties. Most wave propagation studies provide no alternate method for characterizing these statistical distributions. Except in very limited instances (the deep drill hole on the Kola Peninsula in the

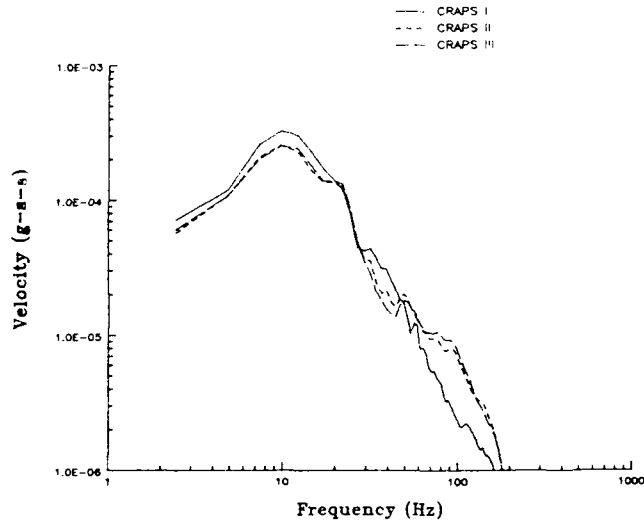


Fig. 10. Comparison of mean vertical velocity spectra for the 10-m range and 1-m depth for the CRAPS I, CRAPS II, and CRAPS III test events.

Soviet Union, for example), it will never be possible to directly probe the earth's crust to depths of tens of kilometers to obtain first hand information regarding the appropriate statistical distribution governing the geologic media through which regional waves propagate. The situation is quite different, however, for shallow, small-scale explosive experiments in alluvium. Experiments of this sort provide a test of wave propagation theory in random media not possible in most areas of seismology or geophysics.

A primitive attempt at correlating subsurface information with observed variability in the wavefield was made for the Art 2 experiment discussed previously. In an effort to quantify the nature of the subsurface heterogeneity at the test site, 18 boreholes were drilled within the confines of the test bed. Standard penetration tests were performed in each hole. The SPT involves determining the number of hammer blows required to drive a sampling tube a unit distance. This blow count is related to the in situ density and compressive strength of the subsurface material [Terzaghi and Peck, 1967]. The set of SPT data suggested a scale length of about 2.0 m. These data were obtained, however, with a sampling interval of about 0.6 m so that shorter wavelength variations are obviously aliased.

An extensive subsurface site characterization effort was part of the CRAPS test series. This investigation employed a variety of techniques including high-resolution surface refraction surveys, cone penetrometer testing, and drilling and sampling.

Cone penetrometer testing, a technique often used by the Civil Engineering community for the estimation of subsurface parameters, offers a method by which unconsolidated materials may be directly probed to obtain an estimate of the appropriate statistical classification of the subsurface. The cone penetrometer is a slender cone-tipped rod which is forced into the soil. A strain gage in the cone tip measures the force on the cone as a function of depth. The frictional force on the cone sleeve is also measured as a function of depth (Figure 11). Cone penetrometers are often used to obtain estimates of the in situ density and degree of compaction [Holtz and Kovacs, 1981]. Rohani and Baladi [1981] describe techniques for relating cone penetrometer data to a full geologic material model. The cone offers the opportunity to obtain a spatial sampling of subsurface materials at small-scale lengths. This data can then be used to produce experimental autocorrelation functions for the material. For the CRAPS experiment, two types of cone penetrometer devices were used, a full-sized cone, which was utilized to make measurements to depths of 6 or 7 meters with data sampling intervals of 3.05 cm, and a mini-cone

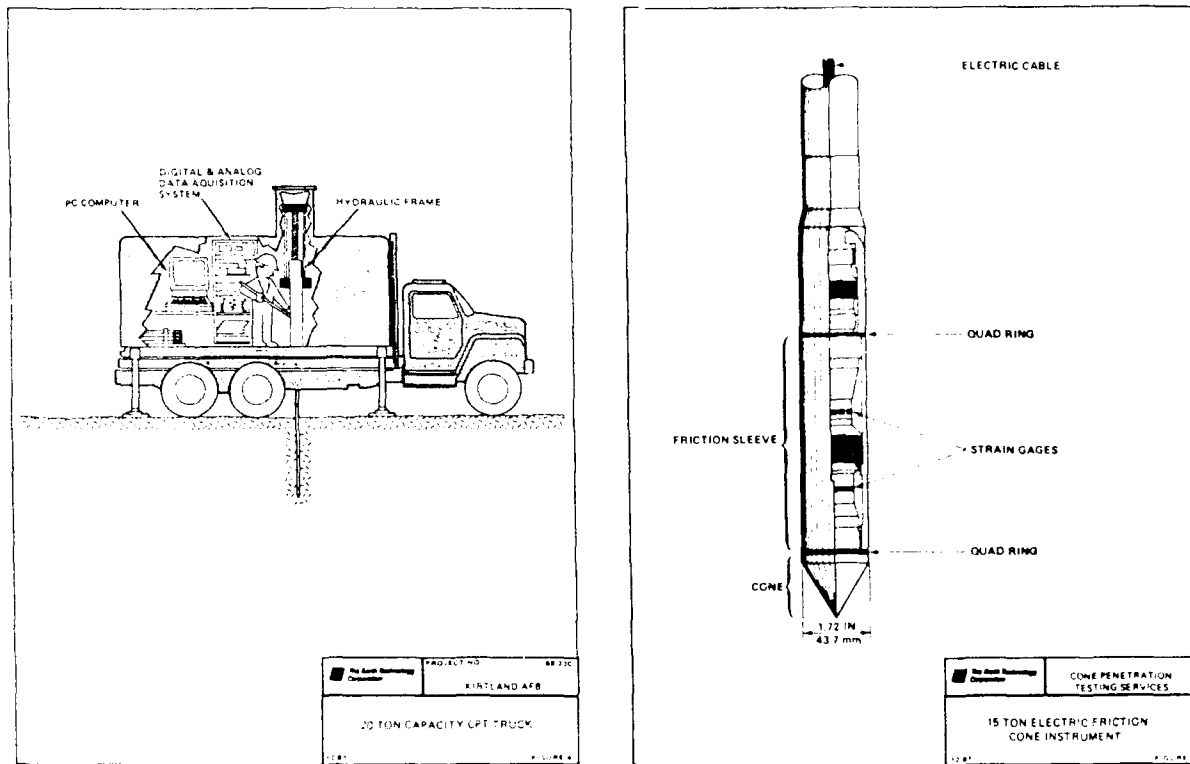


Fig. 11. Drawings of the cone penetrometer truck and cone penetrometer tool. (Courtesy of the Earth Technology Corporation).

which was utilized to make measurements at intervals of 1.27 cm to depths of 2 meters. The test bed sampling pattern is shown in Figure 12. Some of the cone holes were closely spaced in linear and rectangular arrays in order to obtain a statistical characterization of the variability in the horizontal direction; other arrays were designed to obtain the average gross geologic layering across the extent of the entire test bed. The cone penetrometer holds great promise as a tool for quantifying the vertical variability in the statistical sense but estimation of the horizontal variability is more difficult since movement of the cone through the soil disturbs a region about 10 cone diameters (the large cone diameter is 4.37 cm; the mini-cone, 1.90 cm) in radius. The cone hole spacing, therefore, must be larger than these distances in order to obtain unbiased measurements.

A subsurface cross-section constructed from 19 cone holes along the 180/360 radial (Figure 12) is shown in Figure 13. The contours indicate cone tip pressure as a function of depth and range while the solid vertical lines denote the locations of cone test holes. A gross layering system is visible in the cross section. Superimposed on this layering is a significant amount of random spatial variability in material properties. The cone data is used to produce an experimental material autocorrelation function which is compared to theoretical curves in Figure 14. An effort is underway to use the complete set of cone data to develop a statistical model of the subsurface variability at the CRAPS test site. This involves the comparison of theoretical autocorrelation functions with autocorrelations of the data. For purposes of illustration, Figure 14 compares autocorrelations of the data from several cone holes with theoretical curves for the exponential distribution. For the limited data set shown here, the experimental autocorrelations are bounded by the 0.1-m and 0.5-m scale length curves. Other distributions such as the Von Karman and Gaussian distributions have also been used to describe geologic heterogeneity. [Frankel and Clayton, 1986].

An extensive high-resolution surface seismic survey was performed on the CRAPS test bed [Bogaards, 1989]. The intent of the survey was to aid in defining the limits of the deterministic and stochastic wave propagation regimes at the site. The simplest deterministic model usually assumes that velocities change only in the vertical direction. Our initial stochastic model is classified as a distribution of inhomogeneities superimposed upon this velocity-depth profile and is characterized in terms of heterogeneity scale length and velocity contrast [Aki and Richards, 1980]. A set of surface seismic surveys were designed and implemented for the resolution of both the one-dimensional deterministic model as well as the stochastic effects. The field technique involves the retrieval of full wave seismograms at closely spaced intervals.

Figure 3 shows the layout of the full wave refraction survey performed at the CRAPS test site prior to detonation of the full-scale test. The goal of this particular experiment was the characterization of the top 20 m of the site which resulted in spreads of 72 m in length with geophones spaced at 1-m increments. Eight radial refraction lines emanating from a central source were recorded. The deterministic velocity model was constrained by each one-dimensional arm of the survey. High resolution f - k analysis, first arrival time inversion, as well as surface wave analysis were all used to construct a layered deterministic model.

The stochastic portion of the interpretation was performed by treating the eight observations at each range as a statistical ensemble. Frequency domain mean and variance estimates were made. The mean normalized variance or CV was then used as a measure of lateral variability in waveforms (Figure 15). At low frequencies (<30 Hz) the CV values are small ($<.4$) reflecting little spatial variation in the wavefield. As either frequency or range increase, the CV increases approaching 1 at the longer ranges and higher frequencies. In Figure 15 it is evident that the frequency at which a given CV level occurs decreases exponentially with range. Several exponentially shaped striations can be seen in the CV range-

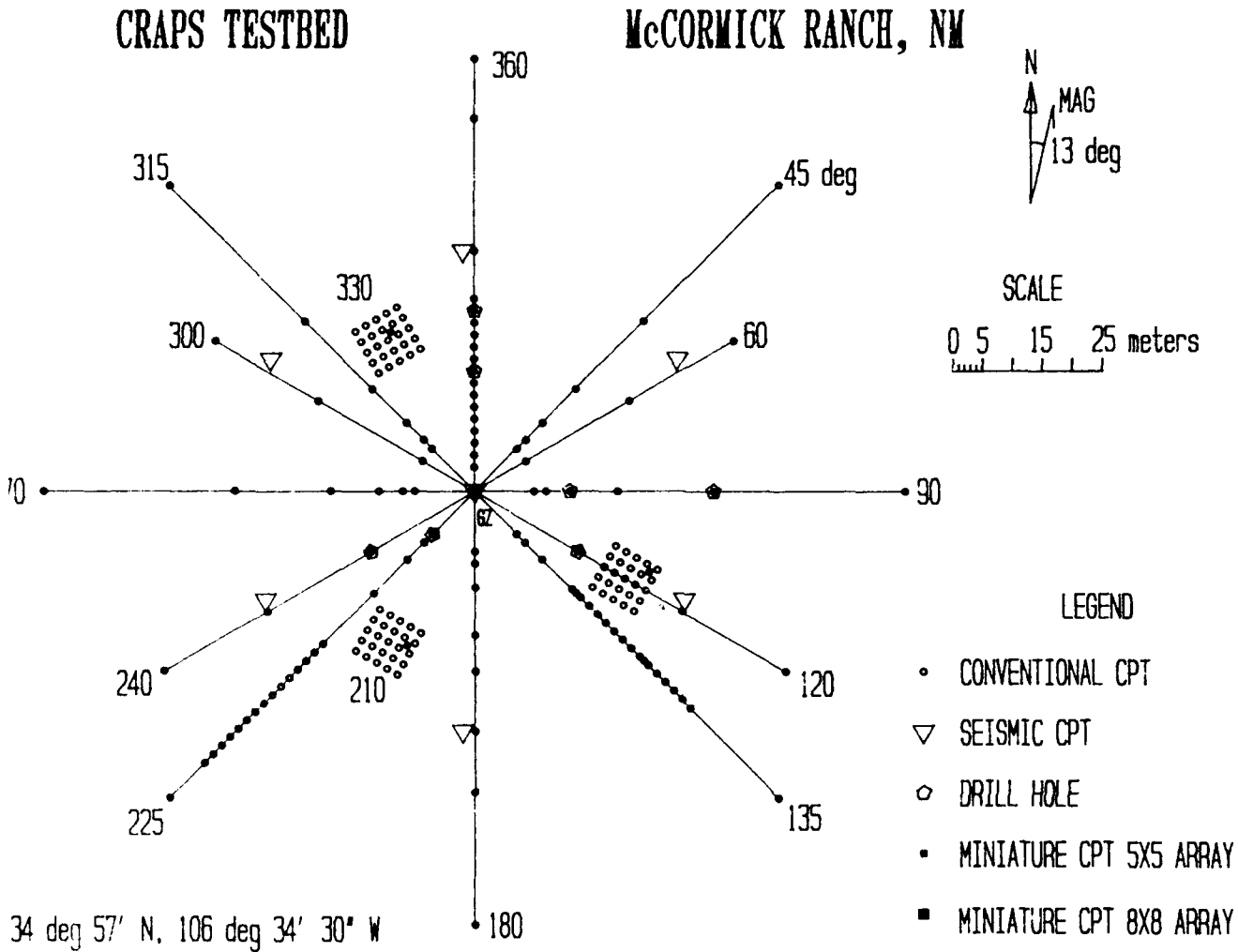


Fig. 12. Plan view showing the relationship of the cone penetrometer test holes to the CRAPS experiment testbed.

frequency plot. This information can then be utilized in constraining the stochastic site model.

The results of the stochastic interpretation of the high resolution seismic survey can aid in predicting the behavior of the full-scale explosive experiment. This point is validated in Figure 16 which compares the CV obtained at the 20-m range from the full wave seismic survey and that determined from data recorded at the same range in the full-scale CRAPS explosive event. The correlation between the seismic results and the CV from the full-scale test is good. The stochastic site characterization technique can be used to estimate the variability in the full scale explosive test.

Modeling and Implications

The results of these ground motion experiments and the site characterization demonstrate the need for the separation of stochastic and deterministic wave propagation effects when interpreting the results of small-scale field tests. Similar degrees of spatial variability in ground motion have been found at other sites. McLaughlin et al. [1983] discuss the station-to-station waveform coherence for near-source explosion accelerograms recorded on a nine-element array at Pahute Mesa, Nevada Test Site. For this array (100-m interelement spacing), at a range of 6

km from a $M_L = 5.6$ nuclear explosion, strong incoherent signals were found above 5 Hz on all components. Vernon et al. [1985] discuss earthquake seismogram coherence for a nine-station array with an interstation spacing of 50 m located near the Pinion Flat observatory in California. Several events with magnitudes between 3.0 and 4.2 and hypocentral distances ranging from 10 to 50 km were analyzed. For this data set, P waves were found to be coherent to 25 to 35 Hz, with S waves coherent to 15 Hz. Menke et al. [1990] discuss the coherence of regional signals recorded at small- (96-200 m spacing) scale arrays on hard rock sites in New England. They found that the spatial coherence at these array sites was on the order of one-sixth to one-half of a wavelength. Strong scattering occurred near the arrays even though they were placed in sites which appeared to be quite homogeneous. Vidale et al. [1990] found a lack of azimuthal symmetry and a large degree of incoherence in small-scale array observations of aftershocks of the Loma Prieta earthquake.

The results of our small field experiments, together with the very limited discussion of similar efforts found in the literature, demonstrate that these stochastic geologic effects pose a potentially serious problem for our current methods of analyzing and modeling ground motion data. For the purposes of illustration let us suppose that CRAPS had been a small-scale high explosive test conducted in the conventional manner with the intent of validating a particular calculational model of explosively

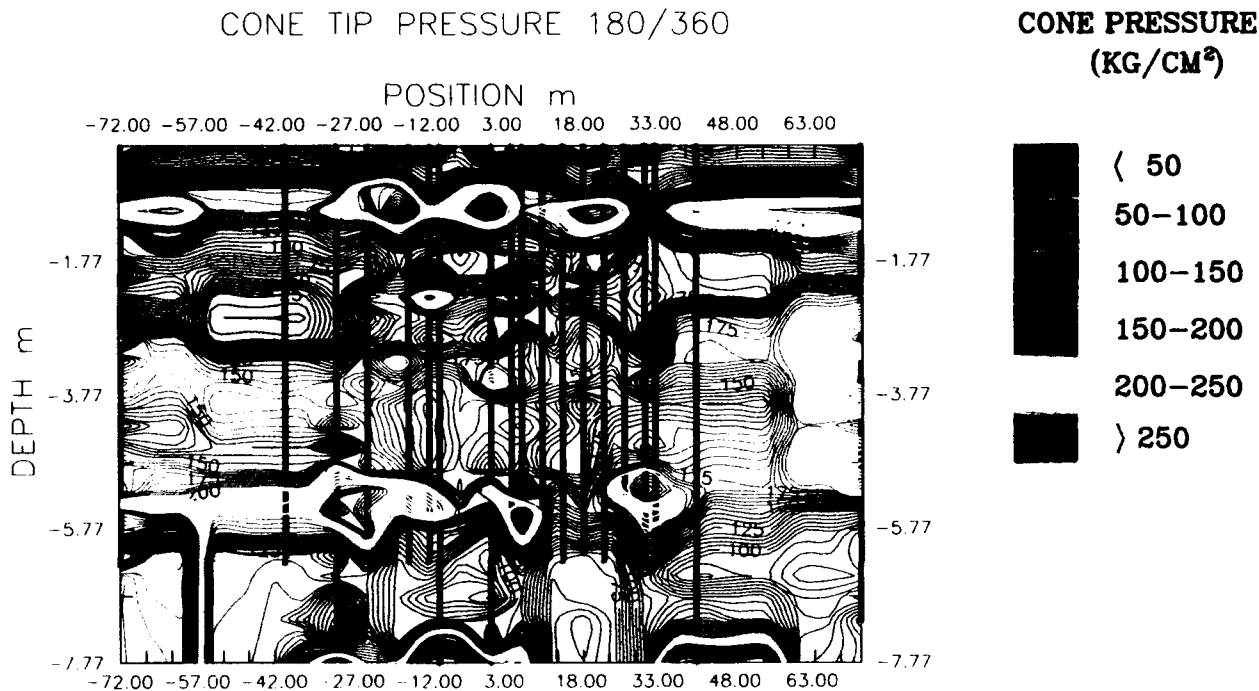


Fig. 13. Cross section of cone tip pressure as a function of depth and range for a north-south line through the center of the CRAPS experiment testbed. The solid vertical lines indicate the locations of cone penetrometer holes. The plot gives an idea of the heterogeneity present beneath the CRAPS testbed. (The depth scale is exaggerated.)

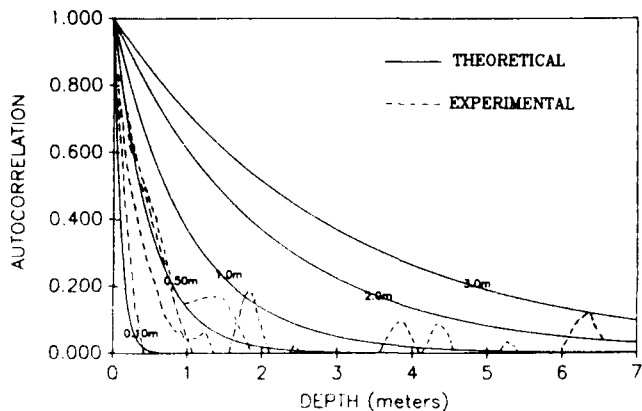


Fig. 14. Theoretical exponential autocorrelation curves for scale lengths from 0.10 to 3.0 m compared with autocorrelations of the cone tip pressure from several holes.

induced ground motion. Typically, gages would not have been fielded on multiple azimuths as shown in Figure 3., but instead would have been placed on at most two azimuths due to funding limitations. In order to develop, improve, or verify the calculational model we would attempt to match the output of the calculation with the recorded waveforms. Various parameters of the calculation would be varied in an attempt to accomplish this task. The recorded waveforms which we obtained from one or two azimuths would not, however, present a complete picture of the physics involved in the field experiment. Figure 17 presents the complete set of waveforms obtained from the 10 m range and 1-m depth on the CRAPS

event. As seen in Figure 17, there is a significant degree of variability in the character of the waveforms from one azimuth to another, particularly at the higher frequencies. The question for our deterministic analysis now becomes: Which waveform is the right one? Furthermore, even if we could decide upon a "right" waveform which we would then attempt to model we would be doing the wrong physics since we employed a uniform plane layered geology in the code. A better representation of the wave propagation phenomena would be best described by random spatial variability in geologic properties superimposed upon a plane layered model.

Once a good statistical model of the subsurface variability is established at a site of interest it must be incorporated in some way into ground motion models. Some workers have performed finite element or finite difference simulations of wave propagation through media with random spatial variability in material properties [Frankel and Clayton, 1986]. Others have approached the problem by means of analytical solutions. Flatte and Wu [1988] present a review of such modeling efforts. Reinke and Stump [1988] applied a simple solution based on the Born approximation in an attempt to model the frequency at which ground motion incoherence first occurred in small-scale field experiments. Modeling of ground motion excitation and propagation by means of techniques such as these is required to define the influence of spatial variability in material properties. These numerical experiments will require development of a methodology to incorporate what is learned from stochastic field characterization efforts into physical models of ground motion excitation and propagation. At the Phillips Laboratory, efforts are currently underway to perform near-source, finite difference simulations of small buried explosive experiments using a spatially random non-linear material model. Information from the extensive site characterization effort performed for the CRAPS experiments is being incorporated into the model.

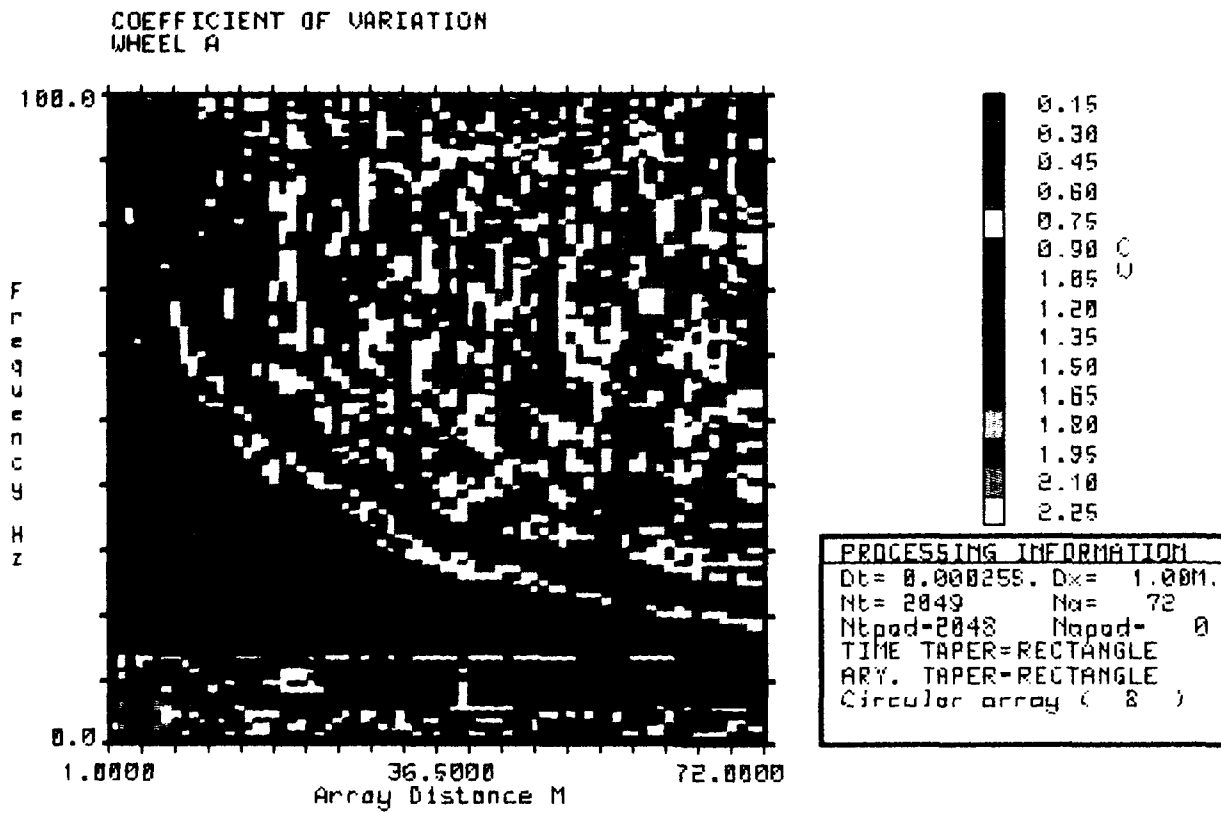


Fig. 15. Coefficient of variation plot for the amplitude spectra of records from the high-resolution seismic survey. The horizontal scale is range in meters, the vertical scale is frequency in Hz, the shadings denote coefficient of variation levels.

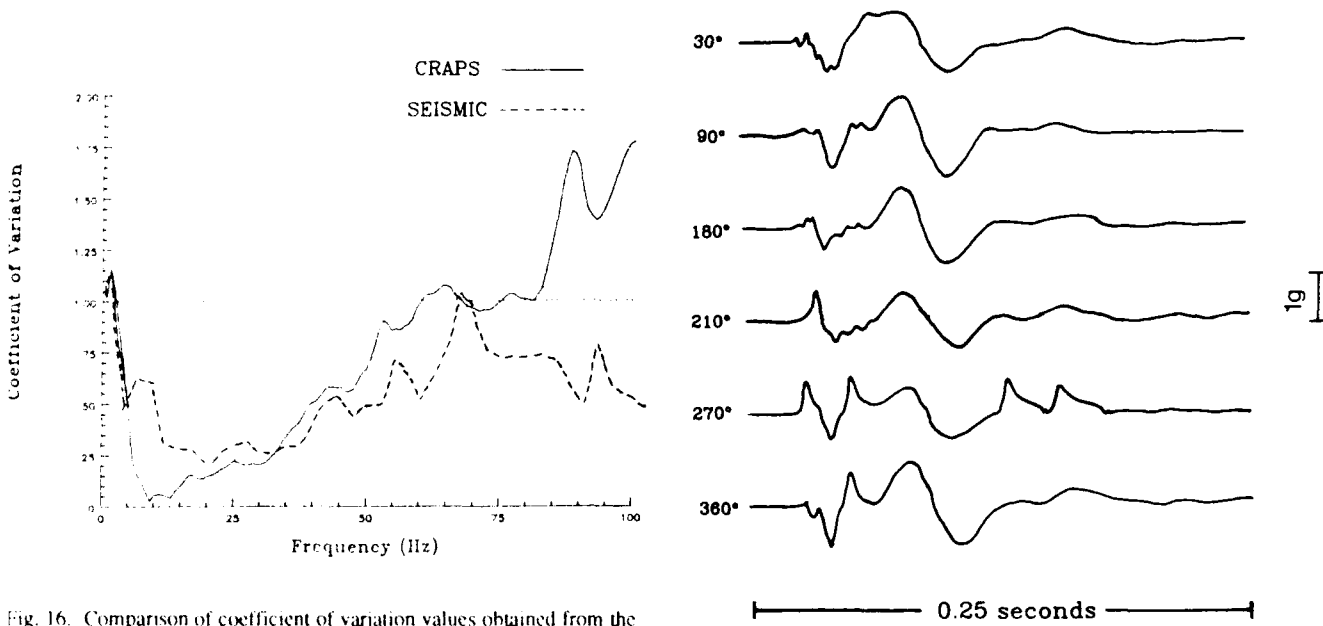


Fig. 16. Comparison of coefficient of variation values obtained from the 20-m range for the high resolution seismic survey with the coefficient of variation curve obtained from the CRAPS I waveforms recorded at the same range.

Fig. 17. Plots of the vertical accelerograms recorded at the 10-m range and 1-m depth for the CRAPS I experiment.

Discussion and Conclusions

The results of these small-scale experiments have demonstrated that heterogeneity in geologic materials exerts a significant influence on the results of small-scale high explosive experiments, at least for the dry alluvial site where the experiments were conducted. Considering that this particular site in general is thought to have a fairly uniform near-surface geologic composition, the degree of azimuthal variation observed from these small tests is remarkable. It is clear that for this site, deterministic interpretations of the data cannot be made above 35 Hz. Effective techniques for dealing with the data above this spectral region are still under development. Attempts are being made to include the results of a stochastic/deterministic site characterization process in finite difference models of explosive experiments. Future experiments of this type will require that stochastic site characterization and modeling considerations be incorporated into the experimental plan.

Although this paper has dealt specifically with small-scale events, it seems likely that the same phenomenology is at work for large events with longer travel paths and lower frequencies. A number of recent array studies in the literature report observations of similar phenomena at a variety of sites and geologies. In a qualitative sense all of these observations have roughly equivalent coherence-separation distance relationships. The upper frequency threshold for coherence of waveforms recorded by elements separated by a few tens of meters is 15-30 Hz; for separation distances of a few hundreds of meters the coherence threshold drops to 5-10 Hz. Some of the stochastic site characterization techniques described in this paper could be useful in defining near-surface stochastic site response effects for small-scale arrays.

Acknowledgments. Funding for these projects was provided by the Air Force Weapons Laboratory Independent Research Program. Additional support was provided by the Air Force Office of Scientific Research under Grant AFOSR-84-0016 to Southern Methodist University. We are indebted to Dr. Art Guenther, former Chief Scientist of the Weapons Laboratory, for his support and encouragement. Mark Bogaards performed the high-resolution seismic survey analysis as part of his Masters Thesis at SMU. The work could not have been accomplished without Al Leverette's field instrumentation efforts. Robert Goerke directed the cone penetrometer field testing. Kent Anderson assisted in analysis of data from the CRAPS experiments. Kerim Martinez constructed the cone penetrometer cross section. Audrey Martinez prepared some of the figures and provided helpful discussion. Constructive suggestions were received from two anonymous reviewers.

References

- Aki, K., and P. Richards, *Quantitative Seismology: Theory and Methods*, W. H. Freeman and Company, San Francisco, 2 vols., 932 pp., 1980.
- Bethea, R., B. Duran, and T. Boullian, *Statistical Methods for Engineers and Scientists*, Marcel Dekker, Inc., 698 pp., 1983.
- Bogaards, M., *Characterization of Whole Wave Seismograms in the Shallow Weathered Zone*, Masters Thesis, Southern Methodist University, Dallas, Texas, 1989.
- Cramer, H., *Mathematical Methods of Statistics*, Princeton University Press, Princeton, 575 pp., 1961.
- Flatte, S. and R. Wu, Small-scale structure in the lithosphere and asthenosphere deduced from arrival time and amplitude fluctuations at NORSAR, *J. Geophys. Res.*, 93, 6601-6614, 1988.
- Foster, M. and N. Guinzy, The coefficient of coherence: its estimation and use in geophysical data processing, *Geophysics*, 32, 602-616, 1967.
- Frankel, A. and R. Clayton, Finite difference simulations of seismic scattering: Implications for the propagation of short-period seismic waves in the crust and models of crustal heterogeneity, *J. of Geophys. Res.*, 91, 6465-6489, 1986.
- Holtz, R., and W. Kovacs, *An Introduction to Geotechnical Engineering*, Prentice-Hall, Englewood Cliffs, NJ, 733 pp., 1981.
- Jenkins, G. and D. Watts, *Spectral Analysis and Its Applications*, Holden-Day, San Francisco, 525 pp., 1968.
- McLaughlin, K., L. Johnson, and T. McEvily, Two-dimensional array measurements of near source ground accelerations, *Bull. Seismol. Soc. Am.*, 73, 349-376, 1983.
- Menke, W., A. Lerner-Lam, B. Dubendorff, and J. Pacheco, Polarization and coherence of 5-30 Hz wavefields at a hard rock site and their relevance to velocity heterogeneities in the crust, *Bull. Seismol. Soc. Am.*, 80, 430-449, 1990.
- Reinke, R. and B. Stump, Stochastic geologic effects on near-field ground motions in alluvium, *Bull. Seismol. Soc. Am.*, 78, 1037-1058, 1988.
- Rohani, B. and G. Baladi, *Correlation of Mobility Cone Index with Fundamental Engineering Properties of Soil*, Miscellaneous Paper SL-81-4, U.S. Army Engineer Waterways Experiment Station, 1981.
- Stump, B., and R. Reinke, Experimental confirmation of superposition from small-scale explosions, *Bull. Seismol. Soc. Am.*, 78, 1059-1073, 1988.
- Terzaghi, K., and R. Peck, *Soil Mechanics in Engineering Practice*, John Wiley and Sons, New York, 729 pp., 1967.
- Toksoz, M., A. Ben-Menahem, E. Charreue, A. Dainty, and R. Gibson, *Seismic Wave Propagation, Attenuation and Scattering over Regional Distances*, Air Force Geophysics Laboratory Technical Report, GL-TR-89-0329, 1989.
- Vernon, F., J. Fletcher, L. Haar, T. Bolswick, E. Sembera, and J. Brune, Spatial coherence of bodywaves from local earthquakes recorded on a small aperture array, *EOS Trans. Am. Geophys. Union*, 66, 954, 1985.
- Vidale, J., O. Bonamassa, and S. Schwartz, Array studies of ground motions using aftershocks from the Loma Prieta Earthquake, *Seismol. Res. Letters*, 61, 24, 1990.